

UNIVERSITY OF NAPLES FEDERICO II

DEPARTMENT OF PHARMACY

SCHOOL OF MEDICINE AND SURGERY



Ph.D. Thesis

XXXI cycle

**NEW TARGET PROTEINS FOR DRUG DISCOVERY
IN COLON CANCER**

ESTER PAGANO

TUTOR: PROF. FRANCESCA BORRELLI

COORDINATOR: PROF. MARIA V. D'AURIA

Ph.D. program in Pharmaceutical Sciences

A.Y. 2015-2018

TABLE OF CONTENTS

ABSTRACT	6
ABBREVIATION LIST	8
INTRODUCTION	11
Chapter I. Colorectal cancer (CRC)	11
1.1 Physiopathology and statistics	11
1.2 Microenvironmental regulation of tumour angiogenesis	12
Chapter II. Monoacylglycerol lipase (MAGL)	19
1.1 Monoacylglycerol lipase (MAGL): biochemistry and physiopathology	19
1.2 2-arachydonoyl glycerol (2-AG) is a MAGL substrate	19
1.3 The role of MAGL and its substrate 2-AG in cancer.....	20
Chapter III. N-acylethanolamine acid amide hydrolase (NAAA)	24
1.1. N-acylethanolamine acid amide hydrolase (NAAA): biochemistry and physiopathology.	24
1.2 Palmitoylethanolamide (PEA) is a NAAA substrate	25
1.3 The role of NAAA and its substrate PEA in cancer	25
Chapter IV. G protein-coupled receptor 35 (GPR35)	31
1.1 Orphan G protein-coupled receptor 35 (GPR35).....	31
1.2 GPR35: evidence supporting its involvement in cancer	32
1.3 Glucose metabolism in cancer	32
AIM	37
MATERIALS AND METHODS	38
1.1 Patients	38
1.2 Mice	38
1.3 Drugs	38
1.4 Cell culture	39
1.4.1 Colorectal cancer cell lines	39
1.4.2 Healthy colonic epithelial cells (HCEC).....	39
1.4.3 Endothelial cell lines	39
1.5 Primary cells isolation and culture	39
1.5.1 Murine bone marrow-derived macrophages (BMDM).....	39
1.5.2 Isolation of Intestinal Crypts and 3D Organoid Culture	40
1.6 In vivo models of colorectal cancer	40
1.6.1 AOM DSS model of colitis associated to cancer (CAC).....	40
1.6.2 AOM model of colorectal cancer	40

1.6.3 APC ^{min} model of sporadic colon cancer.....	41
1.6.4 Xenograft model of colon cancer.....	41
1.6.4.1 Xenograft tumour secretome preparation	42
1.7 Cell viability (neutral red assay)	42
1.8 Proliferation assays	42
1.8.1 BrdU incorporation in colonic epithelial cells	42
1.8.2 EdU incorporation in colonic organoids	42
1.8.3 Proliferation assay in HUVEC	43
1.9 Migration assay	43
1.9.1 Scratch assay in human colon adenocarcinoma cell lines.....	43
1.9.2 Scratch assay in HUVEC	43
1.10 Angiogenesis analysis	44
1.10.1 Tube formation assay	44
1.10.2 CXCL1/KC detection.....	44
1.10.3 Aortic ring assay	44
1.10.4 Quantification of angiogenesis modulators in HUVEC by ELISA	44
1.11 Evaluation of metabolic profile	44
1.11.1 Glucose uptake	44
1.11.2 Seahorse extracellular flux analysis	45
1.11.3 Lactate measurements	45
1.12 BrdU incorporation and quantification	45
1.13 Identification and quantification of endocannabinoids, PEA and related molecules ...	45
1.14 Immunohistochemistry	46
1.15 Immunostaining for CD31	46
1.16 Gene expression analysis by quantitative Real-Time (q)-PCR	47
1.17 Western blot analysis	47
1.18 Statistical analysis	48
RESULTS	51
Chapter I. Pharmacological inhibition of MAGL reduces experimental colon tumorigenesis	51
1.1 MAGL expression in human colorectal carcinoma (HCT 116) cells and xenograft tumour tissues	51
1.2 The MAGL inhibitor URB602 reduces tumour growth in the xenograft model of colon cancer	51
1.3 <i>Effect of URB602 (a MAGL inhibitor) on 2-AG levels in healthy and tumour tissues from xenografted mice</i>	51
1.4 The MAGL inhibitor URB602 drives <i>in vivo</i> angiogenesis output in xenograft tumour tissues	56

1.5 Direct antiangiogenic effect of the MAGL inhibitor URB602 in HUVEC	56
1.6. The MAGL inhibitor URB602 regulates Cyclin D1 in xenograft tumour tissues	56
1.7. URB602 exerts chemopreventive effects in the azoxymethane (AOM) model of colon carcinogenesis	57
Chapter II. NAAA is crucially involved in proliferation, migration and <i>in vivo</i> colon tumorigenesis	65
1.1 NAAA is down-regulated in human CRC tissues.....	65
1.2 The NAAA inhibitor AM9053 reduces tumour growth in the xenograft model of colon cancer	65
1.3 Effect of the NAAA inhibitor AM9053 on NAAA and PEA targets expression in xenograft colon cancer tumours	65
1.4 The incubation with xenograft tumour secretome reduces NAAA expression in colorectal cancer (CRC) cells	69
1.5 The NAAA inhibitor AM9053 and its substrate PEA reduce the number of tumours induced by azoxymethane (AOM).....	69
1.6 AM9053 (NAAA inhibitor) and PEA inhibit the proliferation of colorectal cancer - but not of healthy colonic - cells	69
1.7 AM9053 and PEA treatments lessen the migration of colorectal cancer cells	69
Chapter III. GPR35 promotes glycolysis, proliferation and colon tumorigenesis	76
1.1 <i>Gpr35</i> ^{-/-} BMDM have reduced glucose uptake	76
1.2 The lack of GPR35 impairs the metabolic profile of macrophages	76
1.3 GPR35 influences angiogenesis via macrophages.....	80
1.4 GPR35 is involved in experimental colitis-associated cancer and sporadic colon cancer...	83
1.5 GPR35 affects intestinal epithelial cell turn-over under homeostatic conditions	83
DISCUSSION	87
Part I. Pharmacological inhibition of MAGL reduces experimental colon tumorigenesis ...	87
1.1 <i>Presence of MAGL and 2-AG in the xenograft tumour tissue</i>	87
1.2 <i>Effect of URB602 on 2-AG levels, tumour progression and angiogenesis</i>	87
1.3 <i>Effect of URB602 in the azoxymethane (AOM) model of colon carcinogenesis</i>	89
1.4 Concluding remarks	90
Part II. NAAA is crucially involved in proliferation, migration and <i>in vivo</i> colon tumorigenesis	91
1.1 <i>NAAA and PPAR-α expression in human CRC</i>	91
1.2 <i>Effect of AM9053 on experimental carcinogenesis</i>	91
1.3 <i>Effect of AM9053 and exogenous PEA on proliferation and migration of colorectal cancer cells</i>	93
1.4 Concluding remarks	94
Part III. GPR35 promotes glycolysis, proliferation and colon tumorigenesis	95
1.1 <i>GPR35 controls macrophages metabolism</i>	95

<i>1.2 GPR35 affects angiogenesis</i>	96
<i>1.3 GPR35 has a role in colonic proliferation and tumorigenesis</i>	96
1.4 Concluding remarks	97
GENERAL CONCLUSIONS	98
REFERENCES	100

ABSTRACT

Background: Colorectal cancer (CRC) is one of the most common causes of death in Western countries. Because of the high heterogeneity and incidence of this disease, it is crucial to improve the knowledge on its biology – a fundamental step for drug discovery - and to develop clinically-relevant diagnostic and prognostic biomarkers.

Evidence suggests that MAGL [(a serine hydrolase that converts monoacylglycerols, such as the endocannabinoid 2-arachidonoyl glycerol (2-AG), in glycerol and fatty acid), NAAA [(a cysteine hydrolase responsible of the catabolism of palmitoylethanolamine (PEA)] and GPR35 (an orphan-G protein coupled receptor) affect biological events (*e.g.* proliferation, differentiation, survival) and regulates pathophysiological states (*e.g.* intestinal inflammation) which are suggestive of a possible involvement in CRC. Here, we explored the possible contribution of MAGL, NAAA and GPR35 to colon tumorigenesis.

Material and Methods: The role of MAGL, NAAA and GPR35 was assessed *in vivo*, via genetic or pharmacological blockade, in *APC^{min}* mice as well as in the azoxymethane (AOM), AOM/dextran sodium sulfate (DSS) and xenograft models.

Cell proliferation was evaluated in CRC cells, healthy colonic epithelial cells and colonic organoids 3D culture by using the BrdU and EdU incorporation; migration was examined in CRC and endothelial cells by using the scratch assay. Angiogenesis was assessed in tumour tissues [by microvessel counting and by investigating the expression of vascular endothelial growth factor (VEGF) and fibroblast growth factor-2 (FGF-2) proteins] as well as in the aortic ring model and in endothelial cells by using the tube formation assay. Cell metabolism was measured by the quantification of extracellular acidification rate (ECAR), oxygen consumption rate (OCR), lactate production and glucose uptake in bone marrow derived macrophages (BMDM). MAGL, NAAA and GPR35 expression was evaluated by RT-PCR and immunohistochemistry; 2-AG and PEA levels were measured by liquid chromatography mass spectrometry.

Results: MAGL- The MAGL inhibitor URB602 reduced xenograft tumour growth, the effect being associated to down-regulation of VEGF and FGF-2, reduction in the number of vessels and down-regulation of cyclin D1. A direct antiangiogenic effect was observed in human endothelial cells, too. In experiments aiming at investigating the role of MAGL in chemoprevention, URB602 attenuated AOM-induced preneoplastic lesions and tumours in wild-type but not in MAGL-deficient mice. **NAAA-** NAAA expression was reduced in biopsies of clinically-diagnosed CRC patients as well as in CRC cells incubated with tumour secretome. The NAAA inhibitor AM9053 and its substrate PEA inhibited proliferation and migration in CRC cells. Increased PEA levels *in vivo* (via NAAA inhibition or by its exogenous administration) resulted in chemopreventive effects

in the AOM model of colon carcinogenesis and reduced xenograft tumour growth. **GPR35**- GPR35 deletion resulted in a reduction of cell energetic demand and production in M0-, M1- and M2-BMDM. Also, depletion of GPR35 in M2-BMDM decreased their capability to produce the CXCL1 (pro-angiogenic chemokine) and to stimulate the tube formation of endothelial cells. Also, *GPR35*^{-/-} mice showed a reduced intestinal turnover in physiological conditions and, importantly, a reduced colon tumorigenesis, as highlighted in two different experimental models of colon cancer. It is noteworthy that the protective role of GPR35 in *APC*^{min} mice was confirmed with the conditional deletion of *Gpr35* (Villin-Cre) in the intestinal epithelium.

Conclusions: In summary, by elucidating the physiopathological role of MAGL, NAAA and GPR35 in experimental colon tumorigenesis and by ascertain their dysregulation in intestinal tumours, this PhD thesis put forth such proteins as possible innovative prognostic markers in clinically-diagnosed CRC and as new molecular targets to be explored in drug discovery.

ABBREVIATION LIST

15-LOX	15-lipoxygenase
2-AG	2-arachidonoyl glycerol
2DG	2-deoxy-D-glucose
2DG6P	2-deoxy-D-glucose-6-phosphate
5-FU	5-fluorouracil
AA	arachidonic acid
ABHD12	α/β -hydrolase domain containing 12
ABHD6	α/β -hydrolase domain containing 6
ACF	aberrant crypt foci
Adenosine-A ₃	adenosine A3 receptor
AEA	N-arachidonylethanolamide or anandamide
AOM	azoxymethane
APC	adenomatous polyposis coli
ATCC	American type culture collection
BMDM	bone marrow-derived macrophages cell line
BrdU	2'-deoxy-5-bromo-uridine
BSA	bovine serum albumin
CAC	colitis associated to cancer
Caco-2	human colorectal adenocarcinoma cell line
CAFs	cancer-associated fibroblasts
CB ₁	cannabinoid receptor 1
CB ₂	cannabinoid receptor 2
CD	Crohn's disease
CD31	cluster of differentiation 31
cDNA	complementary DNA
cGMP	cyclic guanosine 3',5'-monophosphate
COX-2	cyclooxygenase 2
CRC	colorectal cancer
CXCL	CXC-chemokine ligand
CXCL17	chemokine ligand 17
DAG	diacylglycerol
DAGL	diacylglycerol lipase
DMEM	Dulbecco's modified eagle medium
DSS	dextran sodium sulphate
ECAR	extracellular acidification rate
ECM	extracellular matrix
ECs	endothelial cells
EDTA	ethylenediaminetetraacetic acid
EdU	edoxyudine
EGF	epidermal growth factor
EGM-2	endothelial growth medium
ELISA	enzyme-linked immunosorbent assay
EMT	endocannabinoid membrane transporter
EVs	extracellular vesicles
FAAH	fatty acid amide hydrolase
FAP	familial adenomatous polyposis
FBS	fetal bovine serum
FGF2	fibroblast growth factor 2

FITC	fluorescein 5-isothiocyanate
FOLFIRI	fluorouracil/leucovorin and irinotecan
FOLFOX	fluorouracil/leucovorin and oxaliplatin
GABA _A	type A γ -aminobutyric acid receptor
GAPDH	glyceraldehyde 3-phosphate dehydrogenase
GDP	guanosine diphosphate
GPCR	G protein-coupled receptor
GPR55	G protein-coupled receptor 55
GTP	guanosine triphosphate
GWAS	genome-wide association study
HCEC	healty human colonic epithelial cells
HCT116	human colorectal adenocarcinoma cell line
HNPCC	hereditary non-polyposis colorectal cancer
HPLC	high performance liquid chromatography
HUVEC	human umbilical vein endothelial cells
IBD	inflammatory bowel disease
IECs	intestinal epithelial cells
IFN α	interferon- α
IFN γ	interferon- γ
IL	interleukin
IL-4	interleukin-4
<i>ip</i>	intraperitoneal administration
K-Ras	Kirsten RAt Sarcoma
LPS	lipopolysaccharide
M1	pro-inflammatory phenotype of macrophages
M2	pro-resolving phenotype of macrophages
MAGL	monoacylglycerol lipase
M-CSF	macrophage colony-stymulating factor
MMP	matrix metalloproteinase
M Φ	macrophages
NAAA	N-acylethanolamine acid amide hydrolase
NAEs	N-acylethanolamines
NAPE-PLD	N-acyl-phosphatidylethanolamine selective phospholipase D
NAT	N-acyl-transferase
NPPE	N-palmythoylethanolamine
NR	neutral red
OCR	oxygen consumption rate
OEA	N-oleoylethanolamide
p53	tumour suppressor protein
PBS	phosphate-buffered saline
PC	prostate cancer
PCR	polymerase chain reaction
PEA	N-palmythoilethanolamide
PGD2	prostaglandin D2
PGE2	prostaglandin E2
PGF2	prostaglandin F2
PGs	prostaglandins
PLC	phospholipase C
PPARs	peroxisome proliferator-activated receptors

PPAR- α	peroxisome proliferator-activated receptor α
PPAR- γ	peroxisome proliferator-activated receptor γ
PSC	primary sclerosing cholangitis
RPMI 1640	Roswell Park Memorial Institute 1640 medium
SDS-PAGE	sodium dodecyl sulfate-polyacrylamide gel electrophoresis
SNP	single-nucleotide polymorphism
SVEC4-10	immortalized murine endothelial cells
TAMs	tumour-associated macrophages
TASCs	tumour-associated stromal cells
TBS	Tris-buffered saline
TGF β	transforming growth factor β
TNF	tumour necrosis factor
TNM	classification of malignant tumours
TRPV1	transient receptor potential cation channel subfamily V type 1
UC	ulcerative colitis
VEGF	vascular endothelial growth factor
VEGFA	vascular endothelial growth factor A
VEGF-R	vascular endothelial growth factor receptor

CHEMICAL NAMES

AM630	[6-iodo-2-methyl-1-(2-morpholin-4-ylethyl)indol-3-yl]-(4-methoxyphenyl)methanone
AM9023	1-isothiocyanatopentadecane
ARA-C	4-amino-1-[(2R,3S,4S,5R)-3,4-dihydroxy-5-(hydroxymethyl)oxolan-2-yl]pyrimidin-2-one
ARN077	5-phenylpentyl-N-[(2S,3R)-2-methyl-4-oxo-oxetan-3-yl]carbamate
ARN726	4-cyclohexylbutyl-N-[(S)-2-oxoazetidin-3-yl]carbamate
DAB	4-(3,4-diaminophenyl)benzene-1,2-diamine
EDTA	2-[2-[bis(carboxymethyl)amino]ethyl-(carboxymethyl)amino]acetic acid
EdU	5-ethyl-1-[(2R,4S,5R)-4-hydroxy-5-(hydroxymethyl)oxolan-2-yl]pyrimidine-2,4-dione
FCCP	2-[[4-(trifluoromethoxy)-phenyl]hydrazinylidene]propanedinitrile
FITC	3',6'-dihydroxy-6-isothiocyanatospiro[2-benzofuran-3,9'-xanthene]-1-one
HEPES	4-(2-hydroxyethyl)-1-piperazineethanesulfonic acid
HU-210	11-hydroxy- Δ^8 -tetrahydrocannabinol
JZL184	(4-nitrophenyl) 4-[bis(1,3-benzodioxol-5-yl)-hydroxymethyl]piperidine-1-carboxylate
MK886	3-[3-tert-butylsulfanyl-1-[(4-chlorophenyl)methyl]-5-propan-2-ylindol-2-yl]-2,2-dimethylpropanoic acid
S-OOPP	N-[(3S)-2-oxooxetan-3-yl]-3-phenylpropanamide
URB602	cyclohexyl N-(3-phenylphenyl)carbamate

INTRODUCTION

Chapter I. Colorectal cancer (CRC)

1.1 Physiopathology and statistics

Colorectal cancer (CRC) represents a common cause of cancer-related deaths. It has been estimated that, in 2018, it will be the third most common cause of deaths in USA, with an equal incidence in males and females (8%) and with a prediction of 140,250 new diagnosed cases (Siegel et al., 2018; Figure 1). Similarly, CRC has been placed at the second position in the oncologic death rank in European countries for 2018 (Malvezzi et al., 2018; Figure 2) and in Italy 53.000 new CRC cases has been estimated to be diagnosed in the same year (www.airtum.it).

The majority of colorectal cancers are sporadic, arising from dysplastic adenomatous polyps. In this case, CRC develops as a consequence of the progressive accumulation of genetic and epigenetic alterations that cause transformation and progression of normal mucosa to adenoma and subsequently to carcinoma (Lao and Grady, 2011) (Figure 3). These alterations are the consequence of mutations in genes involved in cell growth regulation, such as tumour-suppressor genes (*e.g.* APC, Smad4 and p53) or oncogenes (*e.g.* K-Ras, c-myc, c-neu, c-src) (Calvert and Frucht H, 2002). This multi-step process spans 10 to 15 years, thereby providing an opportunity for prevention.

It is also well established that CRC is largely influenced by lifestyle, genetic predisposition and longstanding intestinal inflammation. About 10% of CRCs develops in the setting of well-defined hereditary syndromes *i.e.* hereditary non-polyposis colorectal cancer (HNPCC) and familial adenomatous polyposis (FAP) (Lynch and de la Chapelle, 2003; Rustgi, 2007).

Chronic gut inflammation is one of the main causes of increased risk of developing CRC (Terzic et al., 2010; Ullman and Itzkowitz, 2011) (Figure 3). Patients affected by inflammatory bowel diseases (IBD), such as ulcerative colitis (UC) and Crohn's disease (CD), are at increased risk of developing neoplasia (Gupta et al., 2007; Itzkowitz and Harpaz, 2004), with an extended incidence rate of 2.75 and 2.64 of CRC in patients with UC and CD, respectively (Bernstein et al., 2001). It is worth noting that colitis can promote tumorigenesis by altering microbial composition as well as the expansion of microorganisms with genotoxic capabilities (Richard et al., 2018; Dejea et al., 2018). Other risk factors include obesity, meat and fat-rich diet, smoking, alcohol consumption and hyperinsulinemia (Marley and Nan, 2016; Wynder et al., 1969).

CRC is largely asymptomatic until the latter stages, when the cancer has already metastasized, thus a huge emphasis is also placed on early detection. Standard clinical practice for CRC patients include primarily the surgical resection, followed by neoadjuvant radiotherapy (for patients with rectal cancer), and adjuvant chemotherapy (for patients with stage III/IV and high-risk stage II colon cancer) (Marley and Nan, 2016). 5-fluorouracil (5-FU) is used in several poly-chemotherapy

regimens in CRC advanced patients, such as FOLFOX (Fluorouracil/Leucovorin and Oxaliplatin) and FOLFIRI [Fluorouracil/Leucovorin and Irinotecan (IR)] (Gustavsson et al., 2015). However, intrinsic or acquired resistance to 5-FU may occur (Ahn et al., 2015).

Despite the clear progresses raised in colon cancer diagnosis and therapy, the number of deaths still remain unacceptably high. Therefore, it is crucial to improve the knowledge on CRC pathogenesis, and, importantly, to identify new strategies, including chemoprevention and early diagnosis, in order to reduce the public health burden of this disease.

1.2 Microenvironmental regulation of tumour angiogenesis

Microenvironment plays a crucial role in the tumour growth and a considerable number of key transduction signals are involved in tumour microenvironment progression. Specifically, it is largely reported the importance of angiogenesis for the development of solid tumours, because the dissemination of tumours requires the growth of new blood vessels (Risau, 1997; Hanahan and Folkman, 1996).

Hypoxic cancer cells secrete vascular endothelial growth factor A (VEGFA), which initiates tumour angiogenesis by engaging VEGF receptor 2 expressed on the endothelial cells of neighbouring blood vessels (Potente et al., 2011). In pre-malignant stages of epithelial tumours, a basal lamina precludes the interaction between early lesions and the vascularized peritumoral tissues (Bossi et al., 1995; Bluff et al., 2009) (Figure 4). Instead, in the malignant tumours, cancer cells acquire invasive behaviours and induce a stromal response involving the formation of new blood vessels (Bergers and Benjamin, 2003) (Figure 4). Tumour-associated blood vessels typically acquire an aberrant morphology, which indicates the impaired vascular maturation, poor vessel functionality and incoherent tumour perfusion (Potente et al., 2011; Bergers and Benjamin, 2003; Morikawa et al., 2002). This angiogenic switch, strictly correlated with cancer progression, shows substantial variances in the patterns of tumour vascularization, which reflects differences in tumour type, grade and stage, anatomical site and expression of pro-angiogenic and anti-angiogenic factors (Bluff et al., 2009; Fukumura et al., 1997; Jubb et al., 2011; Morrissey et al., 2008).

Concerning CRC, it is characterised by enhanced VEGF expression and high microvascular densities, - suggestive of increased angiogenic activity - which negatively affect patient survival (Des Guetz et al., 2006). Consistently, therapy with anti-VEGF antibodies improves CRC patient survival, thus emphasising VEGF as a major clinical angiogenic factor (Carmeliet, 2005; Ferrara et al., 2007; Hawinkels et al., 2008).

Although cancer cells play a pivotal role as source of VEGFA and other pro-angiogenic mediators, many signals are produced from various tumour-associated stromal cells (TASCs), including bone marrow-recruited cells (*e.g.* macrophages, lymphocytes and neutrophils) as well as tissue-resident

cells such as vascular cells (i.e. endothelial cells and pericytes) and fibroblasts (Fang and Salven, 2011) (Figure 5).

In mouse models of cancer, macrophages derive mainly from circulating monocytes that extravasate into tumours in response to various chemoattractant *stimuli* (Qian and Pollard, 2010; Lahmar et al., 2016). Thereafter, monocytes differentiate and mature into tumour-associated macrophages (TAMs), i.e. the major constituents of malignant tumours - under the influence of colony-stimulating factor 1 (M-CSF) (Qian and Pollard, 2010; Lahmar et al., 2016).

Current therapeutic interventions often fail to prevent disease progression to metastatic dissemination. Hence, innovative therapeutic approaches include the targeting of specific molecular pathways such as proteins involved in the tumour angiogenesis and metastasis (Gelmon et al., 1999; Goetz et al., 2003).

Estimated New Cases

		Males		Females			
Prostate	164,690	19%			Breast	266,120	30%
Lung & bronchus	121,680	14%			Lung & bronchus	112,350	13%
Colon & rectum	75,610	9%			Colon & rectum	64,640	7%
Urinary bladder	62,380	7%			Uterine corpus	63,230	7%
Melanoma of the skin	55,150	6%			Thyroid	40,900	5%
Kidney & renal pelvis	42,680	5%			Melanoma of the skin	36,120	4%
Non-Hodgkin lymphoma	41,730	5%			Non-Hodgkin lymphoma	32,950	4%
Oral cavity & pharynx	37,160	4%			Pancreas	26,240	3%
Leukemia	35,030	4%			Leukemia	25,270	3%
Liver & intrahepatic bile duct	30,610	4%			Kidney & renal pelvis	22,660	3%
All Sites	856,370	100%	All Sites	878,980	100%		

Estimated Deaths

		Males		Females			
Lung & bronchus	83,550	26%			Lung & bronchus	70,500	25%
Prostate	29,430	9%			Breast	40,920	14%
Colon & rectum	27,390	8%			Colon & rectum	23,240	8%
Pancreas	23,020	7%			Pancreas	21,310	7%
Liver & intrahepatic bile duct	20,540	6%			Ovary	14,070	5%
Leukemia	14,270	4%			Uterine corpus	11,350	4%
Esophagus	12,850	4%			Leukemia	10,100	4%
Urinary bladder	12,520	4%			Liver & intrahepatic bile duct	9,660	3%
Non-Hodgkin lymphoma	11,510	4%			Non-Hodgkin lymphoma	8,400	3%
Kidney & renal pelvis	10,010	3%			Brain & other nervous system	7,340	3%
All Sites	323,630	100%	All Sites	286,010	100%		

Figure 1. Ten Leading Cancer Types for the Estimated New Cancer Cases and Deaths by Sex, United States, 2018 (from Siegel, 2018).

Estimates are rounded to the nearest 10 and cases exclude basal cell and squamous cell skin cancers and in situ carcinoma except urinary bladder. Ranking is based on modeled projections and may differ from the most recent observed data.

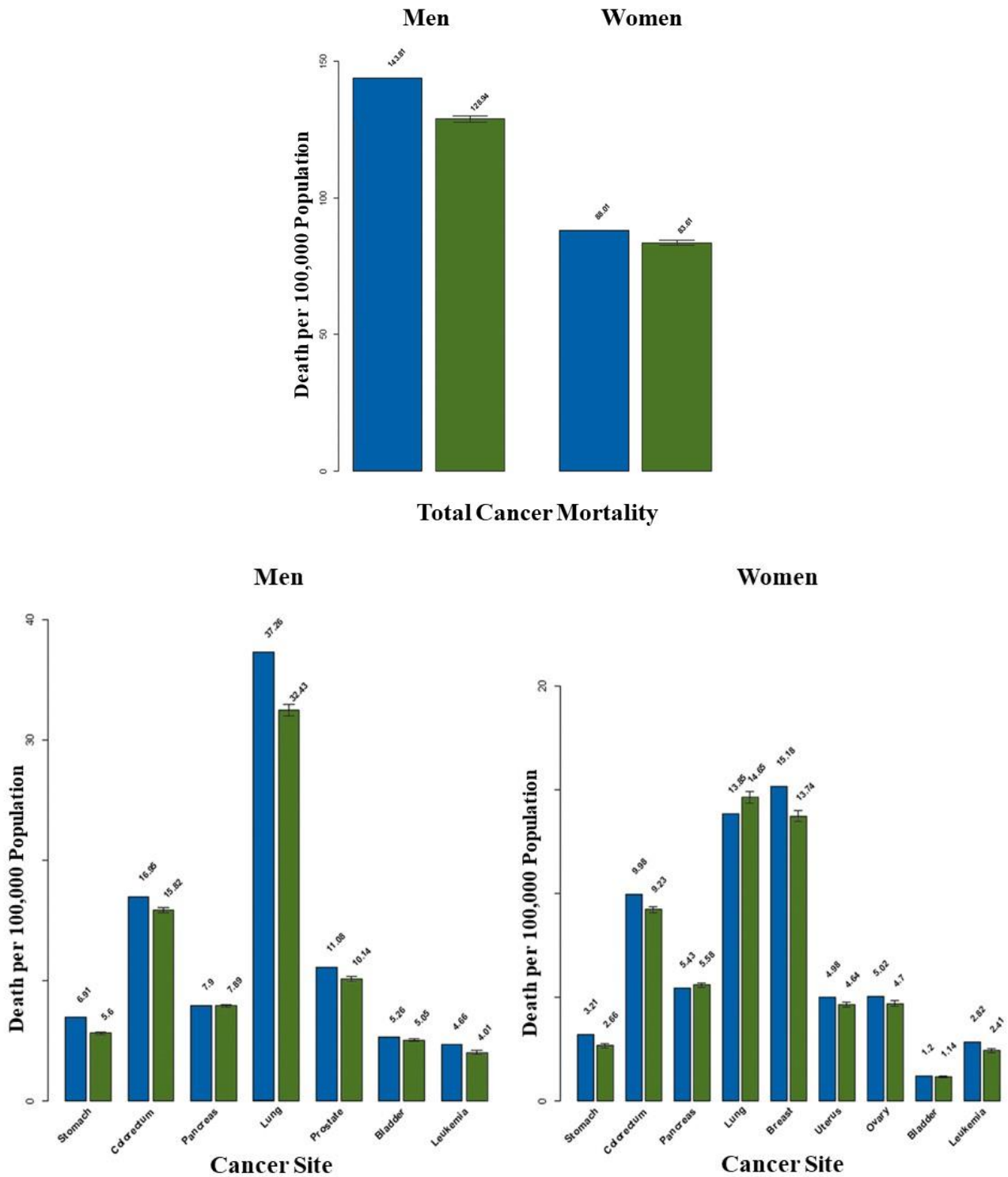


Figure 2. Prediction of cancer mortality in the European Union (EU) for the year 2018 (from Malvezzi et al., 2018).

Bar-plots of age-standardized (world population) death rates per 100 000 persons for the year 2012 (blue) and predicted rates for 2018 (green) with 95% prediction intervals for total cancer and the eight major cancer sites in EU men and women.

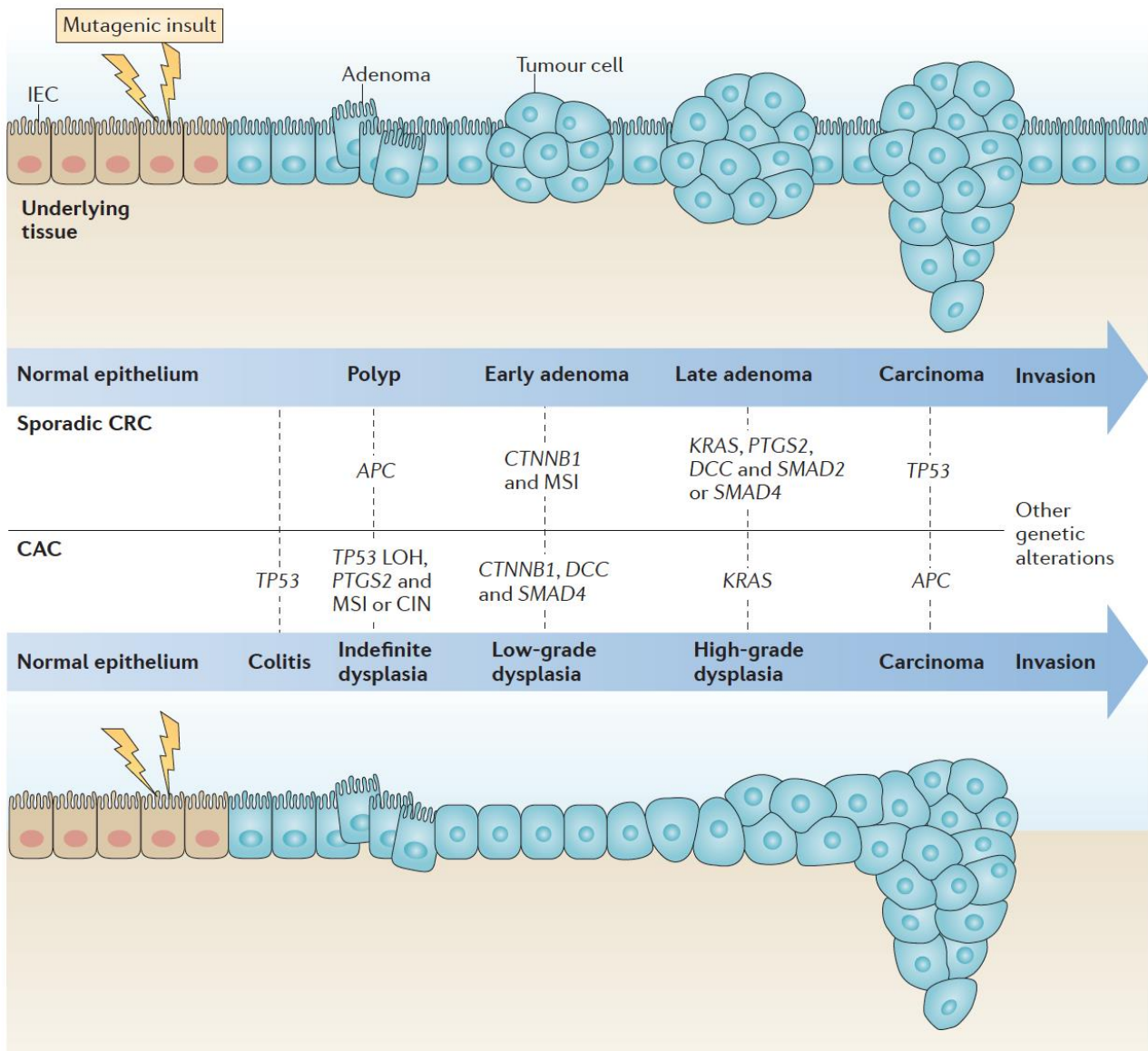


Figure 3. Adenoma to carcinoma sequence (from West et al., 2015)

Canonical mechanisms of sporadic colorectal cancer (CRC) and colitis-associated cancer (CAC) development are shown in the top and bottom panels, respectively. CRC and CAC share similarities in their developmental pathways, including microsatellite instability (MSI), activation of the oncogene KRAS, activation of cyclooxygenase 2 (COX2; encoded by PTGS2), and mutation and eventual loss of heterozygosity (LOH) of TP53, adenomatous polyposis coli (APC), deleted in colon cancer (DCC) and SMAD4. However, the frequency and sequence of these events differs between the cancers. For example, mutation in APC is one of the first events in CRC, whereas it occurs at later stages in CAC. By contrast, TP53 mutations usually occur early in CAC but at a later stage in the progression of CRC. Although CRC shows a clear progression of morphological changes, from polyp to carcinoma, CAC progression involves increasing histological grades of dysplasia that culminate in an invasive carcinoma. CTNNB1, gene encoding β -catenin; CIN, chromosomal instability; IEC, intestinal epithelial cell.

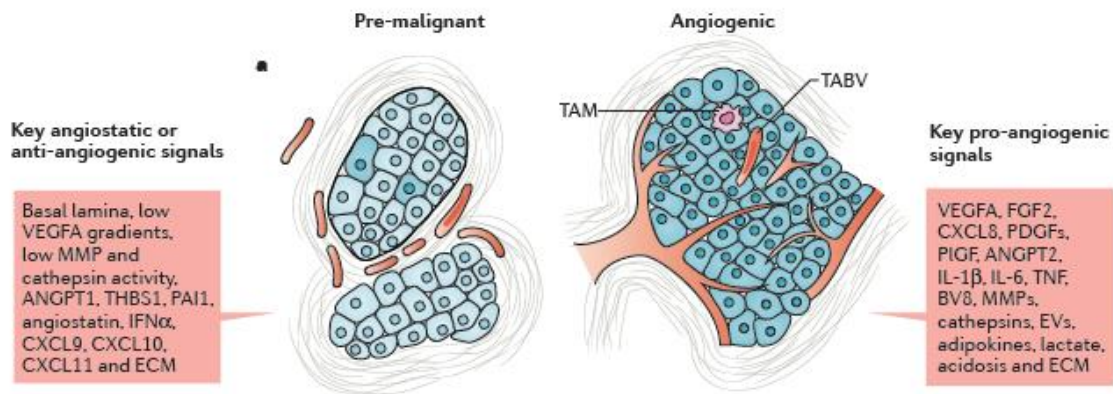


Figure 4. Angiogenesis during malignant progression (from De Palma et al., 2017)

Early-stage (pre-malignant) tumours typically display scant or no intratumoural vascularization, although a vascularized stroma surrounds the tumours and may adjoin parenchymal tumour domains (left panel). In malignant tumours, the cancer cells acquire invasive behaviours and induce a stromal response involving robust intratumoural angiogenesis, along with leukocyte infiltration, fibroblast proliferation and extracellular matrix (ECM) deposition (right panel). In pre-malignant lesions, a basal lamina separates the tumour from the surrounding tissues; this, together with angiostatic signals conveyed by some ECM components, and the relatively low levels of pro-angiogenic factors, prevents intratumoural vascularization or constrains it into a quiescent state. In malignant lesions, angiogenesis is largely controlled through the actions on vascular endothelial cells (ECs) of multiple pro-angiogenic mediators, which include growth factors, cytokines, various ECM proteins, ECM-remodelling enzymes, as well as extracellular vesicles (EVs) and by-products of deregulated tumour metabolism. ANGPT, angiopoietin; CXCL, CXC-chemokine ligand; EV, extracellular vesicle; FGF2, fibroblast growth factor 2; IFN α , interferon- α ; IL, interleukin; MMP, matrix metalloproteinase; PAI1, plasminogen activator inhibitor 1; PDGF, platelet-derived growth factor; PIGF, placental growth factor; TABV, tumour-associated blood vessel; THBS1, thrombospondin 1; TNF, tumour necrosis factor; VEGFA, vascular endothelial growth factor A.

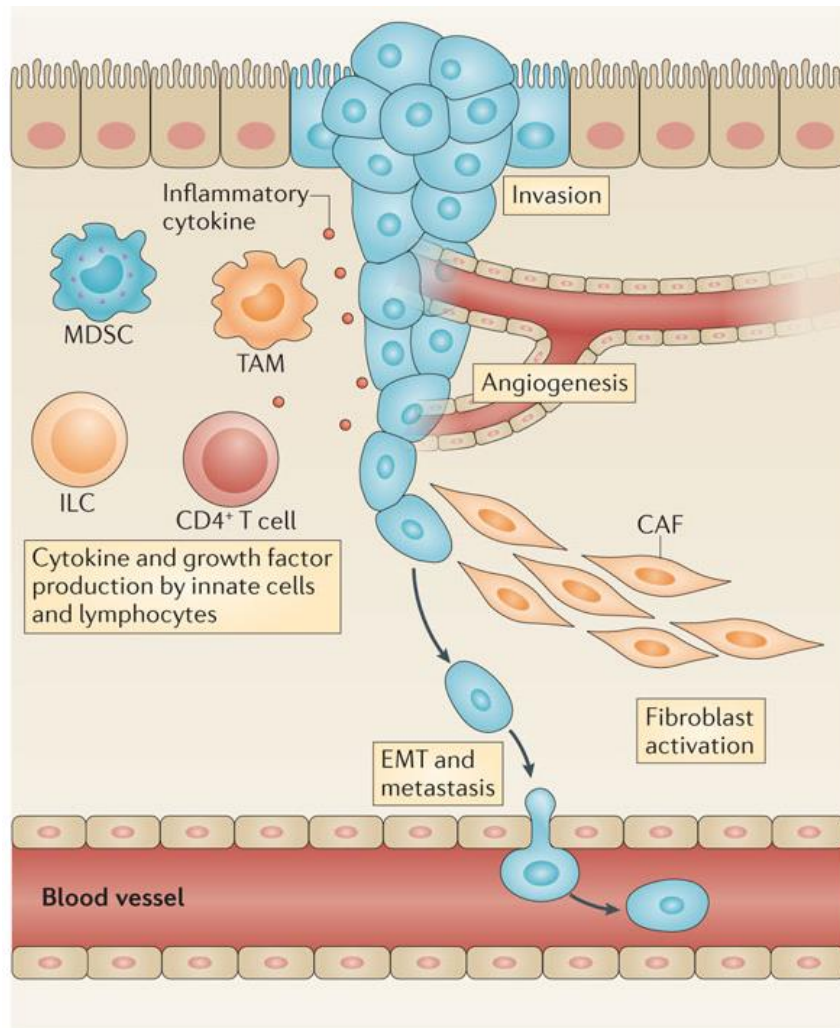


Figure 5. Tumour microenvironment and role of the inflammation (from West et al., 2015)

Production of inflammatory cytokines by several cell types including CD4⁺ T cells, innate lymphoid cells (ILCs) and tumour-associated macrophages (TAMs). Many of the inflammatory cytokines can act directly on transformed intestinal epithelial cells (IECs) to promote proliferation, inhibition of apoptosis, invasion, angiogenesis, epithelial to mesenchymal transition (EMT) and metastasis. More recently, it has been appreciated that these cytokines can activate cancer-associated fibroblasts (CAFs) to produce cytokines and growth factors that modulate both neoplastic cells and the tumour microenvironment.

Chapter II. Monoacylglycerol lipase (MAGL)

1.1 Monoacylglycerol lipase (MAGL): biochemistry and physiopathology

Monoacylglycerol lipase (MAGL) is a serine hydrolase that converts monoacylglycerols, such as the endocannabinoid 2-arachidonoyl glycerol (2-AG) to glycerol and fatty (arachidonic) acid. MAGL consists of two tissue specific isoforms with a molecular weights of 33 kD and 36 kD, which could reflect different splice variants (Karlsson et al., 2001; Long et al., 2009a). The enzyme associates with membranes and its active site resides within the cytosol.

MAGL is localized in different areas of brain and in peripheral tissues, including the gastrointestinal tract (Ahn et al., 2008; Duncan et al., 2008; Izzo and Camilleri, 2009). MAGL blockade shows tissue-specific differences in monoacylglycerol metabolism, with the brain showing the most dramatic elevations in 2-AG and peripheral tissues often showing greater changes in other monoacylglycerols, consistent with the lipolytic role of MAGL as the final step of triglyceride hydrolysis in peripheral tissues (Long et al., 2009b).

In addition to the role of MAGL in terminating 2-AG signaling, MAGL exerts a crucial control over brain prostaglandins production in both basal and neuroinflammatory states. (Nomura et al., 2011a). In fact, through the hydrolysis of 2-AG, MAGL releases arachidonic acid (AA), i.e. the major precursor for the synthesis of pro-inflammatory eicosanoids (Nomura et al., 2011a). MAGL blockade decreases AA levels in the brain, stoichiometrically to 2-AG elevation, which also results in a reduction of lipopolysaccharide (LPS)-induced pro-inflammatory levels of downstream COX-driven prostaglandins [i.e. prostaglandin E2 (PGE2), PGD2, PGF2], and thromboxane production (Nomura et al., 2011a). For this reason, MAGL is an important target for neuroinflammatory and neurodegenerative disorders.

In recent years, the understanding of MAGL role has greatly increased, due to the progress made in the knowledge of the structure of MAGL, the synthesis of highly potent and selective *in vivo* efficacious inhibitors, e.g. JZL184 and URB02, as well as the development of MAGL-deficient mice (Chanda et al., 2010; Long et al., 2009a; Sclosburg et al., 2010) (Figure 6). Consequently, an impressive number of studies have described the therapeutic potential of MAGL inhibitors in a variety of human diseases – including cancer - through the bidirectional manipulation of endocannabinoids, eicosanoids, and other lipid signaling pathways.

1.2 2-arachidonoyl glycerol (2-AG) is a MAGL substrate

MAGL plays a predominant role in catalyzing the hydrolysis of the endocannabinoid 2-arachidonoyl glycerol (2-AG) (Dihn et al., 2002; Dihm et al., 2004; Hohmann et al., 2005). 2-AG is generated “*on demand*” through *stimulus*-dependent cleavage of membrane phospholipid precursors and its levels are regulated by the balance between its production and degradation (Murataeva et al.,

2014). 2-AG is thought to be produced through hydrolysis of phospholipids by phospholipase C (PLC) β or δ to release diacylglycerols (DAG), which are then degraded to 2-AG by diacylglycerol lipase (DAGL) α or β (Gao et al., 2010; Tanimura et al., 2010). (Figure 7).

Genetic or pharmacological inhibition of MAGL reduces 2-AG hydrolysis by >80% in most tissues, including the brain. The remaining amount of 2-AG is metabolized by the hydrolytic enzymes α/β -hydrolase domain 6 (ABHD6), ABDH12, fatty acid amide hydrolase (FAAH) (Blankman et al., 2007; Dihn et al., 2004; Marrs et al., 2010; Goparaju et al., 1998), 15-lipoxygenase (Kozak et al., 2002) and monoacylglycerol acyltransferases/kinases (Simpson et al., 1991). Although the other enzymes may have roles in 2-AG hydrolysis in certain settings, MAGL blockade lead to dramatic elevations, especially in the brain, in 2-AG levels, confirming that MAGL is the primary enzyme involved in degrading 2-AG *in vivo* (Long et al., 2009b; Nomura et al., 2011a; Schlosburg et al., 2010; Fowler, 2012).

2-AG is an endogenous lipid mediator involved in a variety of physiological and physiopathological processes. 2-AG behaves as full agonist for the cannabinoid (CB)₁ and CB₂ receptors (Sugiura et al., 1999; Sugiura et al., 2000). The 2-AG homologues 2-linoleoylglycerol and 2-palmitoylglycerol, which are present in tissues and presumably released together with 2-AG, act as ‘entourage compounds’ to potentiate the effects of 2-AG at CB receptors without themselves having a direct action on CB receptors (Ben-Shabat et al., 1998). In addition, several studies report that 2-AG may also exert physiological effects independently from CB1 and CB2 receptors activation, for example by binding to and activating GABA_A (Sigel et al., 2011), PPAR- γ (Bouaboula et al., 2005), adenosine A3 (Lane et al., 2010), TRPV1 (Iwasaki et al., 2008), and GPR55 (Ryberg et al., 2007) (Figure 7). However, CB1 receptor is the major brain target through which 2-AG exerts its physiopathological effects, including regulation of food intake and metabolism, neuro-inflammation, addiction, anxiety and pain (Baggelaar et al., 2018).

1.3 The role of MAGL and its substrate 2-AG in cancer

MAGL is up-regulated in aggressive human ovarian, prostate, breast cancer cells and in primary tumours, where it promotes migration, invasion, survival, and *in vivo* tumour growth (Mulvihill and Nomura, 2013; Nomura et al., 2010; Nomura et al., 2011b). In cancer cells, MAGL plays a role in controlling global levels of free fatty acids, which serve as building blocks for the synthesis of pro-tumorigenic signalling lipids, such as prostaglandin E2 and lysophosphatidic acid (Qin et al., 2014; Nomura et al., 2010). Recently, it has been reported that MAGL is upregulated in melanoma tissue and its expression in tumour cells is significantly associated with tumour aggressiveness, vascular invasion of the primary lesion and tumour progression (Baba et al., 2017).

Concerning 2-AG, i.e. the main substrate of MAGL, studies have shown that it exerts antiproliferative effects in a number of cancer cell lines (Melck et al., 2000; Costa et al., 2014; Orellana-Serradell et al., 2015), including colorectal cancer cells (Ligresti et al., 2003). For example, the increase of endogenous 2-AG levels as a consequence of MAGL inhibition was shown to reduce prostate cancer invasion *in vitro* (Nomura et al., 2011b). On the other hand, the reduction of physiological endogenous 2-AG levels has been reported to stimulate cell invasion (Nithipatikom et al., 2011).

Our understanding of how MAGL impacts colon cancer progression is so far hindered by under-reported and controversial data (Schicho and Storr, 2011; Izzo et al., 2015), since the enzyme has been associated to both cancerogenic (Sun et al., 2013) and anti-cancerogenic processes (Ye et al., 2011). Nevertheless, the effect and role of MAGL in relation to 2-AG production and angiogenesis have been not evaluated to date.

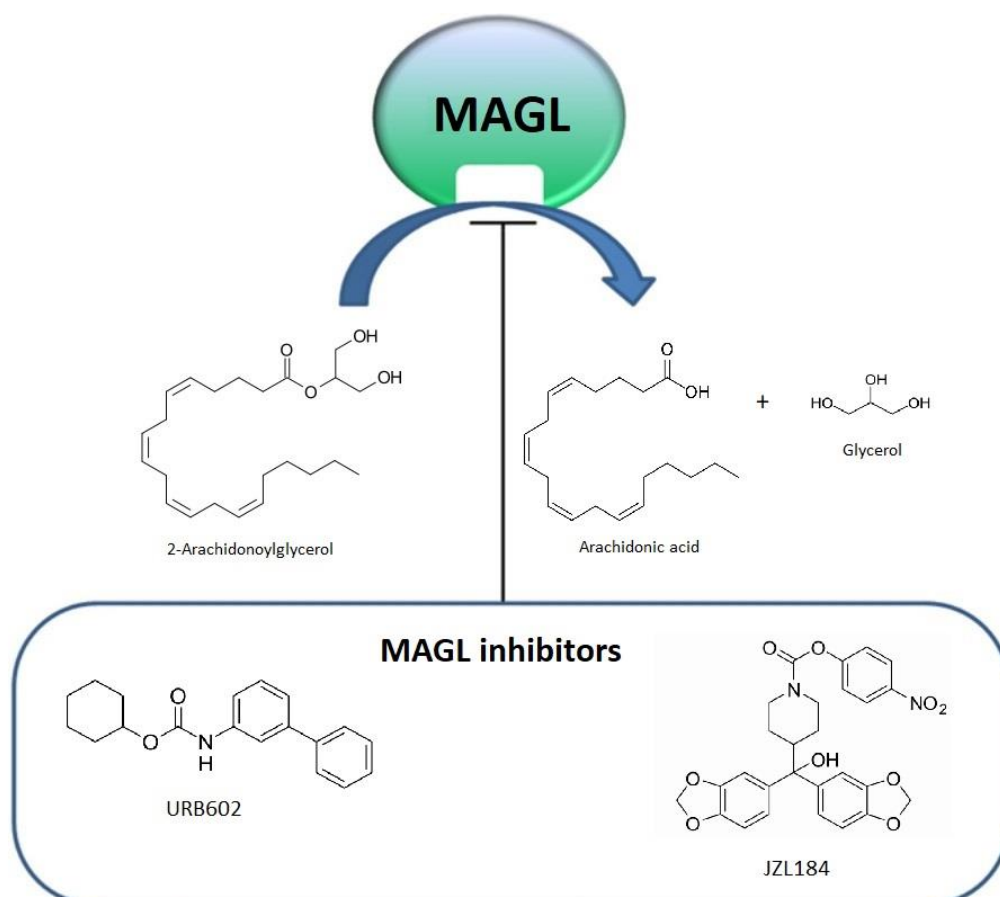


Figure 6. Conversion of 2-Arachidonoylglycerol (2- AG) into arachidonic acid and glycerol by monoacylglycerol lipase (MAGL). MAGL inhibitors such as URB602 and JZL184 increase the endogenous levels of 2-AG.

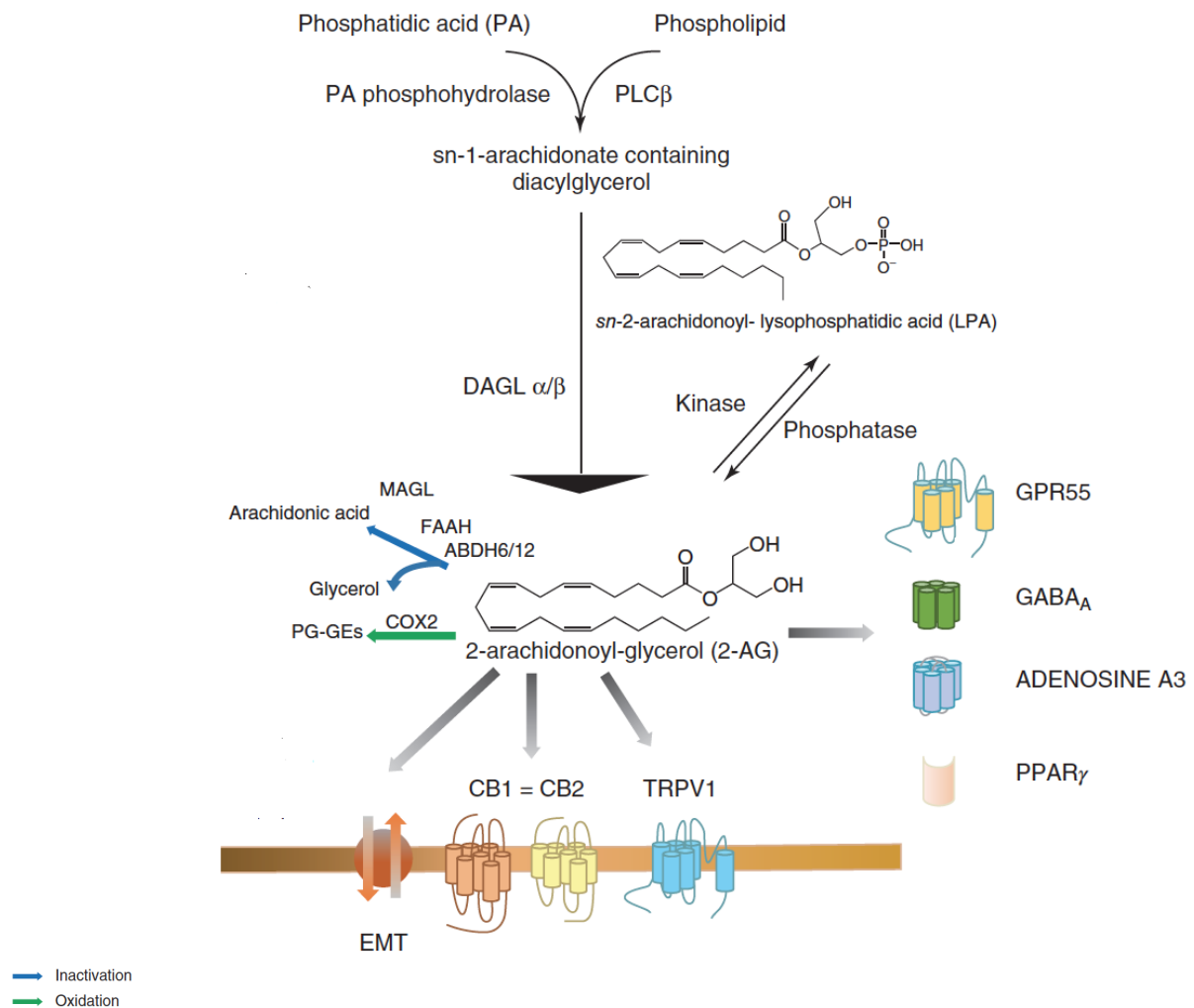


Figure 7. Metabolic pathways and molecular targets of 2-AG (adapted from Iannotti and Piscitelli, 2018).

ABH4/6/12, αβ-hydrolase 4/6/12; CB1/2, cannabinoid receptor 1/2; COX₂, cyclooxygenase 2; DAG, diacylglycerol; EMT, 'endocannabinoid membrane transporter'; FAAH, fatty acid amide hydrolase; GDE1, glycerophosphodiester phosphodiesterase; GPR55, G-protein-coupled receptor 55; PLCβ, phospholipase Cβ; PLD, phospholipase D; PTPN22, protein tyrosine phosphatase, nonreceptor type 22; TRPV1, transient receptor potential, vanilloid subtype 1 receptor; GABA_A, type-A γ-aminobutyric acid receptor; adenosine A3, adenosine A3 receptor; PPAR_γ, peroxisome proliferator-activated receptor gamma; 15-LOX, lipoxygenase-15; PMs, prostaglandin-ethanolamides/prostamides; PG-GEs, prostaglandin-glyceryl esters.

Chapter III. N-acylethanolamine acid amide hydrolase (NAAA)

1.1. N-acylethanolamine acid amide hydrolase (NAAA): biochemistry and pathophysiology

N-acylethanolamine acid amide hydrolase (NAAA) is a N-terminal cysteine hydrolase of the cholesteryl esterase family. Being a lysosomal enzyme, NAAA is produced as an inactive pro-enzyme and autocatalytically activated by cleavage at acidic pH. Human and murine NAAA are similar with 76% sequence identity (Tsuboi et al. 2005). Glycosylation of the enzyme was firstly believed to be necessary to reach its full activity. However, more recent findings have demonstrated that glycosylation is most probably necessary for trafficking of the enzyme to the lysosomes and its maturation, with minimal effects on enzyme activity (Pavlopoulos et al. 2018).

NAAA is responsible of the hydrolysis of N-acylethanolamines (NAEs), mainly PEA and to a very less extent OEA and AEA. Consistently, NAAA inhibitors increase preferentially PEA levels *in vitro* and *in vivo*, making NAAA a promising target for drug discovery (Tsuboi et al. 2005; Ueda et al., 2013; Alhouayek and Muccioli, 2014; Bottemanne et al., 2018) (Figure 8). With the recent molecular identification of NAAA, a number of selective and stable NAAA inhibitors have been synthesised and tested in a variety of disease models. While the first generation of inhibitors were irreversible and moderately potent, in more recent years new potent, reversible, stable and selective inhibitors have been synthesised (Bottemanne et al., 2018; Figure 8). Makriyannis's research group developed a series of isothiocyanate-based NAAA reversible inhibitors such as AM9053 and AM9023 (West et al., 2012; Malamas et al., 2015) (Table 1). Other series of potent NAAA inhibitors were developed by Piomelli and co-workers around β -lactone and β -lactam moieties, such as β -lactone (S)-OOPP, ARN077 and ARN726 (Solorzano et al., 2009; Duranti et al., 2012; Ponzano et al., 2013; Ribeiro et al., 2015; Nuzzi et al., 2016) (Table 1). These new inhibitors are precious tools to study the role of NAAA.

Because NAAA is highly expressed in bone marrow and immune system, especially in macrophages, its pathophysiological role was firstly evaluated in inflammatory processes (Solorzano et al., 2009; Sasso et al., 2013; Yang et al., 2015). Moreover, because NAAA is believed to primarily control PEA levels (Tsuboi et al. 2005; Tai et al., 2012), its inhibition is expected to mimic the anti-inflammatory, neuroprotective and analgesic properties of PEA (Alhouayek and Muccioli, 2014). NAAA is also largely expressed in human and murine small and large intestine (Borrelli et al., 2015; Alhouayek et al., 2015) and its pharmacological inhibition reduces colon inflammation by locally increase PEA levels (Alhouayek et al., 2015). However, it is important to note that NAE levels as well as the expression of NAAA may be altered differently depending on the tissue or the disease considered.

1.2 Palmitoylethanolamide (PEA) is a NAAA substrate

N-acylethanolamines (NAEs) are endogenous lipids consisting of an acyl chain linked by an amide bond to ethanolamine. Although sharing the same basic scaffold, NAEs can bind to several different receptors and exert a plethora of biological effects (Bottemanne et al., 2018). Besides the well characterized NAEs, such as the endocannabinoid N-arachidonoylethanolamine (AEA), N-palmitoylethanolamine (PEA) is one of the most-studied NAEs, being it clinically used for its anti-inflammatory, analgesic and neuroprotective properties mostly mediated by PPAR- α (Alhouayek and Muccioli, 2014; Gugliandolo et al., 2018; Esposito and Cuzzocrea, 2013; Skaper et al., 2015; Iannotti et al., 2016). Despite PPAR α is the main reported target (Lo Verme et al., 2005), additional and pharmacologically relevant targets of PEA have been reported (Petrosino and Di Marzo, 2017) (Figure 9). Thus, PEA has also been shown to be an agonist of orphan G-protein coupled receptor 55 (GPR55) (Ryberg et al., 2007), although this pharmacological implication remains to be clarified. In addition, unlike AEA, PEA does not bind to cannabinoid (CB) receptors, although it can indirectly activate them via the so-called “entourage” effect, i.e. through the inhibition of FAAH, the enzyme responsible for endocannabinoids degradation (Di Marzo et al., 2001; Petrosino et al., 2016). Finally, PEA may directly or indirectly modulate (via enhancement of AEA levels or via PPAR- α activation) transient receptor potential cation channel subfamily V (TRPV)1 channels (De Petrocellis et al., 2002; Ho et al., 2008; Ambrosino et al., 2013; Ambrosino et al., 2014) (Figure 9).

In addition to be an endogenous lipid molecule, PEA is also a food component, first discovered in the late 1950s, when it was shown that the anti-allergic and anti-inflammatory activities exerted by peanut oil or soybean lecithin were due to a specific lipid fraction corresponding to PEA (Coburn et al., 1954; Ganley et al., 1958). PEA has been detected in a wide variety of food sources such as milk, tomato and corn (Venables et al., 2005; Kilaru et al., 2007; Gouveia-Figueira and Nording, 2014) (Table 2).

1.3 The role of NAAA and its substrate PEA in cancer

Several splice variants of NAAA are expressed in human cells. Among these, two code for catalytically inactive proteins which represent up to 20% of the expressed NAAA in certain cell lines, including the human prostate cancer cell line VCAP) (Sakura et al., 2016). The expression and the activity of NAAA were reported in a number of tumour types and the enzyme has been also proposed as a possible biomarker of prostate cancer (Wang et al., 2008). More recently, NAAA expression was found higher in non-aggressive prostate cancer, assuming the enzyme as a promising signature for tumour aggressiveness (Liu et al., 2014). Also, NAAA is highly expressed in aggressive mouse ovarian cancer (Du et al., 2016). Interestingly, it has been recently reported

that pharmacological inhibition of NAAA decreased proliferation and migration and caused cell death in different bladder cancer cell lines (Vago et al., 2017). However, to date there is no information about the possible role of NAAA in colorectal cancer physiopathology.

Concerning PEA, there are some findings which are suggestive of a possible role in cancer. First, some of PEA targets (*e.g.* CB receptors, TRPV1 and PPAR- α) are involved in the carcinogenesis mechanisms. Furthermore, PEA has been shown: i) to slow up melanoma cell survival (Hamtiaux et al., 2012); ii) to induce cell death in high grade astrocytomas/neuroblastoma cells (Stock et al., 2012); iii) to be dramatically decreased in human tumour brain tissues compared to healthy area (Maccarone et al., 2001) and iv) to potentiate the cytotoxic effect of anandamide in human breast cancer cells (De Petrocellis et al., 2002). A recent study on colorectal cancer cells has shown antiproliferative and antiangiogenic effects of PEA, possibly through a selective PPAR- α dependent inhibition of AKT/mTOR pathway (Sarnelli et al., 2016). Nevertheless, the knowledge of PEA role in CRC is still greatly fragmentary, lacking functional studies that corroborate its involvement and potential molecular mechanisms.

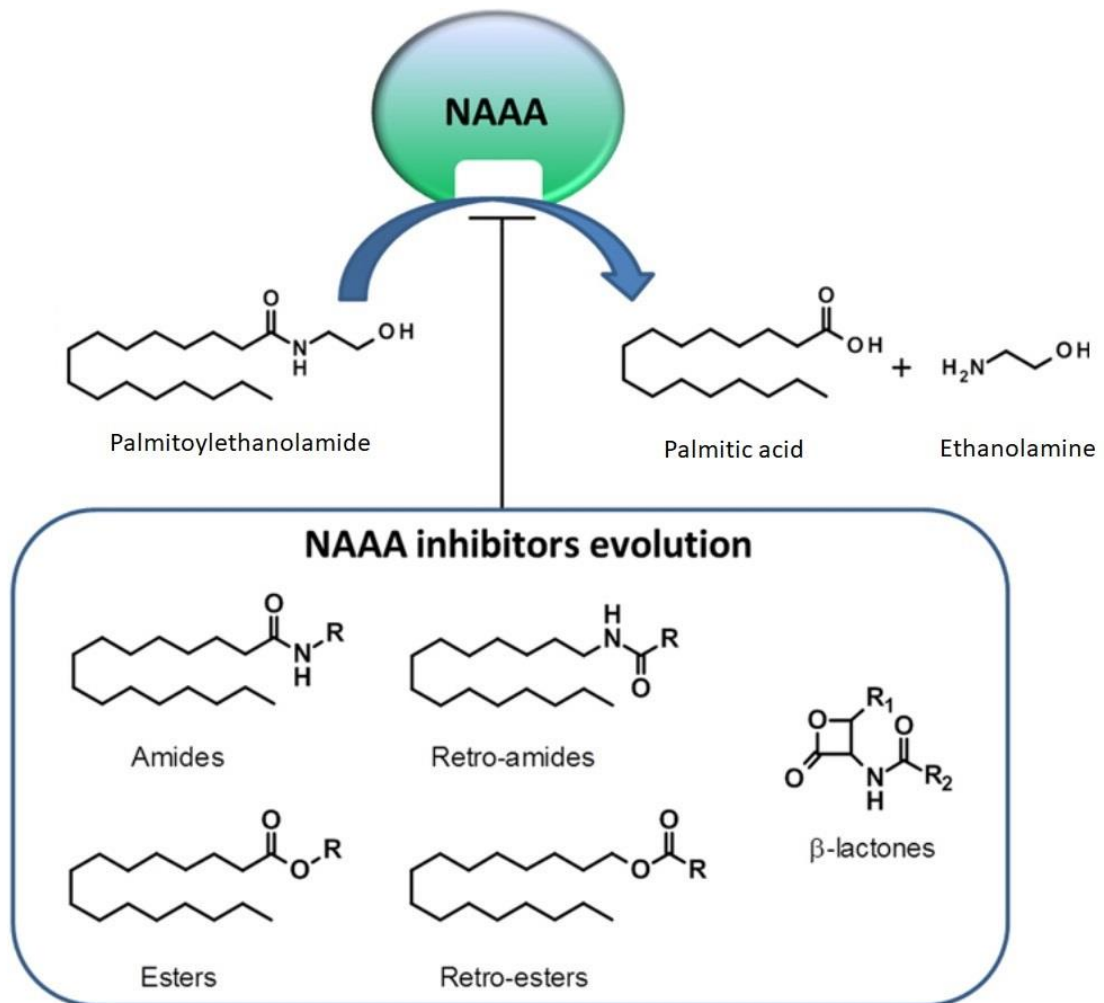


Figure 8. Conversion of palmitoylethanolamide (PEA) into palmitic acid and ethanolamide by acylethanolamine acid amide hydrolase (NAAA) (adapted from Bandiera et al., 2014).

Representative chemical structures of NAAA inhibitors are shown. Specific NAAA inhibitors and their pharmacological properties are reported in Table 1.

TABLE 1 Characteristics of representative NAAA inhibitors

Characteristics of representative NAAA inhibitors						
Inhibitor	<i>In vitro</i>			<i>In vivo</i>		
	NAAA inhibition	FAAH inhibition	Effect on NAE levels	Model	Dose	Effect on NAE levels
Cyclopentyl hexadecanoate	IC ₅₀ = 10 μM (hNAAA)	FAAH: no significant effect (at 50 μM)	Increases PEA levels in NAAA-expressing HEK cells			
Pyrrolidine derivative 16	IC ₅₀ = 2 μM (rNAAA)	FAAH: IC ₅₀ >100 μM	Increases PEA levels in RAW264.7 cells			
AM9023	IC ₅₀ = 0.600 μM (hNAAA)	FAAH: IC ₅₀ >10 μM				
AM9053	K _i = 0.030 μM (hNAAA)	FAAH: IC ₅₀ ≈ 100 μM	Increases NAE levels in J774 cells	DSS-induced colitis	10 mg/kg, b.i.d. (i.p.)	Increases PEA levels in the colon
(S)-OOPP	IC ₅₀ = 0.420 μM (rNAAA)	FAAH: IC ₅₀ >100 μM	Increases PEA levels in RAW 264.7 cells and in NAAA-expressing HEK cells (at 10 μM)	Carrageenan-instilled sponges to recruit leukocytes	25 μg/implanted sponge	Increases PEA levels in carrageenan-recruited leukocytes
				Spinal cord injury in mice	30 μg/mice (intrathecaly)	Not reported
ARN077	IC ₅₀ = 0.01 – 0.130 μM (rNAAA) IC ₅₀ = 0.007 μM (hNAAA)	FAAH: no significant effect (at 10 μM)		Chronic constriction injury	20 μl of a 10% suspension topically administered on the paw skin	Increases PEA levels in the sciatic nerve
				DNFB-induced dermatitis	3% topically administered on the ear skin	Increases PEA levels in the DNFB-treated ear
ARN726	IC ₅₀ = 0.063 μM (rNAAA) IC ₅₀ = 0.027 – 0.073 μM (hNAAA)	FAAH: IC ₅₀ >100 μM		Carrageenan-induced lung inflammation	30 mg/kg (per os)	Increased PEA and OEA levels
				CFA-injected paw	30 mg/kg (i.p.)	Increased PEA and OEA levels
N-O-aryl-substituted derivative 37	IC ₅₀ = 0.006 μM (hNAAA)	FAAH: IC ₅₀ >50 μM		Carrageenan-induced paw inflammation	5–50 μg/paw (intraplantar)	Not reported
F96	IC ₅₀ = 0.270 μM (rNAAA)	FAAH: IC ₅₀ = 41 μM		TPA-induced ear edema	10 mg/kg (i.p.)	Increased PEA and OEA levels in TPA-treated ears
F215	IC ₅₀ = 0.009 μM (rNAAA)	ND				

(from Bottemanne et al., 2018)

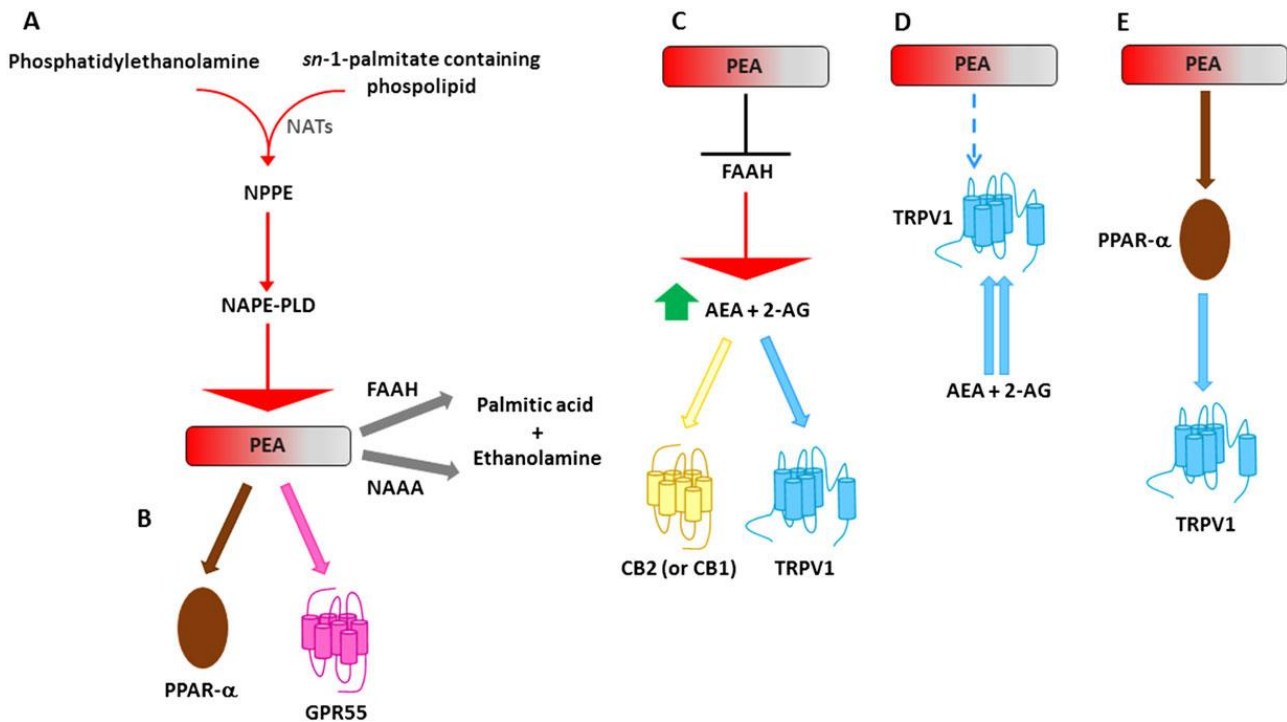


Figure 9. Metabolic pathways and molecular targets of PEA (from Petrosino and Di Marzo, 2017).

(A) PEA is biosynthesized from a membrane phospholipid, N-palmitoylphosphatidylethanolamine (NPPE), via several routes, the most investigated of which is through the direct hydrolysis by NAPE-PLD. PEA can be then degraded to palmitic acid and ethanolamine by either FAAH or NAAA (Iannotti et al., 2016). NAT, N-acyl-transferase.

(B) PEA can directly activate PPAR- α (Lo Verme et al., 2005b) or, more controversially, GPR55 (Ryberg et al., 2007).

(C) PEA, for example through the inhibition of the expression of FAAH, may increase the endogenous levels of AEA and 2-AG, which directly activate CB2 (or CB1) receptors and TRPV1 channels (entourage effect) (Di Marzo et al., 2001; Petrosino et al., 2016).

(D) PEA, possibly through an allosteric modulation of TRPV1 channels, potentiates the activation and desensitization by AEA and 2-AG of TRPV1 channels (entourage effect) (De Petrocellis et al., 2001; Di Marzo et al., 2001; Ho et al., 2008; Petrosino et al., 2016).

(E) PEA may also activate TRPV1 channels via PPAR- α (Ambrosino et al., 2013, Ambrosino et al., 2014).



TABLE 2. Food sources that contain PEA	
Food source	Concentration of PEA (ng·g⁻¹ fresh weight)
Bovine milk	0.25
Elk milk	1.81
Human breast milk	8.98 ± 3.35 nmol·L ⁻¹
Human breast milk (110 ± 32.3 lactation days)	23.4 ± 7.2 nmol·L ⁻¹
Common bean (<i>Phaseolus vulgaris</i>)	53.5
Garden pea (<i>Pisum sativum</i>)	100
Southern or blackeyed peas (<i>Vigna unguiculata</i>)	138
Tomato	100
<i>Medicago sativa</i>	1150
Corn	200
Soybean (<i>Glycine max</i>)	6700
Soy lecithin	950000
Peanut (<i>Arachis hypogaea</i>)	3730

(from Petrosino and Di Marzo, 2017)

Chapter IV. G protein-coupled receptor 35 (GPR35)

1.1 Orphan G protein-coupled receptor 35 (GPR35)

The G protein-coupled receptors (GPCRs) superfamily of transmembrane-spanning proteins is composed of ~1,000 members (Lagerstrom and Schiöth, 2008) and comprises ~3% of the human genome (Insel et al., 2007). Considering their ubiquity and central role in signal transduction, it is not surprising that GPCRs constitute the largest class of drug targets for a wide range of pathological conditions (Santos et al., 2017; Campbell and Smrcka, 2018). Although GPCR-targeted therapies are hampered by undesirable side effects [due to a lack of receptor subtype selectivity (Wang and Lewis, 2013) and/or a pathological interference with physiological signaling (Kenakin, 2005)], GPCRs remain attractive targets for drug design. In last years, more than 140 GPCRs with unknown endogenous ligands have been discovered, including the so-called *orphan receptors* (Levoe et al., 2006). These are involved in different physiological effects and may provide access to signal transduction pathways currently unknown, allowing for new strategies in drug design. Importantly, orphan GPCR-targeted therapies may be more selective than those currently known, resulting in a potential side effects reduction.

G protein-coupled receptor 35 (GPR35) is an orphan receptor discovered in 1988 (O'Dowd et al., 1998) (Figure 10). Despite being able to be activated by high concentration of endogenous molecules, foremost the tryptophan metabolite kynurenic acid (KYNA), 2-oleoyl lysophosphatidic acid (LPA), CXCL17 and cGMP (cyclic guanosine 3'5' monophosphate), it has not been demonstrated that any of these agonists binds selectively to GPR35 (Oka et al. 2010; Wang et al. 2006; Maravillas-Montenero et al., 2015). For example, KYNA shows huge species-dependent differences in potency, which is lowest ($EC_{50} > 10^{-3}$ M) for human GPR35 (Jenkins et al., 2011; Milligan, 2011), and CXCL17 does not act as GPR35 agonist in some experimental system (Park et al., 2018).

A number of synthetic surrogate ligands for GPR35 have been proposed. One of the earliest and most useful GPR35 ligands is the cGMP phosphodiesterase inhibitor zaprinast (2-(2-propyloxyphenyl)-8-azapurin-6-one) (Taniguchi et al., 2006). Despite its wide application as reference GPR35 agonist (with reported potency between 2-8 μ M at the human ortholog), zaprinast, similarly to kynurenic acid and many other synthetic agonists, display a marked animal (human vs rodent) species selectivity (Mackenzie et al., 2014; Jenkins et al. 2010, Jenkins et al. 2012).

GPR35 is mainly expressed in colon, spleen and immune cells (e.g. macrophages and dendritic cells) in both humans and mice (Maravillas-Montero et al. 2015; Divorcy et al. 2015; Taniguchi et al., 2006; Wang et al., 2006). In the rat, high expression of GPR35 has been found in spleen, colon, dorsal root ganglion, and uterus (Taniguchi et al., 2006; Ohshiro et al., 2008).

It has been reported that GPR35 plays a role in a wide range of human diseases, but the signaling pathways have been not elucidated (Sun 2008, Okumura et al., 2004). In terms of classical GPCR signaling, GPR35 appears to couple to various G α subunits depending on the cell type and/or background animal species (Divoraty et al. 2015).

1.2 GPR35: evidence supporting its involvement in cancer

A genome-wide association study (GWAS) identified a single-nucleotide polymorphism (SNP) of GPR35 as novel risk locus for ulcerative colitis (UC) and primary sclerosing cholangitis (PSC) (Ellinghaus et al. 2013). The GPR35 rs3749171 SNP, leading to a threonine to methionine shift at Thr3.44, is located in the third transmembrane helix of the receptor (Ellinghaus et al. 2013). The third intracellular domain with its DRY motif is crucial for keeping the receptor in its inactive state. Only after ligand binding GPCRs change their structure so that the DRY motif allows the activation of downstream signaling. Remarkably, patients with UC and PSC have a higher risk to develop cancer (Krugliak Cleveland et al. 2017, Karlsen et al. 2017, Ullman and Itzkowitz, 2011).

GPR35 is highly expressed in human gastric cancer cells (Okumura et al., 2004). Moreover, GPR35 was identified as a potential receptor for CXCL17, a mucosal chemokine that promotes tumour growth and angiogenesis (Maravillas-Montero et al. 2015, Weinstein et al. 2006). Thus, CXCL17 levels are significantly increased in primary colonic cancers and clinical analyses suggest that CXCL17 could be an important biomarker of CRC poor prognosis (Ohlsson et al. 2016). Recently, it has been proposed a clinical significance of the CXCL17-CXCR8 (GPR35) axis in breast cancer, but the mechanistic basis of this effect remains poorly understood (Guo et al., 2017).

Recently, a significant increase of GPR35 expression, correlating with poor prognosis, has been reported in non-small-cell lung cancer (NSCLC) tissues (Wang et al., 2018). Notably, GPR35 was upregulated in chemoresistance cell model of NSCLC, and GPR35-mediated chemoresistance occurred partially via β -arrestin-2/Akt signalling (Wang et al., 2018).

Despite these findings, GPR35 function as tumour suppressor or inducer in cancers is still uncertain and may be related to cancer/cell types and/or specific microenvironment of the tumour.

1.3 Glucose metabolism in cancer

Cancer cells metabolize glucose in a different manner compared to normal cells (Warburg, 1956). Glucose metabolism and glycolysis is accelerated in cancer cells by preferential expression of transporters and enzyme isoforms that drive glucose flux. While in normoxia, healthy cells use the degradation of glucose to pyruvate and later the TCA (tricarboxylic acid) cycle to produce ATP, neoplastic cells prefer to use glycolysis to produce energy rather than oxidative phosphorylation (Warburg, 1956) (Figure 11). Indeed, tumour cells switch metabolism with high lactate production, even in aerobic conditions, and mitochondrial metabolism suppression. This metabolic adaptation is

called “aerobic glycolysis” or the “Warburg effect” (Warburg, 1956) (Figure 11). In solid tumours, the hypoxic environment supports glycolytic metabolism and provides resistance to therapy as well as an optimal niche for the maintenance of cancer stem cells (Trèdan et al., 2007; Persano et al., 2011; Fidoamore et al., 2016). Several genes (*e.g.* oncogenes) involved in the glycolytic pathway regulate the adjustment of cancer cells to the metabolic switch, suggesting them as possible target in cancer therapy.

Activation of macrophages or dendritic cells with a range of stimuli, including LPS (Krawczyk et al., 2010), the TLR3 ligand poly(I:C) (Pantel et al., 2014) and type I interferon (IFN) (Pantel et al., 2014), induces a metabolic switch from OXPHOS to glycolysis, in a phenomenon similar to the Warburg effect (Pantel et al., 2014; Kelly and O’Neill, 2015) (Figure 12). Recent immunometabolism studies have shown that alterations in the metabolic profile of macrophages shape their activation state and function (Kelly and O’Neill, 2015). Thus, metabolic reprogramming of macrophages could become a therapeutic approach to treat diseases, such as cancer, with a high macrophage involvement (Geeraerts et al., 2017).

Here, we took advantage of macrophages in order to investigate the metabolic role of GPR35 and the possible impact on experimental models of colorectal cancer.

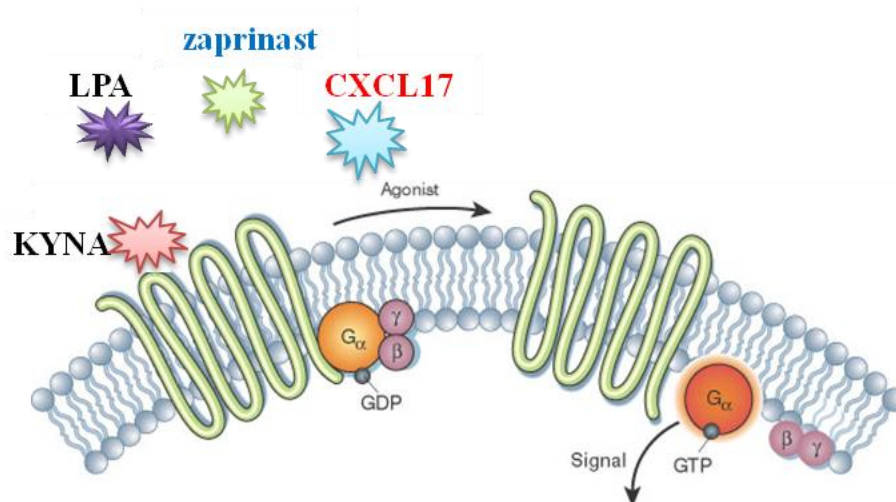
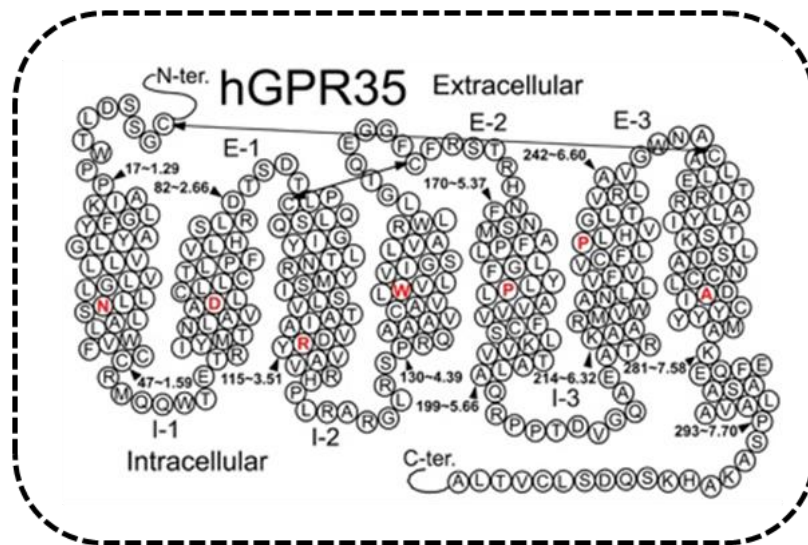


Figure 10. Helix net representation of human GPR35 receptor structure (from Shore and Reggio, 2015) and **simplified activation of GPR35 by endogenous or synthetic ligands.**

The most highly conserved residue in each transmembrane helix (among Class A GPCRs) is shown in red. Possible disulfide bridges are indicated by double-headed arrows.

Tryptophan metabolite kynurenic acid (KYNA), 2-oleoyl lysophosphatidic acid (LPA),

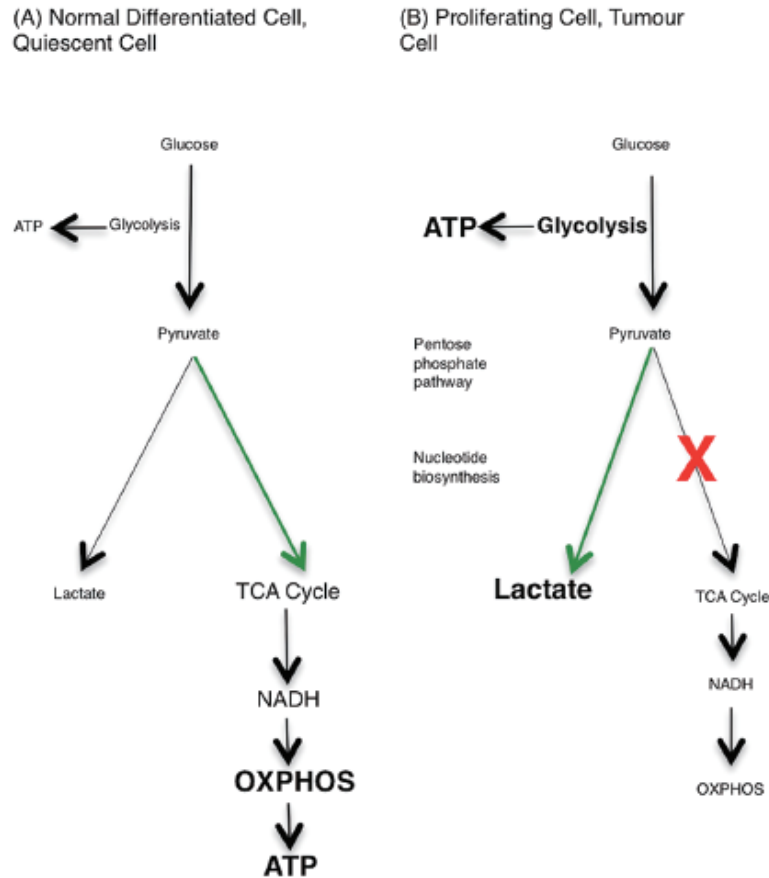
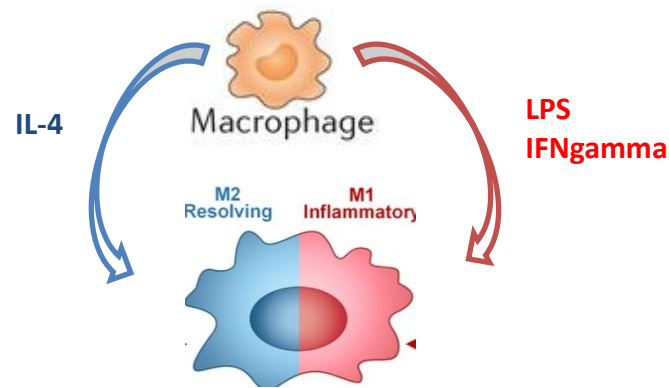


Figure 11. The Warburg effect (from Kelly and O'Neill, 2015)

(A) In resting cells, glucose is metabolized to pyruvate via glycolysis. Some pyruvate is converted to lactate, but most is directed to the TCA cycle via acetyl-CoA. The TCA cycle generates NADH, which donates electrons to the mitochondrial electron transport chain so that OXPHOS can progress.

(B) In highly proliferative or tumour cells, the metabolic profile switches from OXPHOS to aerobic glycolysis, known as the Warburg effect. Mature innate immune cells also rely on glycolysis, although they do not proliferate after activation. The majority of the pyruvate generated by glycolysis is converted to lactate, and glycolytic intermediates build up, meeting the high energy demand of the cell. Glycolysis is the source of ATP in these cells, and also provides glucose-6-phosphate for nucleotide biosynthesis in the PPP.



- Th2 responses
- Tissue remodelling
- Angiogenesis and tumour progression
- Th1 responses
- Pro-inflammatory
- Antitumour immunity

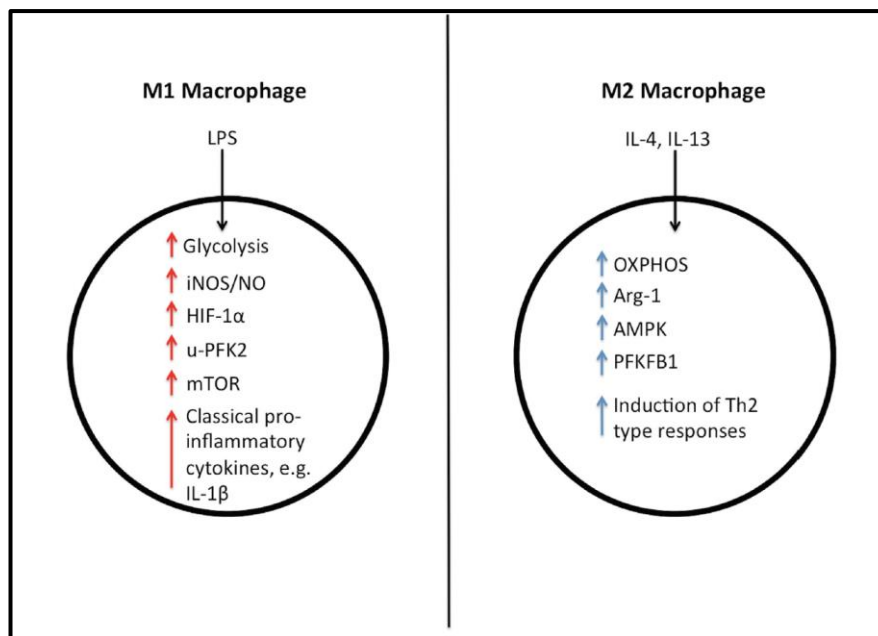


Figure 12. Physiological and metabolic differences between M1 and M2 phenotypes of macrophages (Adapted from Kelly and O'Neill, 2015)

M1 macrophages (pro-inflammatory phenotype) rely on glycolysis for ATP production and have increased levels of iNOS, HIF-1 α and u-PFK2, while M2 macrophages (pro-resolving phenotype) are fueled by OXPHOS and have increased levels of Arg-1, AMPK and PFKFB1. M1 macrophages release pro-inflammatory cytokines such as IL-1 β , while M2 macrophages are involved in the response to parasite infection, as well as in wound healing, and they release the anti-inflammatory cytokine IL-10. In fact, it is thought that a spectrum of macrophage activation exists, with different populations of macrophages exhibiting different inflammatory and metabolic phenotypes.

AIM

The general aim of this work is to investigate the possible role of three specific targets, namely two enzymes [i.e. monoacylglycerol lipase (MAGL) and N-acylethanolamine acid amide hydrolase (NAAA)] and the G protein-coupled receptor (GPR) 35 in colorectal cancer (CRC).

To adequately pursue our objective, both pharmacological and genetic blockade of MAGL, NAAA and GPR35 were exploited in well-established models of sporadic colon cancer (i.e. AOM-induced preneoplastic lesions, polyps and tumours and *APC^{min}* mice), in a model of colitis associated to cancer (tumours induced by the AOM/DSS combination) and in xenograft CRC tumours.

More in depth studies were performed in colorectal cancer cell lines (in order to evaluate proliferation and migration), in endothelial cells (to evaluate the angiogenic process) and in bone marrow-derived macrophages (to evaluate the impact on metabolic profile).

Finally, we have measured the expression of these targets in human colonic biopsies of CRC patients, which is of obvious translational value.

In few words, the ultimate goal of my PhD thesis is to provide potential innovative therapeutic targets for CRC.

MATERIALS AND METHODS

1.1 Patients

Human studies were approved by Ethical Committee of the University of Naples Federico II, Department of Medicine (protocol number 245_2015). Patients with a well-established diagnosis of colorectal cancer (CRC, stage II-IV) were included. Human colon samples were obtained by surgical colorectal resection. Healthy tissues, obtained from the peritumoral or distal resection margins of tumour, were used as control. All patients provided written informed consent.

1.2 Mice

All procedures performed in studies involving animals were carried out in accordance with the Italian D.L. no. 116 of 27 January 1992 and associated guidelines in the European Communities Council Directive of 24 November 1986 (86/609/ECC and 2010/63/UE). Experiments were conducted in UK with the approval of the UK home office and in Italy with the approval of the Institutional Animal Ethics Committee for the use of experimental animals. Male ICR mice (weighting 25–30 g) and athymic nude female (4-weeks old) mice were purchased from Harlan Italy (S. Pietro al Natisone, UD, Italy) and fed *ad libitum* with standard food (Mucedola srl, Settimo Milanese, Italy). MAGL knock-out (*Mgll^{-/-}*) mice were a kind gift of R. Zechner and R. Zimmermann, University of Graz, Austria. GPR35 knock-out (*Gpr35^{-/-}*) mice were obtained from the KOMP repository and the intestinal epithelia-specific GPR35 were generated by outbreeding the FlpO and then crossing into mice carrying *Villin-Cre*. Ear-biopsy genomic DNA was used for routine genotyping of all mice. GPR35 mice were bred and maintained in specific pathogen-free conditions at the Central Biomedical Services (CBS) facility, University of Cambridge. Athymic female mice, fed *ad libitum* with sterile mouse food, were maintained under pathogen-free conditions at the Department of Pharmacy, University of Naples Federico II. All mice were used after 1 week-acclimation period (temperature 23±2 °C; humidity 60%, free access to water and food).

1.3 Drugs

Azoxymethane (AOM) was purchased from Sigma (Milan, Italy). URB602 and Matrigel™ were obtained from Cayman Chemical (Cabru SAS, Arcore, Italy) and BD Biosciences (Buccinasco, Milan, Italy), respectively. DSS was obtained from MP Biomedicals (Canada). PEA was a kind gift from Epitech Group. AM9053 was synthesized in the laboratory of A. Makriyannis and M. Malamas. All reagents for cell cultures were obtained from Sigma, Bio-Rad Laboratories (Milan, Italy) and Microtech Srl (Naples, Italy). The vehicles used for *in vivo* (10% ethanol, 10% Tween-

20, 80% saline, 2 ml/kg) and *in vitro* (0.1% DMSO or 0.1% ethanol) experiments had no effect on the responses under study.

1.4 Cell culture

1.4.1 Colorectal cancer cell lines

For *in vitro* experiments, two human colon adenocarcinoma cell lines (i.e. Caco-2 and HCT116, ATCC from LGC Standards, Milan, Italy), with a different genetic profile (APC gene and p53 mutated in Caco-2 cells, K-RAS mutated in HCT116 cells) have been used (Ahmed et al. 2013). These cell lines were cultured in Dulbecco's modified Eagle's medium (DMEM) containing 10% fetal bovine serum (FBS), 100 U/ml penicillin and 100 µg/ml streptomycin, 1% non-essential amino acids, 2 mM L-glutamine and 1 M HEPES, in conformity with the manufacturer's protocols. Cell viability was evaluated by trypan blue exclusion.

1.4.2 Healthy colonic epithelial cells (HCEC)

The immortalized healthy human colonic epithelial cells (HCEC), derived from human colon biopsies, have been used as a comparison with tumoural cells. HCEC were a kind gift of Fondazione Callerio Onlus (Trieste, Italy). HCEC were cultured in Dulbecco's modified Eagle's medium (DMEM) supplemented with 10% FBS, 100 Units/ml penicillin, 100 µg/ml streptomycin, 200 mM L-Glutamine, 100 mM Na-pyruvate and 1 M HEPES. Cell viability was evaluated by trypan blue exclusion.

1.4.3 Endothelial cell lines

The human umbilical vein endothelial cell line (HUVEC, Promocell, Heidelberg, Germany) and immortalized murine endothelial cells (SVEC4-10, ATCC from LGC Standards, UK) were used. Cells were routinely maintained in 75 cm² polystyrene flasks, at 37 °C in a 5% CO₂ atmosphere, in Dulbecco's modified Eagle's medium (DMEM) for SVEC4-10 or in endothelial growth medium (EGM-2) for HUVEC. DMEM was supplemented with 10% foetal bovine serum (FBS), 100 U/ml penicillin, 100 µg/ml streptomycin, 1% non-essential amino acids and 2 mM L-glutamine. EGM-2, containing VEGF, R3-IGF-1, hEGF, hFGF, hydrocortisone, ascorbic acid, heparin and GA-1000 (Clonetics, Cambrex Bio Science Walkersville, USA) was supplemented with 10% FBS.

1.5 Primary cells isolation and culture

1.5.1 Murine bone marrow-derived macrophages (BMDM)

Bone marrow was flushed out of the murine femur and tibia with macrophages culture medium (RPMI 1640, supplemented with 1 mM HEPES pH 7.4, 50 U/ml PenStrep and 10 % FBS). Cells were then filtered through 70 µm cell strainer and incubated for 6 days in culture medium supplemented with 100 ng/ml (h)M-CSF in plates. After harvesting and seeding, BMDM were

polarized for 16 h toward M1 or M2 phenotype with LPS (20 ng/ml) plus IFN γ (50 ng/ml) or IL-4 (20 ng/ml), respectively.

1.5.2 Isolation of Intestinal Crypts and 3D Organoid Culture

The small and large intestine was flushed with cold PBS, cut longitudinally and into 5 mm pieces. To dissociate the crypts, pieces were placed in 25mM EDTA/PBS for 1h at 4°C and suspended in PBS. Isolated crypts were washed, counted and pelleted. A total of 200 crypts were mixed with 40 μ l of Matrigel and plated in 24-well plates (Sato et al. 2009). After polymerization of Matrigel, 500 μ l of IntestiCult Organoid Growth Medium (Stem Cell) containing Wnt-3a (50 ng) was added. Medium was changed every 3 days. For passage, organoids were removed from Matrigel and mechanically dissociated into single-crypt domains, and then transferred to fresh Matrigel. Passage was performed once per week with a 1:2 split *ratio*.

1.6 In vivo models of colorectal cancer

1.6.1 AOM DSS model of colitis associated to cancer (CAC)

6-8-week-old wild type and *Gpr35*^{-/-} mice were injected i.p. with azoxymethane (12.5 mg/kg, AOM). Colitis was induced by two cycles of 2.5% dextran sodium sulfate (DSS) in drinking water for 5 days, followed by a 16 day tap water period (Greten et al., 2004). The final DSS cycle (2%) was administered for 4 days, followed by a 10 day tap water period. The size and number of colonic tumours were evaluated at day 61 microscopically in longitudinally cut and formalin fixed specimen. The typical features of the AOM DSS model are depicted in Table 3.

1.6.2 AOM model of colorectal cancer

AOM (40 mg/kg in total, i.p.) was administered in mice at the single dose of 10 mg/kg at the beginning of the first, second, third and fourth week. The drugs were given i.p. three times a week starting one week before the first administration of AOM. All animals were euthanized by asphyxiation with CO₂ three months after the first injection of AOM. Based on our laboratory experience, this time (at the used dose of AOM) was associated with the occurrence of a significant number of aberrant crypt foci (ACF, which are considered pre-neoplastic lesions), polyps and tumours (Izzo et al. 2008) (see table 3 for the AOM model features).

For ACF, polyps and tumours determination, the colons were rapidly removed after sacrifice, washed with saline, opened longitudinally, laid flat on a polystyrene board and fixed with 10% buffered formaldehyde solution before staining with 0.2% methylene blue in saline. Colons were examined using a light microscope at 20X magnification (Leica Microsystems, Milan Italy). The detection and quantization of ACF, polyps and tumours on the colon were performed as previously reported (Izzo et al., 2008). Briefly, in comparison to normal crypts, aberrant crypts have greater size, larger and often elongated openings, thicker lining of epithelial cells, compression of adjacent

crypts, and are more darkly stained with methylene blue. The criterion to distinguish polyps from tumours was established considering the main characteristic features of these two lesions (i.e. crypt distortion around a central focus and increased distance from luminal to basal surface of cells for polyps and high grade of dysplasia with complete loss of crypt morphology for tumours) (Izzo et al., 2008).

URB602 (MAGL inhibitor), AM630 (NAAA inhibitor) and PEA were intraperitoneally administrated at doses of 5 mg/kg, 20 mg/kg and 10 mg/kg, respectively.

In some experiments, MAGL-ko mice were used. In this set of experiments, AOM (40 mg/kg in total, i.p.) was administered at increasing doses (four doses of 1, 2, 3 and 4 mg/kg in a week) during the first, second, third and fourth week. This protocol of administration was selected on the basis of preliminary experiments, in which MAGL-deficient mice were found to be more sensitive the AOM action.

1.6.3 APC^{min} model of sporadic colon cancer

APC^{min} mice were obtained from the Jackson Laboratory and crossed with mice lacking *gpr35* globally or conditionally in their intestinal epithelial cells. At the age of 15 weeks mice were sacrificed and after flushing with PBS the intestine was longitudinally cut, formalin fixed and tumours count was assessed microscopically. Samples were embedded as swiss rolls in paraffin for further analysis. APC^{min} model of sporadic colon cancer main characteristics are reported in table 3.

1.6.4 Xenograft model of colon cancer

The effect of URB602 (a MAGL inhibitor) was evaluated on tumour formation induced by subcutaneous injection of HCT116 cells (2.5×10^6) into the right flank of athymic female mice for a total volume of 200 μ l [50% cell suspension in phosphate buffer solution (PBS) and 50% MatrigelTM] (see table 3 for xenograft tumour features). Ten days after inoculation (once tumours had reached a size of 250-300 mm³), mice were randomly assigned to control and treated groups, and treatments were initiated. Tumour size was measured every day by digital caliper, and tumour volume was calculated according to the modified formula for ellipsoid volume (volume = $\pi/6 \times$ length \times width²). Mice were euthanized when the endpoint tumour volume was of 2000 mm³. The MAGL inhibitor URB602, at the dose of 5 mg/kg, was given intraperitoneally (i.p.) every day for all the duration of the experiment. URB602 dose was selected on the basis of previous published work which showed selective inhibitory effects of URB602 on MAGL enzyme without psychoactive effects (Comelli et al. 2007). Xenograft tumour tissue as well as healthy tissue (derived from contralateral paw of the inoculated mice) were collected and analyzed after 8 days of treatment.

The effect of AM9053 (a NAAA inhibitor) and PEA were evaluated on tumour formation induced by subcutaneous injection of HCT116 cells (2.5×10^6) into the back of athymic female mice for a total volume of 200 μL of PBS. The NAAA inhibitor AM9053 at the dose of 20 mg/kg was given peritumorally three times per week for all the duration of the experiment. Tumour size was measured three times per week by digital caliper, and tumour volume was calculated as reported above. AM9053 dose was selected on the basis of previous published work in which AM9053 selectively inhibits NAAA during the experimental colitis (Alhouayek et al. 2015).

1.6.4.1 Xenograft tumour secretome preparation

Nude mice were sacrificed 21 days post-injection, untreated tumours excised and cultured in DMEM (without foetal bovine serum) for 24 h. The conditioned medium was collected and added to Caco-2 cells for 24h at 37°C. Then, the Caco-2 cells were washed in PBS and homogenized in 1.0 mL of TRIzol for further analyses.

1.7 Cell viability (neutral red assay)

Cell viability was evaluated by measuring the neutral red uptake (NR assay). Cells were seeded in presence of 10% FBS in 96-well plates at a density of 1×10^4 cells per well (Caco-2, HCT116 and HCEC cells and allowed to adhere for 24 h). After this period, the human colonic cells were incubated with medium containing 10% FBS in presence or absence of increased concentrations of AM9053 (0.01–10 μM) and PEA (0.1–30 μM) for 24 h. Subsequently, cells were incubated with NR dye solution (50 $\mu\text{g}/\text{ml}$ in 10% FBS) for 3 h at 37°C and then lysed with 1% acetic acid. The absorbance was read at 532 nm (iMark™ microplate reader, Bio-Rad). All results are expressed as percentage of cell viability ($n = 3$ experiments including 8–10 replicates for each treatment).

1.8 Proliferation assays

1.8.1 BrdU incorporation in colonic epithelial cells

HCT 116, Caco-2 and HCEC were seeded in 96-well plates (1.0×10^4 cells per well), allowed to adhere (within 24h) and starved by serum deprivation for 24h. Cells were then treated with NAAA-inhibitor AM9053 (0.1–3 μM) and PEA (1–30 μM). After 24 hours of treatment, cells were incubated with BrdU (10 μM) in the cell medium for 2 hours. Thereafter, the proliferation of the cells was determined by using the BrdU proliferation ELISA kit (Roche, Milan, Italy) according to the manufacturer's instructions. All results are expressed as percentage of cell proliferation ($n = 3$ experiments including 8–10 replicates for each treatment).

1.8.2 EdU incorporation in colonic organoids

For EdU incorporation, 40 μl of the matrigel containing colonic organoids was seeded in 8-well chamber-slide. 10 μM EdU was added to the wells 6 h prior to fixation. The proliferation marked by

EdU incorporation was detected with Click-iT Edu Imaging Kits (Invitrogen) in according to the supplier's instructions.

1.8.3 Proliferation assay in HUVEC

For proliferation assay, HUVEC were seeded in 96-well plates at a density of 1×10^3 cells per well and after adherence (3-4 h) they were serum starved for 12 hours. Cells under basal condition [0.1% fetal calf serum (FCS)] or stimulated for 24 h with either 1% FCS or FGF-2 (20 ng/ml) were treated with URB602 (0.1 and 1 μ M). Cells were then fixed, stained and randomly counted at 20 x magnification (Donnini et al. 2006). Data are expressed as counted cells/well.

1.9 Migration assay

1.9.1 Scratch assay in human colon adenocarcinoma cell lines

The migration “wound healing” scratch assay was performed as previously described by Liang and colleagues (Liang et al., 2007). Sub-confluent adenocarcinoma cell line, i.e. HCT116 and Caco-2, were trypsinized and plated into culture-insert two wells (ibidi GmbH, Munich, Germany) inserted on a 24-well plate (condition: 5×10^4 cells suspended in 70 μ l per well of the insert) and leaved to adhere overnight. After this time, the insert was removed, cells were washed with phosphate buffer saline (PBS 1X) and treated with mitomycin C 30 μ g/ml (Sigma-Aldrich, Milan, Italy) in serum-free media, in order to completely inhibit cell proliferation. After 2 hours, HCT116 and Caco-2 cells were treated with the NAAA-inhibitor, AM9053 (3 μ M) or PEA (30 μ M) for 24 hours. Wound area recovery was observed under a phase-contrast microscope (iRiS Digital Imaging System, Twin Helix, Rho, Italy) and photographed at the time zero point (right after the mitomycin C removal) and after the 24-hour-treatment. Successively, by using the ImageJ software, the size of the opened area was measured from the digital images. The results are expressed as % of scratch closure (time zero/time 24h*100). Two imagines were acquired for each well and at least 3 replicates were analyzed for each treatment. Three independent experiments were independently carried out.

1.9.2 Scratch assay in HUVEC

HUVEC were seeded into 24-well plates (1×10^5 cells/well) and incubated for 24 h to confluence. Then, the monolayer was scraped using a sterile micropipette tip to create a wound of ± 1 mm width. Cells were washed twice with PBS, and fresh medium containing URB602 (0,1-1 μ M) was added with ARA-C (2.5 μ g/ml) to inhibit cell proliferation. Images of the wound in each well were acquired from 0 to 8 h under a phase contrast microscope at 20 x magnification. After 8 h cells were stained with Hoechst 33342 and image acquisition and analysis were performed by a Nikon digital camera DS-5MC and NIS Element software, using a Nikon Eclipse TE 300 inverted microscope (Nikon, Tokyo, Japan). Results are expressed as percentage of area of wound (Monti et al. 2010).

1.10 Angiogenesis analysis

1.10.1 Tube formation assay

SVEC4-10 cells were stained with calcein AM for 30 min at 37°C. After counting, SVEC4-10 cells were seeded (7×10^4 cells/well) on growth factor-reduced matrix (Geltrex) -coated 24-well plates and were cultured for 6h with conditioned medium of M2-polarized macrophages. Pictures of tube formation were acquired at confocal microscope and Angiogenesis Analyzer for ImageJ was used for quantification of tube networks.

1.10.2 CXCL1/KC detection

CXCL1/GRO alpha, also known as KC in mouse and CINC-1 in rat, is a member of the CXC family of chemokines. KC was detected in macrophages supernatants by using Quantikine Mouse KC Immunoassay ELISA (R&D system).

1.10.3 Aortic ring assay

Murine thoracic aortas were collected from mice lacking GPR35 or their wildtype littermates. After flushing and removing the connective tissue, aortas were cut into 0,5-1 mm long rings and serum-starved overnight at 37 °C and 5% CO₂ in Opti-MEM. Then the aortic rings were individually embedded in rat type I collagen (Millipore, MA, USA), feed with Opti-MEM supplemented with 2.5% FBS and 30ng/mL VEGF. The aortic rings from GPR35^{+/+} and GPR35^{-/-} mice were treated with vehicle or CXCL17 (0.2mg/mL). The growth medium was changed on days 3, 6 and 8. On day 8 the number of microvessels sprouting was counted using the microscope (Baker et al., 2011).

1.10.4 Quantification of angiogenesis modulators in HUVEC by ELISA

FGF-2 and endostatin levels were measured in conditioned media by ELISA kits (R&D System, Minneapolis, MN, USA). HUVEC were exposed to URB602 (1 μM, 18 h) in 0.1% or 1% FCS. Cell culture supernatants were collected, stored at -80°C and analysed following manufacturer instructions. Data are reported as pg/mL (FGF-2) or ng/mL (endostatin) (means ± SEM). Experiments were run in triplicate.

1.11 Evaluation of metabolic profile

1.11.1 Glucose uptake

BMDM were seeded (5×10^4 cells/well) in white 96-well plates, polarized for 16h as described above or used as M0 macrophages. We used a luminescence-based glucose uptake assay (Glucose Uptake Glo, Promega, USA). Cells were washed once with PBS and then incubated with PBS containing 1 mM 2-deoxy-D-glucose (2-DG) for 60 min. The reaction was stopped at different time points and the detection reagent for 2-deoxy-D-glucose-6-phosphate (2DG6P) was added. Luminescence was measured thereafter. We used a standard curve of 2DG6P to extrapolate the concentration of 2DG6P in the sample and calculate the rate of glucose uptake over time per cell.

1.11.2 Seahorse extracellular flux analysis

BMDM were seeded (7.5×10^4 cells/well) in 96-well XFe Seahorse plates, differentiated for 16 h as described above or left undifferentiated. 1 hour prior to the start of extracellular flux measurements, the medium was changed to Agilent Seahorse XF Base Medium supplemented with 1 mM L-glutamine and 10 mM D-glucose. Medium pH was set to 7.4 after warming to 37 °C. Oxygen consumption rate (OCR) was measured using the XFe96 Seahorse extracellular flux analyser (Agilent, USA) over the course of 2 hours. Oligomycin (1 μ M), FCCP (1.5 μ M) and Rotenone/Antimycin A (both 1 μ M) were injected sequentially to allow assessment of respiratory chain functionality. Glycolysis was assessed through measurement of extracellular acidification rate (ECAR) after sequential injections with D-glucose (10 mM), Oligomycin (1 μ M) and 2-deoxyglucose (100 mM).

1.11.3 Lactate measurements

BMDM were seeded (5×10^4 cells/well) in dialyzed medium in 96-well plate, differentiated for 16h as described above. Lactate concentration was measured in 5 μ L of media collected at experimental time points (12, 24 and 48h) using a luminescence based assay (Lactate Glo, Promega) in according to the supplier's recommendations. Plates were mixed briefly and incubated for 1h at 37°C before reading luminescence. Lactate concentration was determined by comparison to a lactate standard curve.

1.12 BrdU incorporation and quantification

BrdU at dose of 2.5 mg/kg was injected i.p 24 h before euthanizing mice. Paraffin embedded samples were then de-paraffinised in xylene and de-hydrated with ethanol. Cells positive for BrdU were detected using a BrdU staining kit (BD). Proliferation was revealed as BrdU+ cells along the crypt-villus.

1.13 Identification and quantification of endocannabinoids, PEA and related molecules

Endocannabinoids [anandamide (AEA) and 2-arachidonoylglycerol (2-AG)], palmitoylethanolamide (PEA) and oleoylethanolamide (OEA) levels were measured in tumour and healthy tissues of xenografted mouse as well as in HCT116 cells (used for inoculation) by isotope dilution liquid chromatography-atmospheric pressure-chemical ionization mass spectrometry as previously described (Di Marzo et al., 2008). Briefly, collected samples were immediately immersed into liquid nitrogen and stored at -80°C until extraction of endocannabinoids (AEA and 2-AG), PEA and OEA. Samples were extracted with chloroform/methanol (2:1, by volume) containing each 5 pmol of d8-anandamide, d4-PEA, d4-OEA and d5-2-AG, synthesized as described previously (for the former two compounds) or provided by Cayman Chemicals (for d5-2-AG, AnnArbor, MI). The lipid extracts were purified by silica column chromatography and the

fractions containing anandamide, PEA, and 2-AG were analyzed by isotope dilution liquid chromatography–atmospheric pressure–chemical ionization mass spectrometry. Results were expressed as picomoles per milligram of lipid extract.

1.14 Immunohistochemistry

The animals were deeply anesthetized with pentobarbital (100 mg/kg) and then perfused transcardially with 0.9% saline solution for 5 min, followed by 100ml of fixative containing 4% paraformaldehyde (wt/vol)/0.1M phosphate buffer (pH 7.4). After fixation tumour slices were cut with a Leica CM3050S cryostat in serial frozen sections (10 µm-thick) and processed for immunofluorescence. Immunohistochemical study of MAGL expression in tumour slices collected from xenografted mice was performed by incubation of sections with goat anti-MAGL (1:200, Abcam, Milan, Italy) revealed by specific Alexa-594 secondary donkey anti-IgGs antibody (Invitrogen Life Technology, Paisley, UK) and counterstained with 40 ,6-diamidino-2-phenylindole. Immunoreactivity for MAGL was analyzed by DMI6000 microscope equipped with appropriate filters and deconvolution software MetaMorph LAS AF 2.2.0 software (Leica, Germany).

1.15 Immunostaining for CD31

Collected xenograft tumours were immediately embedded in Tissue-Tek O.C.T. (Sakura, San Marcos, CA), cooled in isopentane and frozen in liquid nitrogen for immunostaining and histological analysis. Seven µm-thick cryostat sections from a xenograft tumour were stained with hematoxylin and eosin and adjacent sections were used for immunohistochemical staining with anti CD31 (Chemicon, Millipore, Milan, Italy) antibody. For immunohistochemistry, cryostat sections were firstly fixed in acetone at -20°C and incubated for 10 min in 3% H₂O₂, washed (3 x 5 min) in Tris-buffered saline (TBS) and then incubated in a Blocking reagent (KIT Immunoperoxidase Secondary Detection System, Chemicon, Millipore, Milan, Italy). Mouse monoclonal anti-CD31 antibody diluted 1:100 in TBS, 0.05% bovine serum albumin (BSA) was applied. Negative controls were produced by eliminating the primary antibodies from the diluents. Sections were then washed (3 x 5 min in TBS) and incubated for 10 min in the appropriate species–specific biotinylated secondary antibodies (goat anti mouse IgG, KIT Immunoperoxidase Secondary Detection System, Chemicon). Following washings (3 x 5 min in TBS), the sections were incubated for 10 min in streptavidin-conjugated HRP and then exposed to 3,3-diaminobenzidine tetrahydrochloride (DAB, detection kit, Millipore, Milan, Italy) for 8 min to produce a brown reaction product. Finally, sections were counterstained in hematoxylin and mounted in Aquatex (Merck, Milan, Italy) (Finetti et al. 2012).

For CD31 immunofluorescence labelling, sections were fixed in acetone, and aspecific binding sites were blocked by using 3% BSA. Slides were incubated with a rat anti-mouse CD31 antibody (Millipore, Billerica, USA). Immunoreactions were revealed by using FITC anti-rat secondary antibodies. Images were analyzed using Nikon Eclipse T200, and quantification of human CD31 and vessel lumina were performed counting 10 random field/section for slides.

1.16 Gene expression analysis by quantitative Real-Time (q)-PCR

Healthy tissues and tumours collected from both xenografted mice as well as from patients were immediately immersed into RNA Later and stored at -80°C until RT-PCR analysis.

RNA from macrophages was isolated using the RNeasy Mini kit (QIAGEN). RNA was then reverse transcribed with M-MLV RT (Invitrogen), and SYBR-Green (Eurogentec) qPCR was performed using MX-3000 (Agilent Technologies).

Tumours and colorectal cancer cells were homogenized in 1.0 mL of TRIzol (Invitrogen) following the manufacturer's instructions. Total RNA from murine and human tissues was purified, quantified, characterized and retrotranscribed as previously described (Iannotti et al., 2010). Final preparation of RNA was considered DNA- and protein-free if the integrity number (Bionalyzer 2100, Agilent) was greater than 8 relative to a 0–10 scale. Quantitative real-time PCR was carried out in a iCycleriQ5 system (Biorad, MI, Italy) by use of SYBR Green detection. Selective primers were designed using Allele-Id software version 7.0 (Biosoft International, Palo Alto, CA, USA) and synthesized by MWG-Biotech (HPLC purification grade) (see Table 4). Each sample was amplified simultaneously in a quadruplicate in one-assay run (maximum DCt of replicate samples <0.5), and a standard curve from consecutive fivefold dilutions (100–0.16 ng) of a cDNA pool representative of all samples was included for PCR efficiency determination. Data normalization was performed by using as a control the ct from S16 and/or HPRT, both constitutively expressed proteins; differences in mRNA content between groups were calculated as normalized values by use of the $2^{-\Delta\Delta\text{ct}}$ formula (Iannotti et al., 2010).

1.17 Western blot analysis

The expression of vascular endothelial growth factor (VEGF), fibroblast growth factor-2 (FGF-2) and endostatin was assessed in xenograft tumour tissue of animals treated or not with URB602, the MAGL inhibitor. Samples were fragmented in liquid nitrogen, lysed in Cell Lytic buffer (Invitrogen) and centrifuged at 14000 rpm for 15 min. Supernatant was collected and protein concentration was determined by Bio-Rad Protein Assay (Bio-Rad); lysate aliquots containing 50 μg of proteins were separated by SDS-PAGE (4–12% PA, NuPAGE, Invitrogen) and transferred to a nitrocellulose membrane using iBlot2 (Life Technologies, Monza, Italia). After blocking in 5% w/v nonfat dry milk (1X PBS) buffer, membranes were incubated overnight with anti-FGF-2

(1:1000, Upstate), polyclonal anti-VEGF (1:1000, Millipore) or anti-endostatin (1:1000, Millipore); after washing, secondary antibody anti-mouse or anti-rabbit IgG (1:2500, Promega), linked to horseradish peroxidase, was added. The signal was visualized by enhanced chemiluminescence using Chemidoc XRS (Biorad) and analyzed using Quantity One Software version 4.6.3. The membranes were probed with anti- β -actin antibody (1:1000, Sigma) to normalize the results, which were expressed as ratio of densitometric analysis of each protein/ β -actin bands.

1.18 Statistical analysis

Data are expressed as the mean \pm SEM or SD of n experiments. To determine statistical significance, Student's t-test was used for comparing a single treatment mean with a control mean, and a one-way ANOVA followed by a Tukey multiple comparisons test was used for analysis of multiple treatment means. P-value < 0.05 was considered to be significant. G Power was used for sample size calculation.

TABLE 3 Mouse models of colorectal cancer

Model	Primary location	Invasiveness	Driver	Sporadic CRC vs CAC
<i>APC</i>^{+/-}	Small intestine	Adenomas	Mice are heterozygous for an <i>Apc</i> loss-of-function mutation Increased WNT- β -catenin signalling occurs following allelic loss of wild-type <i>Apc</i>	Sporadic CRC
<i>Xenografts</i>	Usually subcutaneous or orthotopic	Variable	Variable	NA
<i>DSS-AOM</i>	Colon	Aberrant crypt foci and adenomas	Intestinal barrier dysfunction and inflammation driven by the chemical irritant DSS, combined with AOM-induced mutagenesis	CAC
<i>AOM</i>	Colon	Aberrant crypt foci, polyps and adenomas	AOM-induced mutagenesis	Sporadic CRC

(adapted from West et al., 2015)

AOM, azoxymethane; APC, adenomatous polyposis coli protein; CAC, colitis-associated cancer; CRC, colorectal cancer; DSS, dextran sodium sulfate; NA, not applicable.

TABLE 4. Sequences of primers. List of genes screened by Quantitative Real-Time Polymerase Chain Reaction.

Targeted gene	FORWARD Sequence (5'→3')	REVERSE Sequence (5'→3')
Sequences for <i>Homo sapiens</i> primers		
<i>FAAH</i>	GGCGGAGTGCGACAGCGTAG	GCCACTCTTGCTGAGGCGGT
<i>PPAR-α</i>	TTCGCAATCCATCGGCGAG	CCACAGGATAAGTCACCGAGG
<i>TRPV1</i>	CCTGCGTCTAGCTGGTTGCACA	CTGGGACAGCAGCCTGGCAC
<i>CB1</i>	TCTGTTCATCGTGTATGC	CTTGGCTAACCTAATGTCC
<i>CB2</i>	TAGTGCTGAGAGGACCCA	CGCTATCCACCTTCCTACAA
<i>NAAA</i>	TTAAAGAATGGGCAGATT	CCTTTATCTCGTTCATCA
<i>GPR55</i>	GAAAACCCTACAGTTTGCAGTCC	GAGGTGGCAGCATAATCGGG
<i>MAGL</i>	GCCACGGACAGAGCGAAG	CCAGAAGGAAGACAGGAAGCC
<i>p27kip</i>	AACCGACGATTCTTCTACTCAA	CTTCTTGGGCGTCTGCTC
<i>VEGF</i>	CTTGCTCTTATTGTGA	TAGTATGTAGATGTATATTGAA
<i>Cyclin D1</i>	GACCTTCGTTGCCCTCTG	AGGCGGTAGTAGGACAGG
<i>β-actin</i>	AAATCGTGCGTGACATTAAG	ATGGAGTTGAAGGTAGTTTCG
<i>β-actin</i>	GGGGTACTTCAGGGTGAGGA	GATGCCCCCGGGCCGTCTT
<i>RNA POL</i>	ACGACTTTGATGATGTGG	GGAGGATCTCGACATTCT
<i>GAPDH</i>	GGAGCGAGATCCCTCCAAAAT	GGCTGTTGTCATACTTCTCATGG
<i>GPR35</i>	GCTCACCCCAGCTTCACTTC	TAGGTGCCATTCATGGTCTCTGC
Sequences for <i>Mus musculus</i> primers		
<i>FAAH</i>	ACTTGGACGTGGTGCTAACC	GCCTATACCCTTTTTCATGCC
<i>PPAR-α</i>	AGAGCCCCATCTGTCTCTC	ACTGGTAGTCTGCAAAACCAAA
<i>TRPV1</i>	CCACTGGTGTGAGACGCC	TCTGGGTCTTTGAACTCGCTG
<i>CB1</i>	GGGCACCTTCACGGTTCTG	GTGGAAGTCAACAAAGCTGTAGA
<i>CB2</i>	AGAAAGCCCTCGTACCTGTTC	ATGGTCACACTGCCGATCTTC
<i>NAAA</i>	CCAAGACTCCCCTCATTGC	CTCAACTCGGAACCACTCTC
<i>GPR55</i>	CTGGCAGTCCATATCCCAC	GCACCAGCAGTAAATCGAAAACA
<i>GPR35</i>	AAATCCCCACCTTTCAGCACA	CATGGTCCTAGGGCTCATCTG
<i>GLUT1</i>	TGGCGGGAGACGCATAGTTA	AACTCCTCAATAACCTTCTGGGG
<i>SGLT1</i>	ACGTGCACCTGTACCGTTTG	CCTTTATCCTGGTCCAGCCC
<i>SGLT2</i>	GTGTTGGCTTGTGGTCTATGT	TCCACTCAAATCCAGCCACC
<i>β-actin</i>	GCCCTGAGGCTCTTTTCCAG	TGCCACAGGATTCCATAACC

RESULTS

Chapter I. Pharmacological inhibition of MAGL reduces experimental colon tumorigenesis

Adapted from: Pagano et al., 2017 Pharmacol Res. 2017;119:227-236. doi: 10.1016/j.phrs.2017.02.002.

1.1 MAGL expression in human colorectal carcinoma (HCT 116) cells and xenograft tumour tissues

In order to elucidate the role of MAGL in colorectal tumorigenesis, we generated xenograft tumours by inoculating human colorectal cancer (HCT116) cells in athymic mice. Human MAGL mRNA was weakly expressed in HCT116 cells, but it displayed about 5-fold increase in the xenograft tumour tissue (Figure 13A). MAGL was undetectable in the mouse controlateral paw, used as negative control (data not shown). Immunostaining revealed high expression of MAGL protein in tumour tissues (Figure 13B), although the precise localization of the enzyme within the cell was not detectable.

1.2 The MAGL inhibitor URB602 reduces tumour growth in the xenograft model of colon cancer

We evaluated the potential antitumoral effect of the MAGL inhibitor URB602 by using a xenografted tumour model generated as described above. On day 10 after s.c. cells inoculation, all mice developed tumours, with a mean volume (\pm SEM) of 288 ± 37 mm³. Thereafter, mice were treated daily either with vehicle or URB602 (5 mg/kg, i.p.) until the sacrifice of the animals (i.e. after eight days). As shown in Figure 14, URB602 significantly reduced tumour growth compared to vehicle. Eight days after drug (or vehicle) administration, the average tumour volume in the control group was 1980 ± 269 mm³, whereas the average tumour volume in the URB602-treated group was 956 ± 180 , exhibiting a 52% of tumour growth inhibition (Figure 14).

1.3 Effect of URB602 (a MAGL inhibitor) on 2-AG levels in healthy and tumour tissues from xenografted mice

The levels of 2-AG found in tumour tissues of xenografted mice were higher than those detected in CRC (HCT116) cell line (Figure 15A, insert) and in healthy tissues derived from the contralateral paw of xenografted mice (Figure 15A). URB602, at the daily i.p. dose of 5 mg/kg, significantly increased, by approximately four-folds, the levels of 2-AG in healthy tissues, but it was not able to further increase the already elevated 2-AG levels in tumour tissues (Figure 15A).

In order to verify URB602 selectivity vs its target (i.e. MAGL), we measured the levels of anandamide and related acylethanolamides following URB602 treatment. The MAGL inhibitor did not significantly change anandamide levels in both healthy and tumour tissues (Figure 15B).

Similarly, levels of PEA and OEA, both in healthy (PEA pmol/mg: control: 105.6 ± 46.64 , URB602: 220.2 ± 120.1 ; OEA pmol/mg: control: 11.02 ± 3.86 , URB602: 23.12 ± 6.447 ; mean \pm S.E.M., n=5 mice for each experimental group) and in tumour (PEA pmol/mg: control: 121.1 ± 41.79 , URB602: 124.5 ± 44.19 ; OEA pmol/mg: control: 12.0 ± 1.597 , URB602: 9.50 ± 2.132 ; mean \pm S.E.M., n=5 mice for each experimental group) tissues, were unchanged. Collectively these results suggest the selectivity of URB602 for MAGL vs acylethanolamide-hydrolyzing amidases.

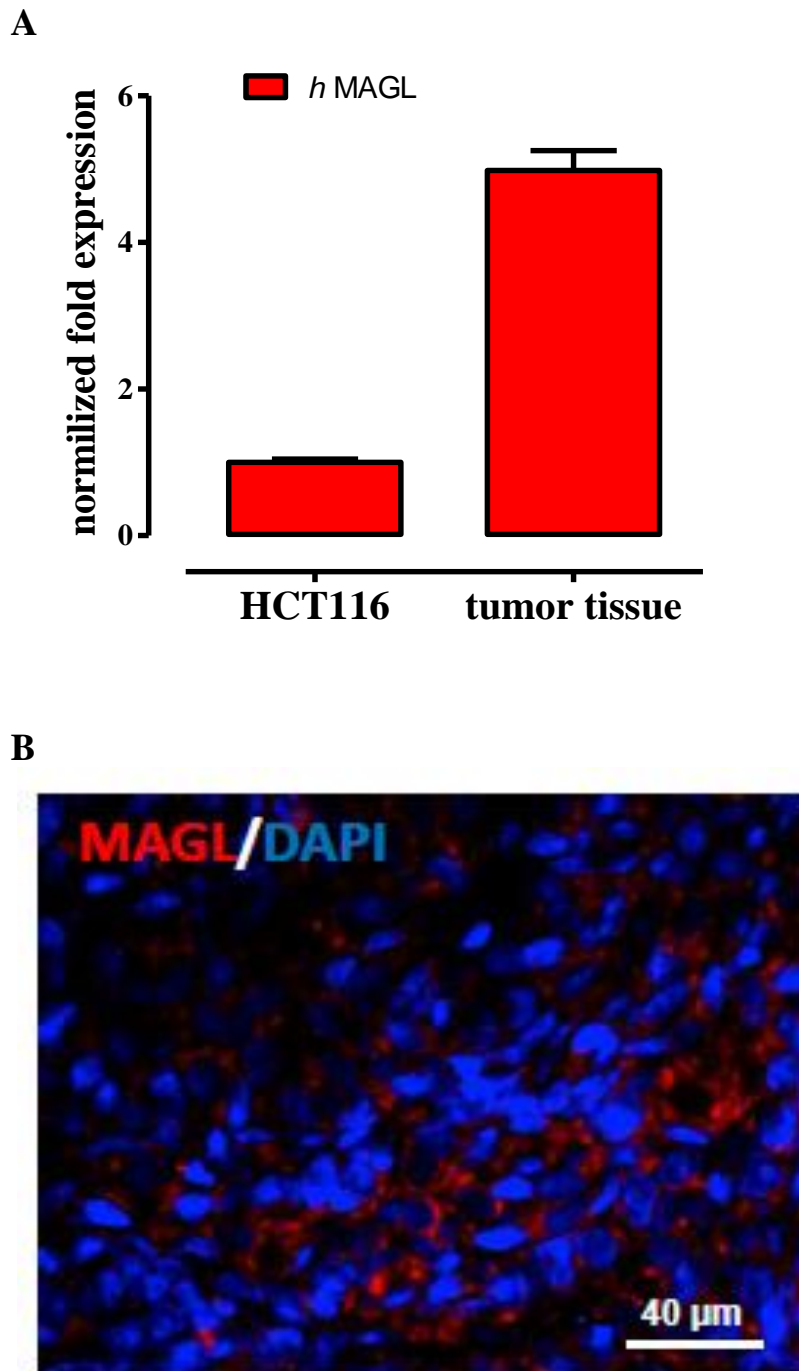


Figure 13. Expression of MAGL in the xenograft model of colon cancer.

(A) Human MAGL mRNA was evaluated by quantitative (real-time) RT-PCR analysis in human colorectal cancer (HCT 116) cells and in xenograft tumour tissues (mean \pm SEM of 5 independent experiments). Data were not statistically analyzed because cells are phenotypically different.

(B) Immunohistochemical analysis of MAGL in tumour tissues (xenograft model of colon cancer).

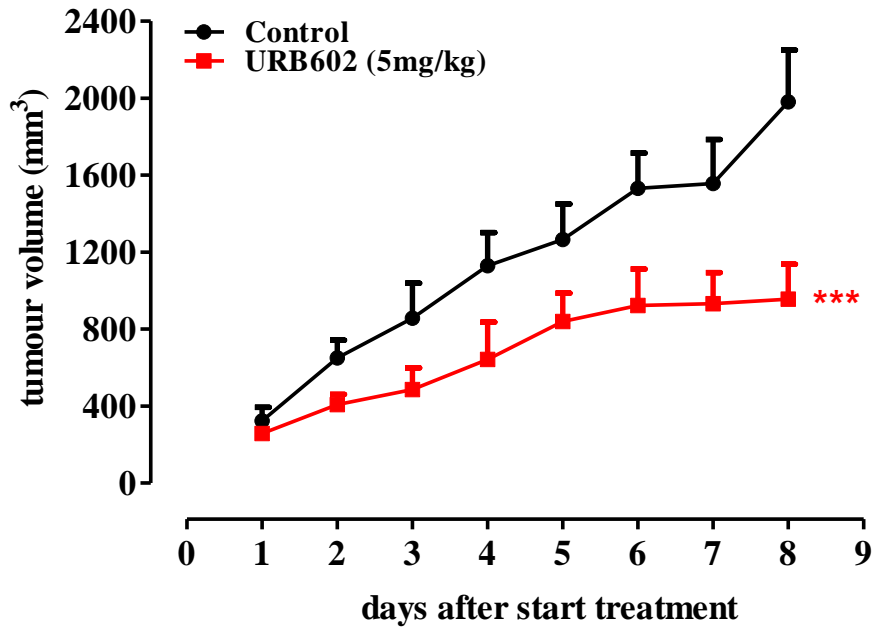


Figure 14. Inhibitory effect of URB602 (a MAGL inhibitor) on tumour formation in the xenograft model of colon cancer.

Tumours were induced by subcutaneous injection of colorectal cancer (HCT 116) cells into the right flank of athymic female mice. Tumour size was measured every day by a digital caliper, and tumour volume was calculated. URB602 (5 mg/kg, i.p.) treatment started 10 days after cell inoculation and continued daily until the sacrifice of the animals. Results represent the mean \pm SEM of 9–11 mice. * $p < 0.05$ and *** $P < 0.001$ vs control (vehicle-treated nude mice).

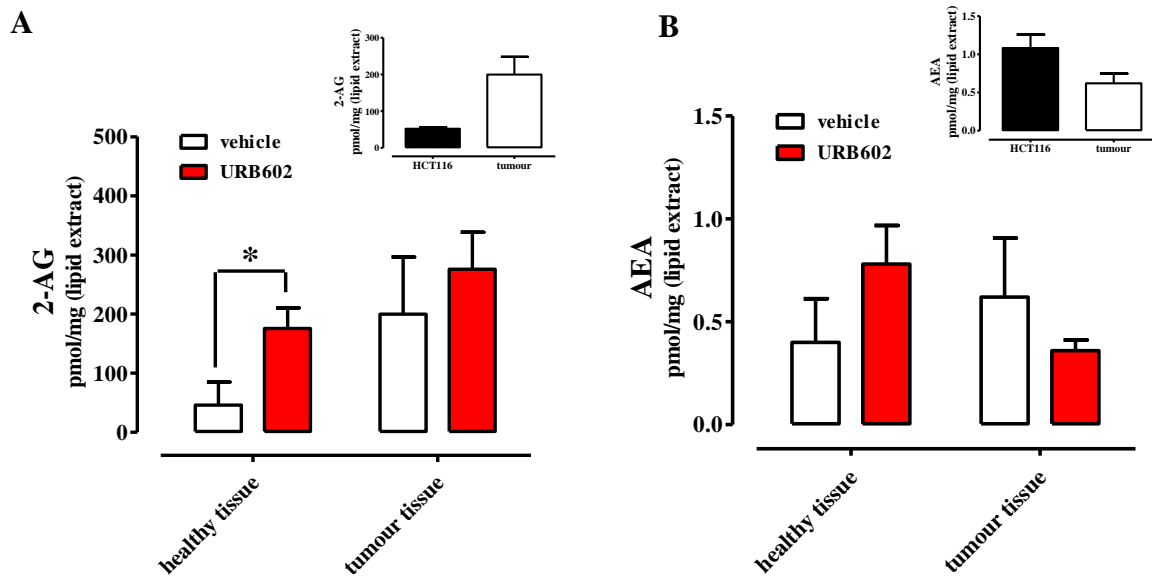


Figure 15. Effect of URB602 (a MAGL inhibitor) on endocannabinoids levels in the xenograft model of colon cancer.

2-arachydonylglycerol (2-AG, A) and anandamide (AEA, B) levels were evaluated in healthy tissues [derived from contralateral flank of the xenografted mice (i.e. the flank not injected with xenografted cells)] and in the tumour tissue. The inserts show a comparison between the levels of 2-AG (insert to A) and anandamide (insert to B) in colorectal cancer (HCT116) cells and in xenograft tumour tissue. Data of the insert were not statistically analyzed because cells are phenotypically different. URB602 (5 mg/kg, i.p.) treatment started 10 days after cell inoculation and it was administered every day until the sacrifice of the animals. Assays were performed 8 days after the first injection of URB602 (i.e. the day of animal sacrifice). Results are mean \pm SEM of 5 independent experiments for each experimental group. *P < 0.05 vs vehicle-treated nude mice.

1.4 The MAGL inhibitor URB602 drives *in vivo* angiogenesis output in xenograft tumour tissues

Figure 16 shows a panel of angiogenesis modulators following URB602 treatment. URB602 (5 mg/kg daily) decreased the expression of pro-angiogenic factors (i.e. VEGF and FGF-2), while it had no effect on the expression of endostatin, an anti-angiogenic modulator in tumour tissues. We also evaluated, by RT-PCR, mRNA expression of VEGF, the most important pro-angiogenic factor (Shibuya et al., 2011; Ferrara, 2004). Results, depicted in the insert to Figure 16B, showed that URB602 treatment decreased VEGF mRNA transcription.

Tumour samples were also analyzed for microvessel density (by counting CD-31 positive neovessels), structure and composition. All these parameters were significantly reduced by URB602 (Figure 17). Collectively, such results suggest antiangiogenic effects *in vivo*.

1.5 Direct antiangiogenic effect of the MAGL inhibitor URB602 in HUVEC

To verify if URB602 exerts a direct antiangiogenic effect, the MAGL inhibitor was tested in HUVEC stimulated with FGF-2 or 1% FCS. Both FGF-2 or 1% FCS (24 h stimulation) increased cell proliferation (Figure 18). The stimulated cell proliferation was inhibited by non-cytotoxic concentrations of URB602 (0.1 and 1 μ M) (Figure 18). In un-stimulated cells (0.1% FCS), URB602, at the 0.1 μ M concentration, stimulated proliferation (Figure 18). Concentrations higher than 1 μ M were not used because they resulted in a cytotoxic effect.

The antiangiogenic effect of URB602 was corroborated by the observation that the inhibitor, at the 1 μ M concentration, significantly reduced migration of adherent cells induced by both FGF-2 and 1% FCS (8 h incubation) (Figure 19). Specifically, the angiogenic factors reduced wound area and URB602 impaired the closure of wounds [see the quantification of scratch reported as percentage of healing in Figure 19 (bottom) and the representative pictures in Figure 19 (top)]. In un-stimulated cells (0.1% FCS), URB602 increased migration (Figure 19). Finally, we analyzed the balance of pro- and anti-angiogenic factors released by HUVEC in the culture media. The increase of FCS concentration (from 0.1% to 1%) induced a significant increase in FGF-2 release and a significant decrease in endostatin levels, as a sign of endothelial activation (Figure 20, see white columns). Both these changes were restored by URB602 treatment (Figure 20). Collectively, such data suggest a direct effect of URB602 on endothelial cells, through the modulation of endothelial cells functional response and production of autocrine/paracrine modulators of angiogenesis.

1.6. The MAGL inhibitor URB602 regulates Cyclin D1 in xenograft tumour tissues

In order to investigate the antiproliferative effects of URB602 *in vivo*, the expression of two cell cycle regulator genes (i.e. cyclin D1 and p27KIP) was evaluated in tumour xenograft tissues.

URB602 decreased the mRNA expression of cyclin D1 (Figure 21A), a factor that, by promoting cell DNA synthesis and cell growth, stimulates cancer cell proliferation (Motokura and Arnold, 1993). No significant effects of URB602 on the cycle-negative regulator p27KIP was observed (Figure 21B).

1.7. URB602 exerts chemopreventive effects in the azoxymethane (AOM) model of colon carcinogenesis

The carcinogenic agent AOM up-regulated colonic mRNA MAGL expression (mRNA fold expression of MAGL \pm SEM: control: 1.0 \pm 0.06, AOM: 1.7 \pm 0.04*; n=4 *p<0.05 vs control) and induced the expected appearance of ACF (Figure 22A), polyps (Figure 22B) and tumours (Figure 22C) after a three months treatment. URB602 significantly reduced AOM-induced ACF (Figure 22A) and tumours (Figure 22C), while it showed a trend to decrease the number of polyps (Figure 22B). URB602 (5 mg/kg), given alone (i.e. in absence of AOM), did not induce ACF, polyps and tumours, thus demonstrating that this compound is devoid of tumour-initiating activity in this experimental model (data not shown).

URB602 did not modify significantly AOM-induced ACF (Figure 22A), polyps (Figure 22B) and tumours (Figure 22C) in MAGL-deficient mouse, confirming the MAGL involvement in its antitumour activity.

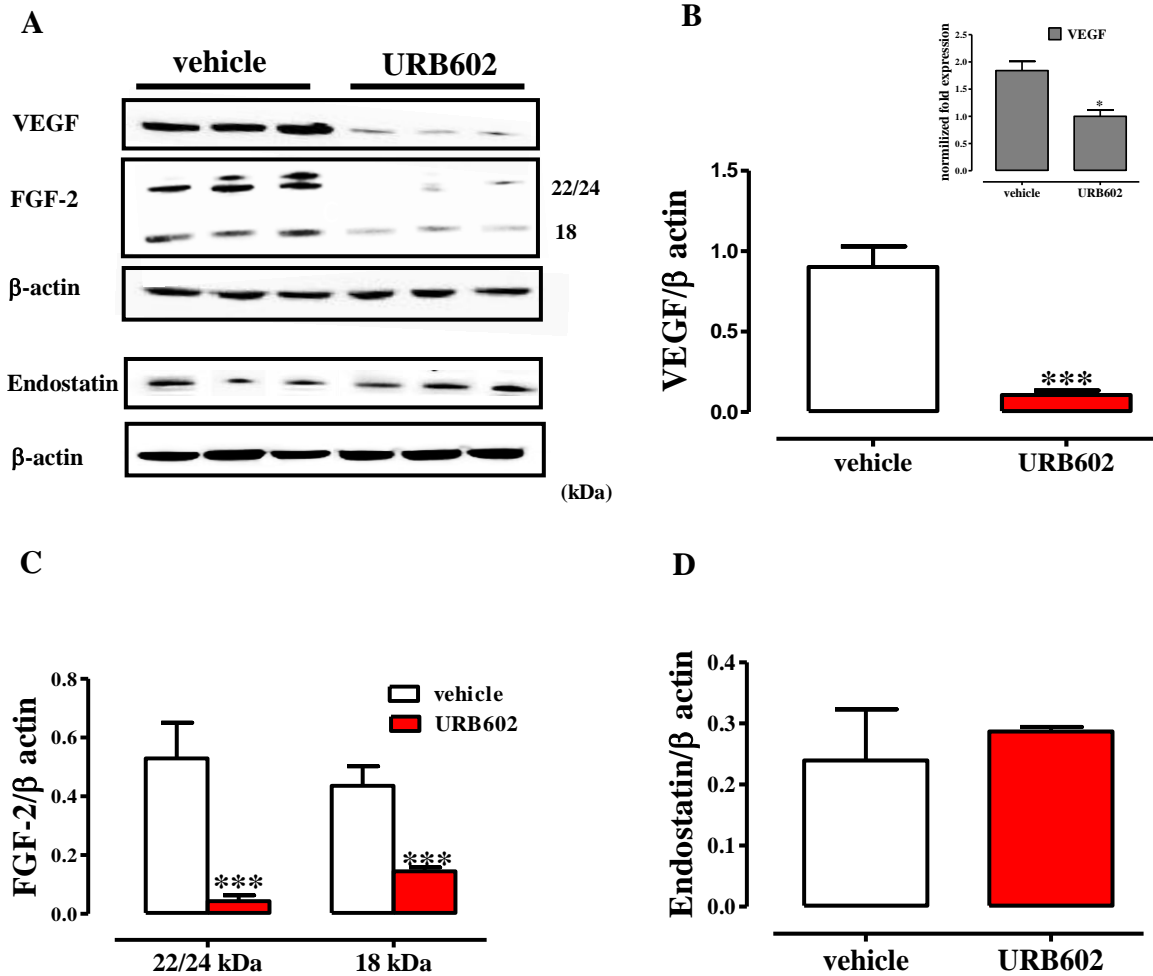


Figure 16. Effect of URB602 (a MAGL inhibitor) on angiogenic factors in the xenograft model of colon cancer.

The effect of URB602 was evaluated on VEGF (A), FGF-2 (B), and endostatin (C) expression in the tumour mass. URB602 (5 mg/kg, i.p.) treatment started 10 days after cell inoculation and it was administered every day until the sacrifice of the animals. Assays were performed 8 days after the first injection of URB602. (A) Representative blots, (B–D) results expressed as ratio of densitometric analysis of each protein/β-actin bands (means ± SEM of 3 tumours from three different mice. Each experiment was in triplicate). ***P < 0.001 vs vehicle-treated nude mice. The insert shows the mRNA expression of VEGF in the tumour tissue (HCT116 xenograft model) from animals treated or not by URB602. *P < 0.05 vs vehicle-treated nude mice.

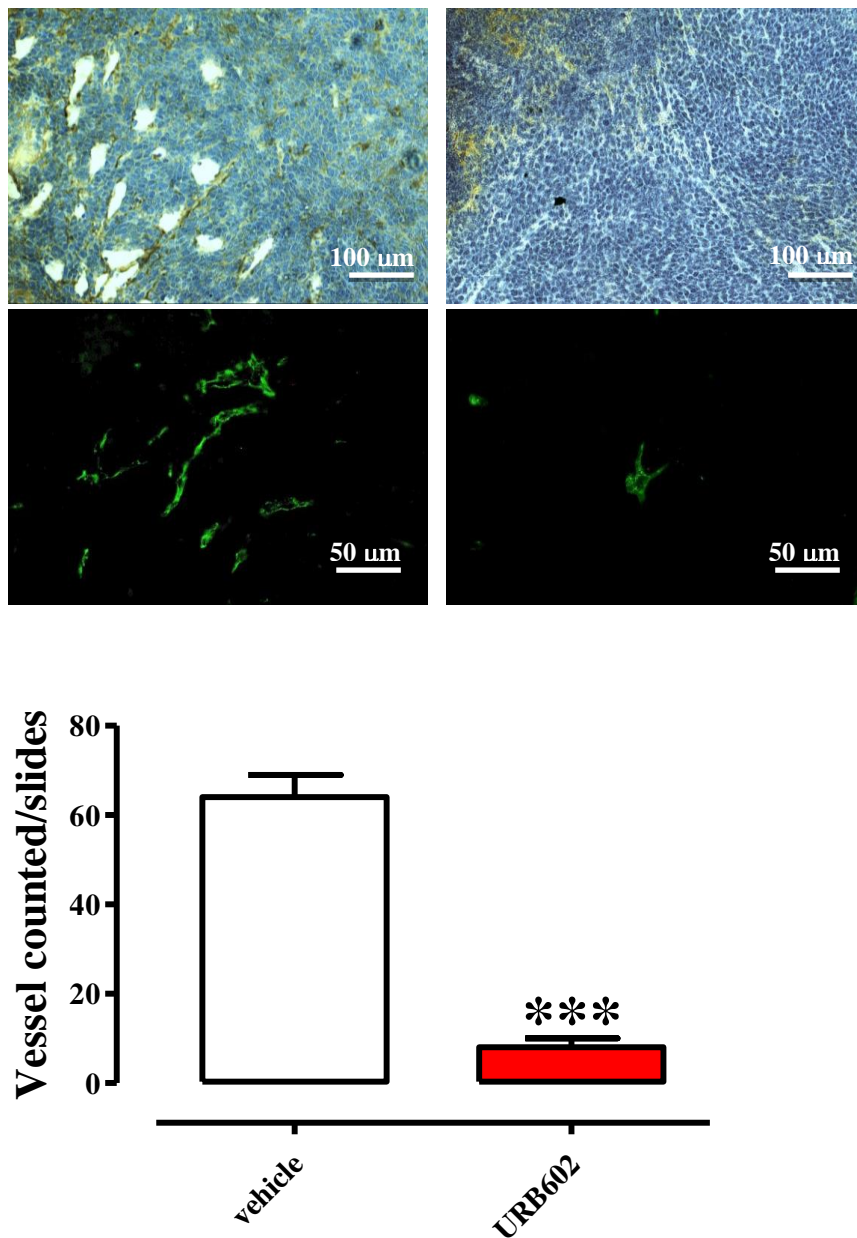


Figure 17. Effect of URB602 (a MAGL inhibitor) on CD31 positive cells in the xenograft model of colon cancer.

Representative images of CD31 immunostaining (upper) or immunofluorescence (bottom) in tumour sections from untreated (vehicle) and URB602-treated mice (URB602). Scale bars indicate 100 (upper) or 50 (bottom) μm . Images obtained by fluorescence microscope (Eclipse TE300, Nikon) at 20 \times (upper) or 40 \times (bottom) magnification and taken by a digital Q10. camera. Bar graph represents the number of CD31 positive vessels, calculated counting 8 random fields/section for slides, each slide having five sections. URB602 (5 mg/kg, i.p.) treatment started 10 days after cell inoculation and it was administered every day until the sacrifice of the animals. Assays were performed 8 days after the first injection of URB602. Results are mean \pm SEM tumours from three different mice. Each experiment was in triplicate. *** $P < 0.001$ vs vehicle-treated nude mice.

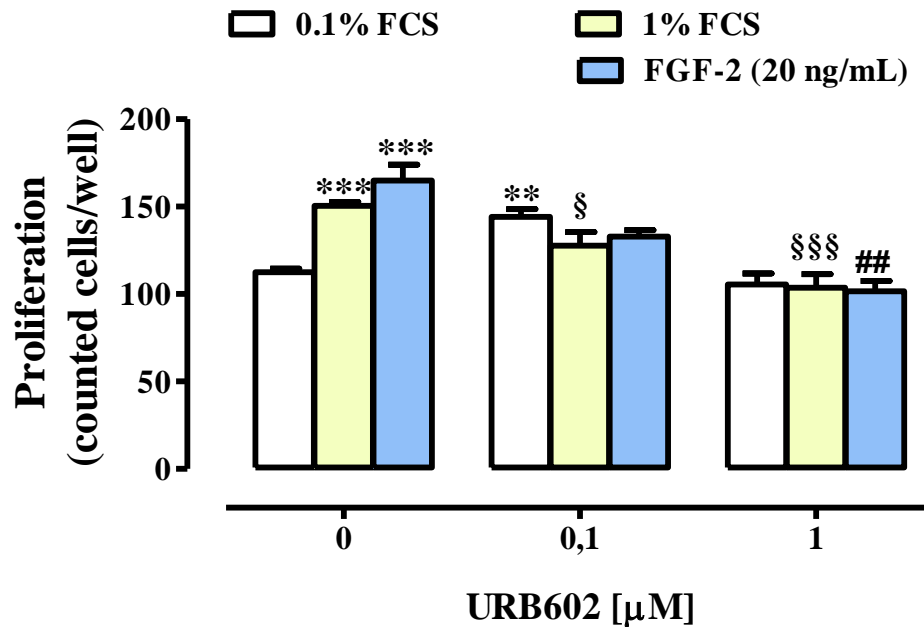


Figure 18. Effect of URB602 (a MAGL inhibitor) on endothelial cell proliferation *in vitro*.

URB602 was tested on cell proliferation in human umbilical vein endothelial cells (HUVEC) under basal condition (0.1% FCS) or in cells stimulated for 24 h with either 1% FCS or FGF-2 (20 ng/ml). (A) URB602 (0.1–1 μ M) was added to the cell media 30 min before stimulation. Data are expressed as counted cells/well \pm SEM from 4 independent experiments. **p < 0.01 and ***p < 0.001 vs 0.1% FCS URB602-untreated cells, §p < 0.05 and §§§p < 0.001 vs 1% FCS URB602-untreated cells; ##p < 0.01 vs FGF-2 URB602-untreated cells.

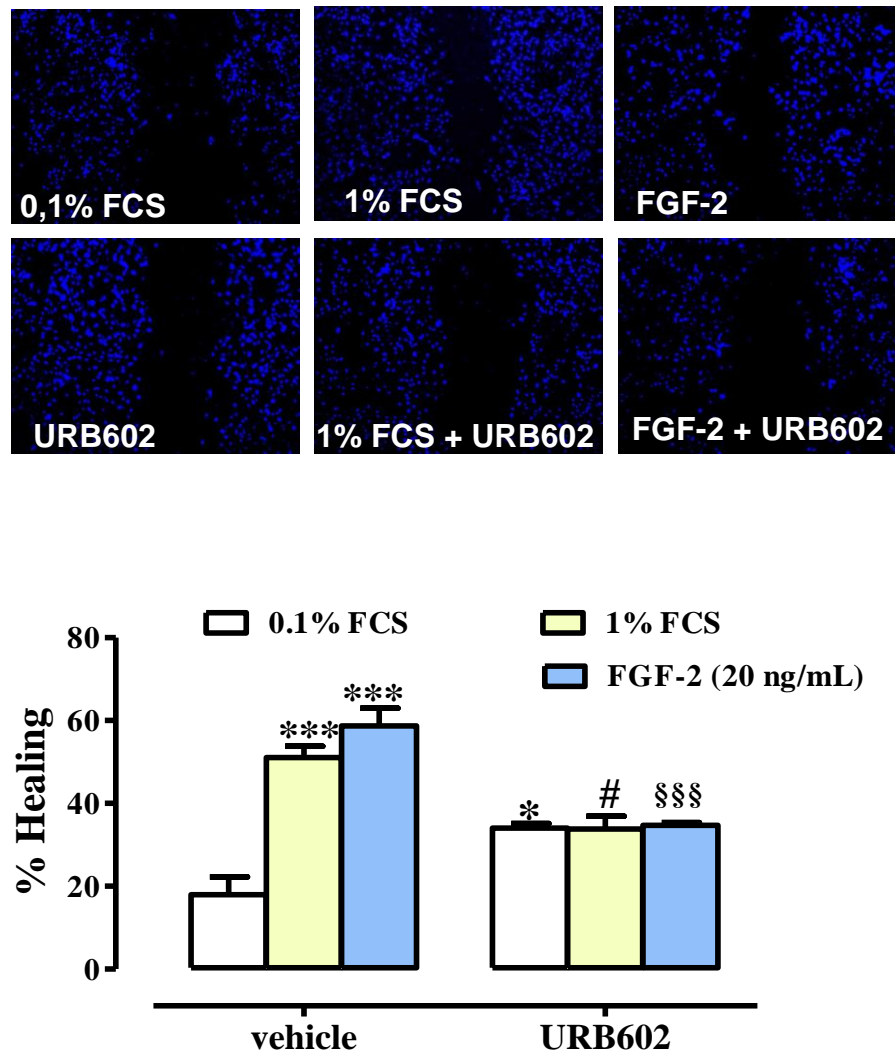


Figure 19. Effect of URB602 (a MAGL inhibitor) on endothelial cell migration *in vitro*.

URB602 was tested on cell migration in human umbilical vein endothelial cells (HUVEC) under basal condition (0.1% FCS) or in cells stimulated for 24 h with either 1% FCS or FGF-2 (20 ng/ml). Bottom: effect of URB602 (1 μ M) in HUVEC monolayers. URB602 was added to the cell media 30 min before stimulation. The graph shows the percentage of healing of the wound area. * $p < 0.05$ and *** $p < 0.001$ vs. 0.1% FCS URB602-untreated cells, # $p < 0.05$ vs. 1% FCS URB602-untreated cells and \$\$\$ $p < 0.001$ vs. FGF-2 URB602-untreated cells.

Top: Representative pictures (of 4 experiments) of Hoechst 33342 labelled cells.

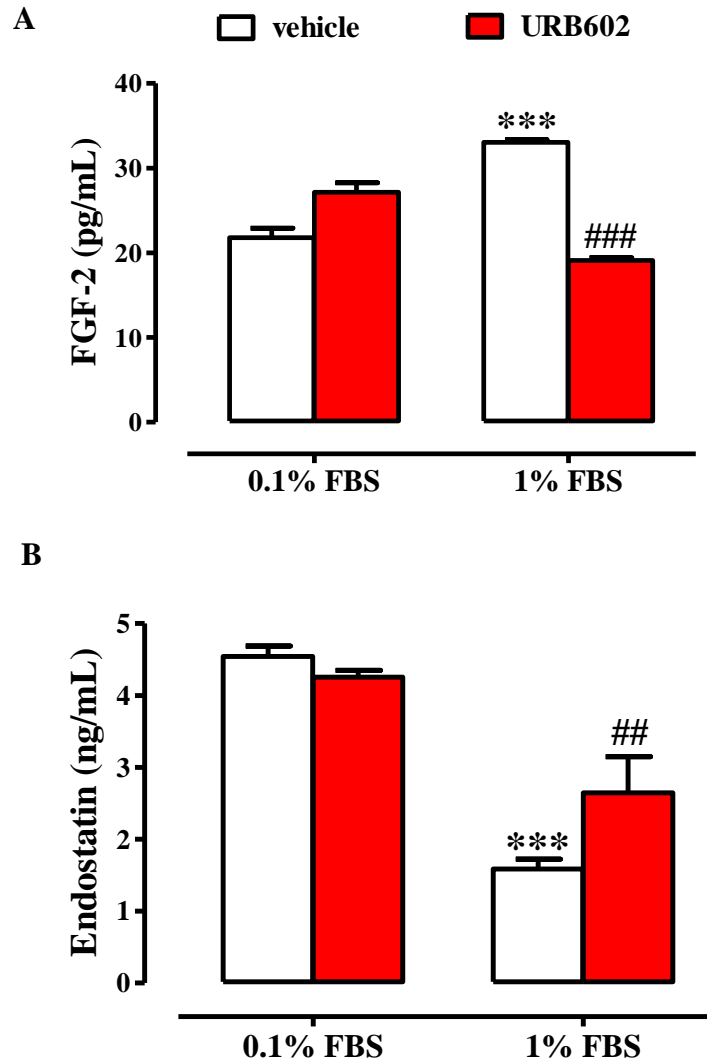


Figure 20. Effect of URB602 (a MAGL inhibitor) on angiogenic factors *in vitro*.

URB602 (1 μ M) was tested on FGF-2 (A) and endostatin levels (B) in human umbilical vein endothelial cells (HUVEC) under basal condition (0.1% FBS) or in cells stimulated for 18 h with either 1% FBS. Data are reported as pg/ml (FGF-2) or ng/ml (endostatin) (means \pm SEM) from 3 independent experiments (in triplicate). *** p <0.001 vs. 0.1% FBS URB602-untreated cells, ## p <0.01 and ### p <0.001 vs 1% FBS URB602-untreated cells.

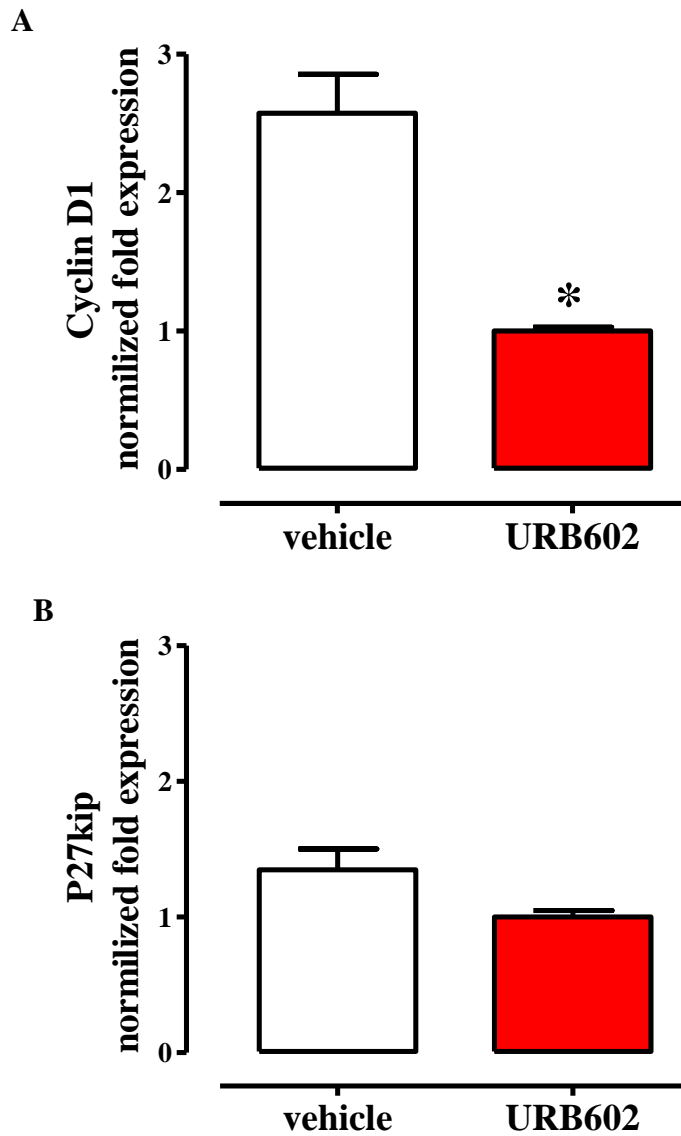


Figure 21. Effect of URB602 (a MAGL inhibitor) on expression of cycle regulator genes in the xenograft model of colon cancer.

Cyclin D1 (A) and P27kip (B) mRNA expression were evaluated by quantitative (real-time) RT-PCR analysis in the tumour mass of vehicle- and URB602-treated mice. URB602 (5 mg/kg, i.p.) treatment started 10 days after cell inoculation and it was administered every day until the sacrifice of the animals. Assays were performed 8 days after the first injection of URB602. *P < 0.005 vs vehicle-treated nude mice.

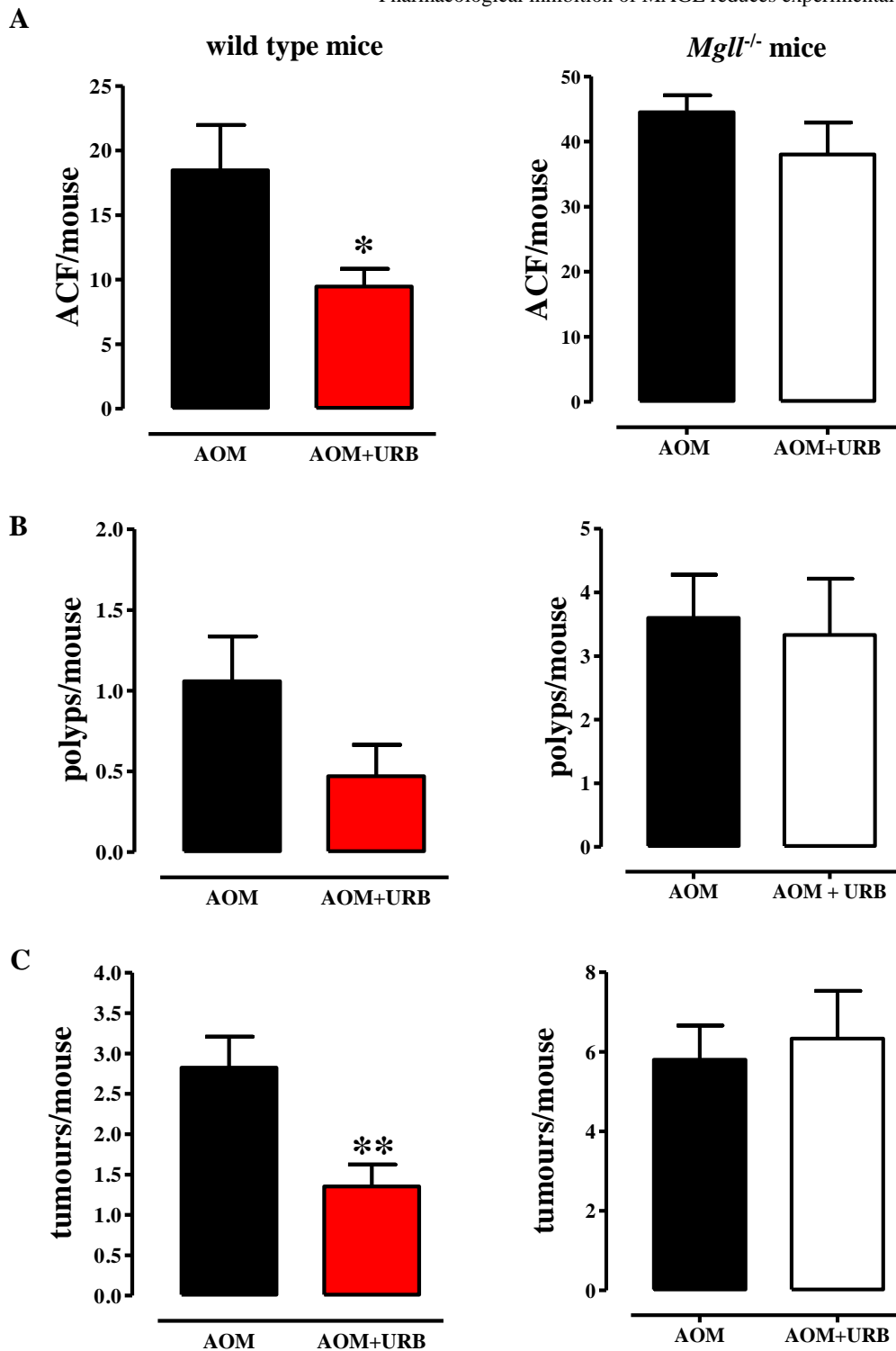


Figure 22. Azoxymethane (AOM) model of colon carcinogenesis: effect of URB602 (a MAGL inhibitor) in wild type and in *Mgll*^{-/-} deficient mice.

The inhibitory effect of URB602 was evaluated on aberrant crypt foci (ACF) (A), polyps (B) and tumours (C) induced in the wild type (left) and MAGL-deficient (right) mice by AOM. URB602 (5 mg/kg, i.p.) was given three times a week for the whole duration of the experiments starting 1 week before the first administration of AOM. Measurements were performed 3 months after the first injection of AOM. The criterion to distinguish polyps from tumours was established considering the main characteristic features of these two lesions. Results represent the mean \pm SEM of 9–11 mice. * $p < 0.05$ and ** $p < 0.01$ vs AOM alone

Chapter II. NAAA is crucially involved in proliferation, migration and *in vivo* colon tumorigenesis

1.1 NAAA is down-regulated in human CRC tissues

Using a web accessible data base named GENT (available at <http://medicalgenome.kribb.re.kr/GENT>), which provides the gene expression patterns across different kind of human cancer and healthy tissues, we found that hNAAA enzyme is significantly downregulated in colonic biopsies of patients with colorectal cancer compared with corresponding normal tissues (Figure 23A). Therefore, we examined the gene expression of hNAAA in colonic tumours of patients at different stages of CRC by RT-PCR. As shown in Figure 23B, a significant reduction of NAAA was observed in tumour specimens (compared to their corresponding non-cancerous controls) at different stages (pT2, pT3 and pT4 of CRC).

We also measured the expression of PPAR- α mRNA, i.e. the main target of PEA, in CRC biopsies. We found that PPAR- α mRNA was differently expressed in CRC tissues with a trend toward a reduction in patients with stage pT3 and pT4 tumours compared to normal tissues (Figure 23C).

1.2 The NAAA inhibitor AM9053 reduces tumour growth in the xenograft model of colon cancer

To assess the *in vivo* involvement of NAAA in murine carcinogenesis, we used AM9053, a selective NAAA inhibitor, in the xenograft model of colon cancer. CRC (HCT116) cells subcutaneously injected into immunodeficient mice gave rise to exponentially growing tumours. After 1 week, when the tumours became measurable, mice were treated (peritumorally, three times per week) with vehicle or AM9053 (20 mg/kg) until the sacrifice of the animals. AM9053 caused a significant reduction of xenograft tumour growth compared to vehicle-treated mice (Figure 24A). At the end of the pharmacological treatment (day 21), the tumour volume (mean \pm SEM) for the vehicle and AM9053 groups were 1006.6 ± 211 mm³ and 764.4 ± 177 mm³, respectively. Also, we found a trend in reduction in the weight of tumours treated with AM9053 (Figure 24C).

1.3 Effect of the NAAA inhibitor AM9053 on NAAA and PEA targets expression in xenograft colon cancer tumours

In addition to PPAR- α , PEA can directly or indirectly activate GPR55, cannabinoids receptors and TRPV1 channel (Di Marzo et al., 2001, Ryberg et al., 20017, Petrosino and Di Marzo, 2017). Thus, we analyzed, by RT-PCR, the expression of such targets as well as of NAAA in xenografts tumours treated or not with AM9053. All the investigated targets were expressed in xenograft tumours, but the NAAA inhibitor AM9053 significantly reduced PPAR- α mRNA expression only (Figure 25).

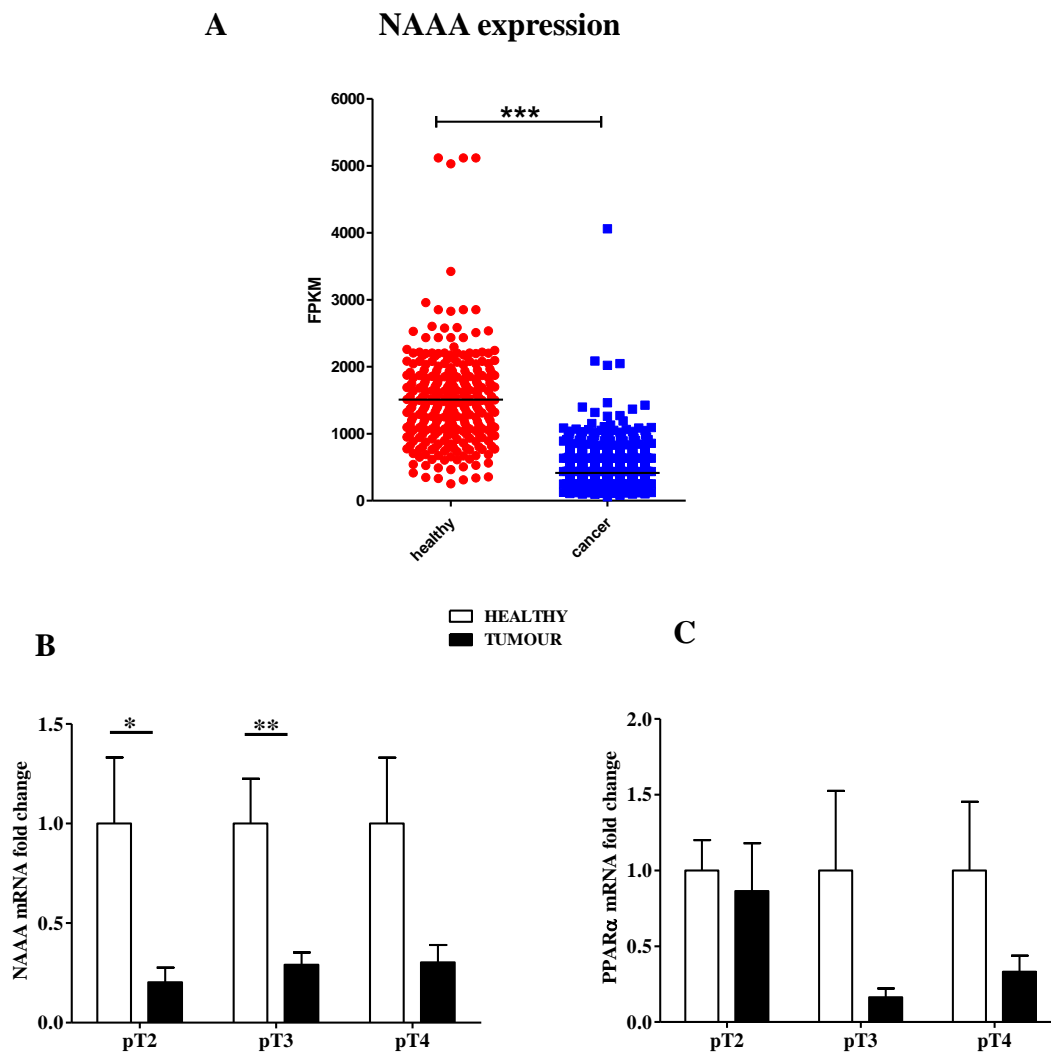


Figure 23. Expression of NAAA and PPAR- α at different TNM stages of colorectal cancer (CRC) patients.

(A) Expression of hNAAA in colorectal cancer [data available in the web-accessible database GENT (Gene Expression across Normal and Tumour tissue)]. *** $p < 0.001$ vs corresponding healthy tissues.

NAAA (B) and PPAR- α (C) mRNA expression was evaluated in colonic biopsies of patients at different stages (pT2, pT3 and pT4) of CRC. mRNA was evaluated by quantitative (real-time) RT-PCR analysis (mean \pm SEM of 3 patients). * $p < 0.05$ and ** $p < 0.01$ vs corresponding healthy tissues (i.e. adjacent non-tumour tissues)

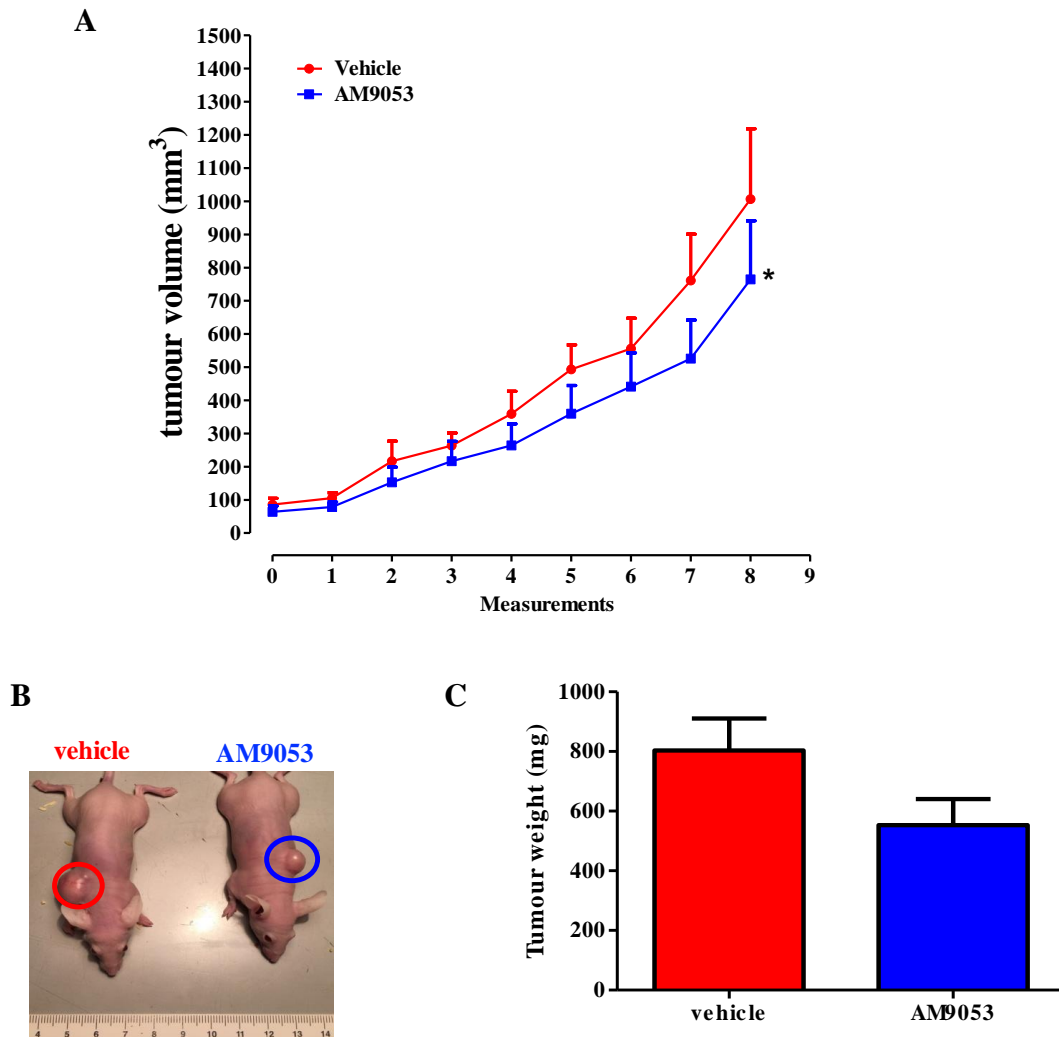


Figure 24. Inhibitory effect of AM9053 (a NAAA inhibitor) on tumour formation in the xenograft model of colon cancer.

Tumours were induced by subcutaneous injection of colorectal cancer (HCT116) cells on the back of athymic female mice.

(A) Tumour growth was measured three times per week by a digital caliper, and tumour volume was calculated. AM9053 (20 mg/kg, peritumorally) treatment started 7 days after cell inoculation and it was administered three times per week for three weeks until the sacrifice of the animals.

(B) Representative images of mice after three weeks-treatment with vehicle or AM9053.

(C) Tumour weight calculated after the sacrifice of mice.

Results represent the mean \pm SEM of 5 mice. * $p < 0.05$ vs vehicle-treated nude mice.

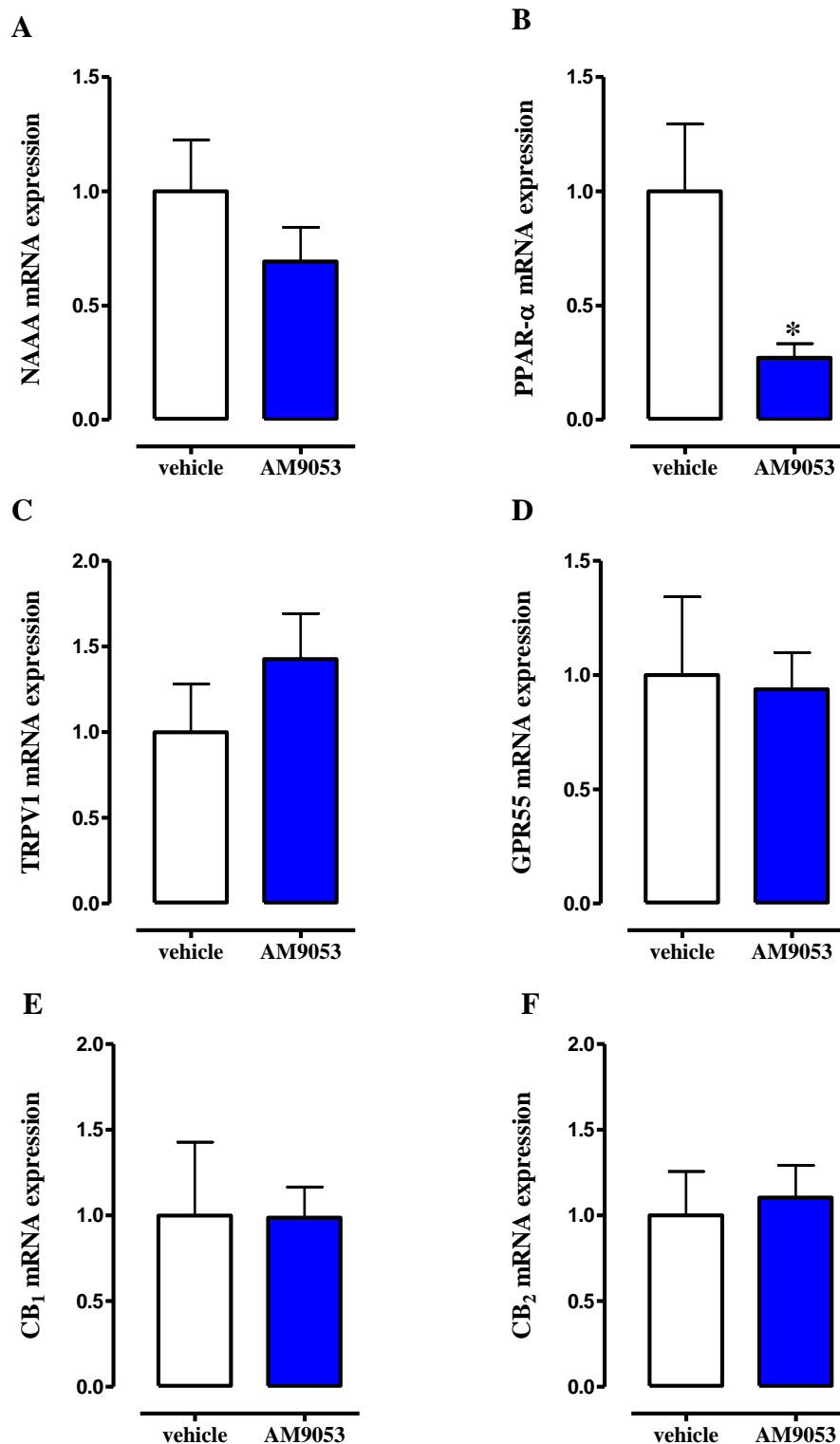


Figure 25. Expression of NAAA and PEA targets in the xenograft model of colon cancer

Human mRNA expression of NAAA (A), PPAR- α (B), TRPV1 (C), GPR55 (D), CB₂ (E) and CB₁ (F) was evaluated by quantitative (real-time) RT-PCR analysis (mean \pm SEM of 5 mice) in xenograft tumour tissues. AM9053 (20 mg/kg, peritumorally) treatment started 7 days after cell inoculation and it was administered three times per week for three weeks until the sacrifice of the animals. *p < 0.05 vs vehicle-treated nude mice.

1.4 The incubation with xenograft tumour secretome reduces NAAA expression in colorectal cancer (CRC) cells

In preliminary experiments, we assessed NAAA mRNA expression in colorectal (HCT116 and Caco-2) cancer cells. Results showed the enzyme to be highly expressed in both cell lines (Table 5). Evidence from literature suggests that tumour secretome, consisting of factors derived from cancer stem cells, non-stem cells and stroma, plays a key role in cancer progression (Xue et al., 2008; Cordani et al., 2016). For this reason, we incubated the CRC (i.e. Caco-2) cells with conditioned medium derived from xenograft tumours and found that the tumour secretome reduced significantly NAAA (Figure 26).

1.5 The NAAA inhibitor AM9053 and its substrate PEA reduce the number of tumours induced by azoxymethane (AOM)

The AOM model of CRC was used to assess the *in vivo* chemopreventive potential of the NAAA inhibitor AM9053 and its substrate PEA. AOM treatment causes the formation of colonic tumours (Figure 27), which was significantly reduced by AM9053 (20 mg/kg, i.p.) or PEA (10 mg/kg, i.p.) (Figure 27). These results confirm a key role of NAAA and its substrate in experimental colon carcinogenesis.

AM9053 was well tolerated with control mice showing no weight loss or other signs of toxicity during treatment (data not shown)

1.6 AM9053 (NAAA inhibitor) and PEA inhibit the proliferation of colorectal cancer - but not of healthy colonic - cells

To evaluate the effect of AM9053 and PEA on cancer cell proliferation, we used the BrdU incorporation assay. We tested a number of non-cytotoxic concentrations of AM9053 (0.1-3 μ M) and PEA (1-30 μ M) on HCT116 cells. Both AM9053 and PEA significantly reduced the proliferation of colorectal cancer cells in a concentration-dependent manner after 24h of treatment (Figures 28A-B). Importantly, AM9053 at concentration of 3 μ M inhibits NAAA and has no effect on FAAH activity, for which concentration of about 100 μ M are needed (Bottemanne et al., 2018). In order to evaluate the selectivity of AM9053 and PEA (tumoural *vs* non tumoural cells), the highest concentrations of both compounds (i.e. AM9053 3 μ M and PEA 30 μ M) were tested on healthy colonic epithelial cells (HCEC). Both compounds did not affect the proliferation of healthy cells, thus suggesting a selective antiproliferative effect *vs* tumoural cells (Figure 28C).

1.7 AM9053 and PEA treatments lessen the migration of colorectal cancer cells

To assess the effect of AM9053 (3 μ M) and PEA (30 μ M) on cell migration, a scratch assay was performed in two different cancer cell lines (i.e. Caco-2 and HCT116). Briefly, the capability of the epithelial cells to cover the scratch created by the insert is directly correlated to the cell migration.

The distance between the edge of the cell sheet and the scratched line was measured. Both AM9053 (3 μM) and PEA (30 μM) (both 24-h treatment) significantly reduced the closure of wounds compared to vehicle-treated cells, as shown in the quantification of scratch expressed as percentage of healing in Figure 29 (top) and in the representative pictures in Figure 29 (bottom).

TABLE 5. Detection of NAAA and GAPDH mRNA by quantitative (real-time) RT-PCR analysis in human colorectal (Caco-2 and HCT116) cells. (Threshold Cycle (Ct) \pm S.E.M.)

<i>Target</i>	Caco-2	HCT116
NAAA	25.53 \pm 0.399	23.37 \pm 0.079
GAPDH	17.60 \pm 0.590	15.08 \pm 0.138

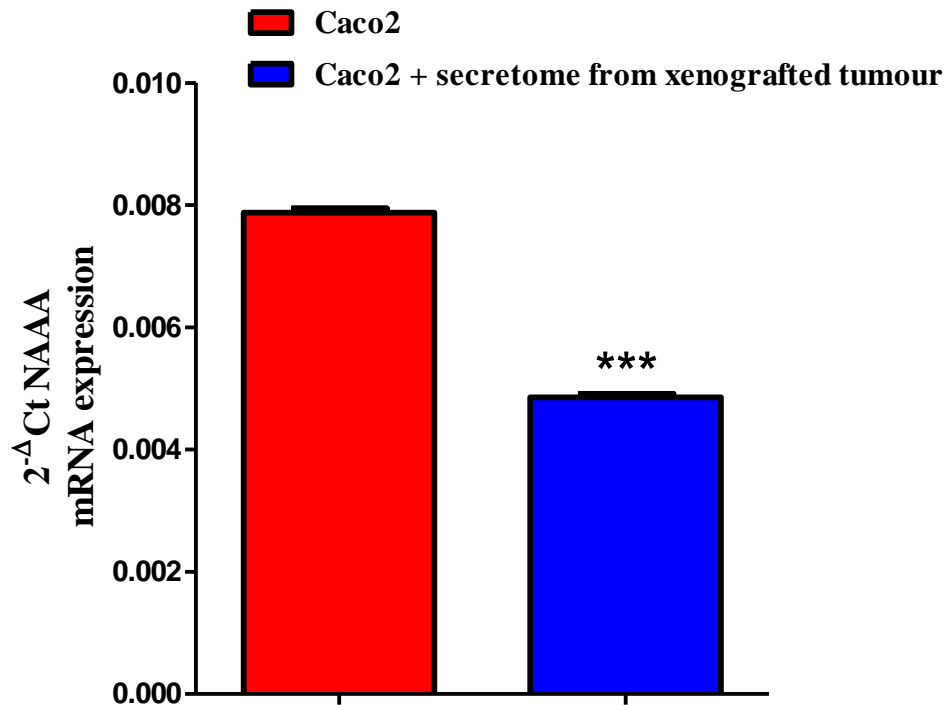


Figure 26. Expression of NAAA in Caco-2 and HCT116 cells incubated with secretome

Caco-2 or HCT116 cells were cultured for 24h at 37°C in presence of secretome (i.e. conditioned medium derived from the tumour mass of the xenograft model of colon cancer). Control cells were incubated with normal medium. Human mRNA was evaluated by quantitative (real-time) RT-PCR analysis (mean ± SEM of 3 different experiments). ***p < 0.001 vs DMEM-treated Caco-2.

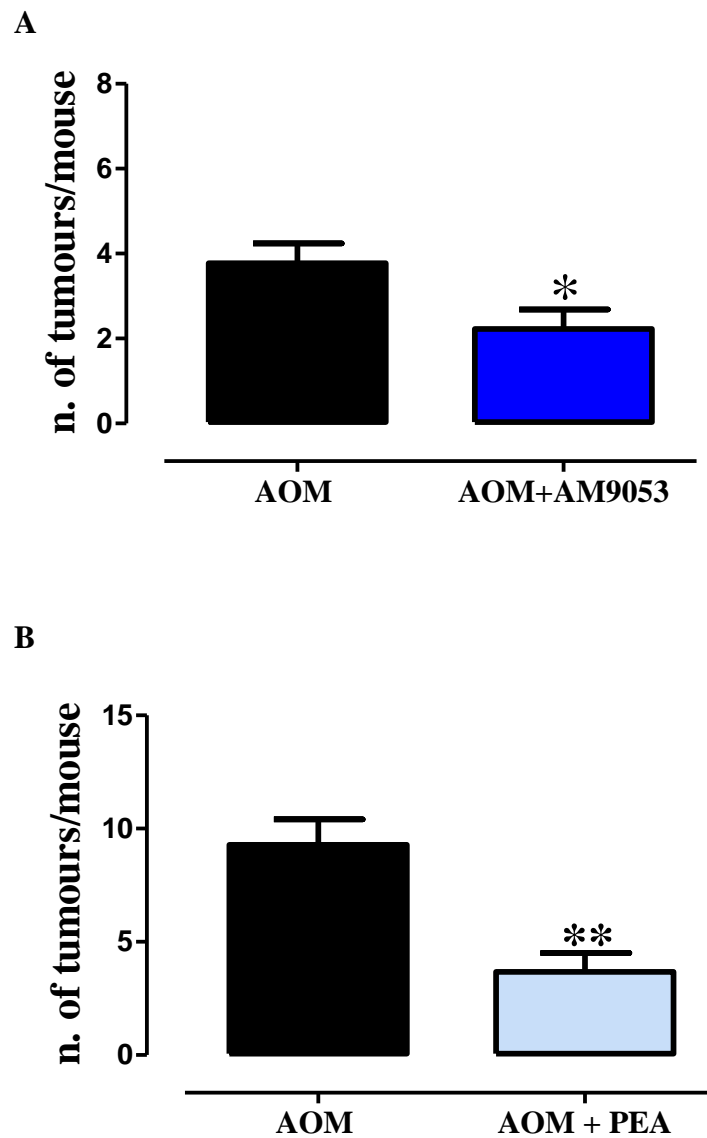


Figure 27. Azoxymethane (AOM) model of colon cancer: chemopreventive effect of AM9053 (a NAAA inhibitor) and PEA.

AM9053 (A, 20 mg/kg, i.p.) or PEA (B, 10 mg/kg, i.p.) were given three times a week for the whole duration of the experiment starting 1 week before the first administration of AOM. Measurements were performed 3 months after the first injection of AOM. Results represent the mean \pm SEM of 9 mice. * $p < 0.05$ and ** $p < 0.01$ vs AOM alone

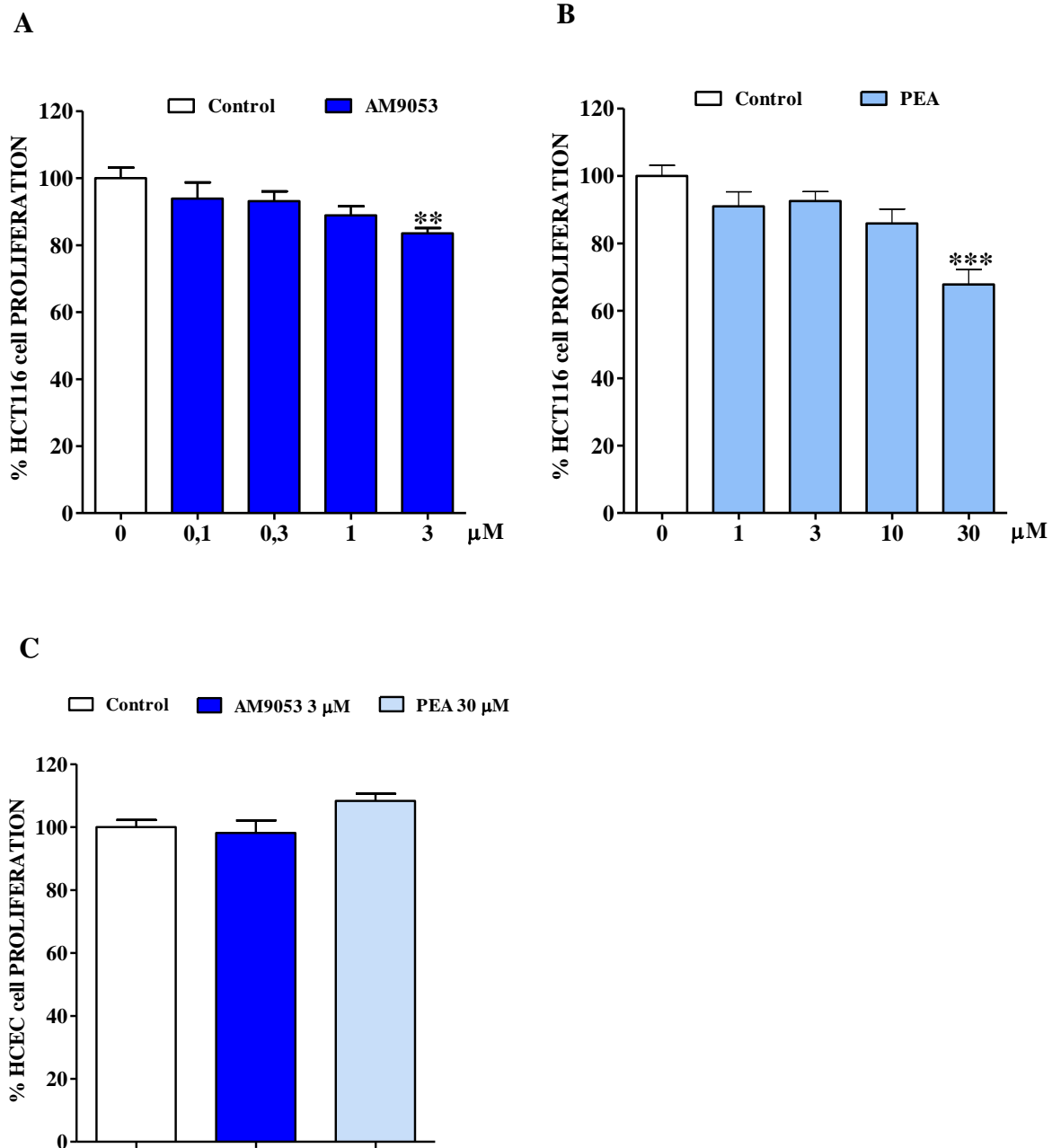


Figure 28. Effect of AM9053 (a NAAA inhibitor) and PEA on colonic epithelial cell proliferation.

(A) AM9053 (0.1-3 μM) and (B) PEA (1-30 μM) were tested on proliferation of colorectal cancer (HCT116) cells by using the BrdU incorporation assay. Cells were incubated with increasing concentrations of compounds (24h-exposure). Each bar represents the mean \pm SEM of three independent experiments. * $p < 0.05$ and *** $p < 0.001$ versus control (vehicle-treated cells).

(C) Effect of AM9053 (3 μM) or PEA (30 μM) on proliferation in healthy colonic epithelial cells (HCEC).

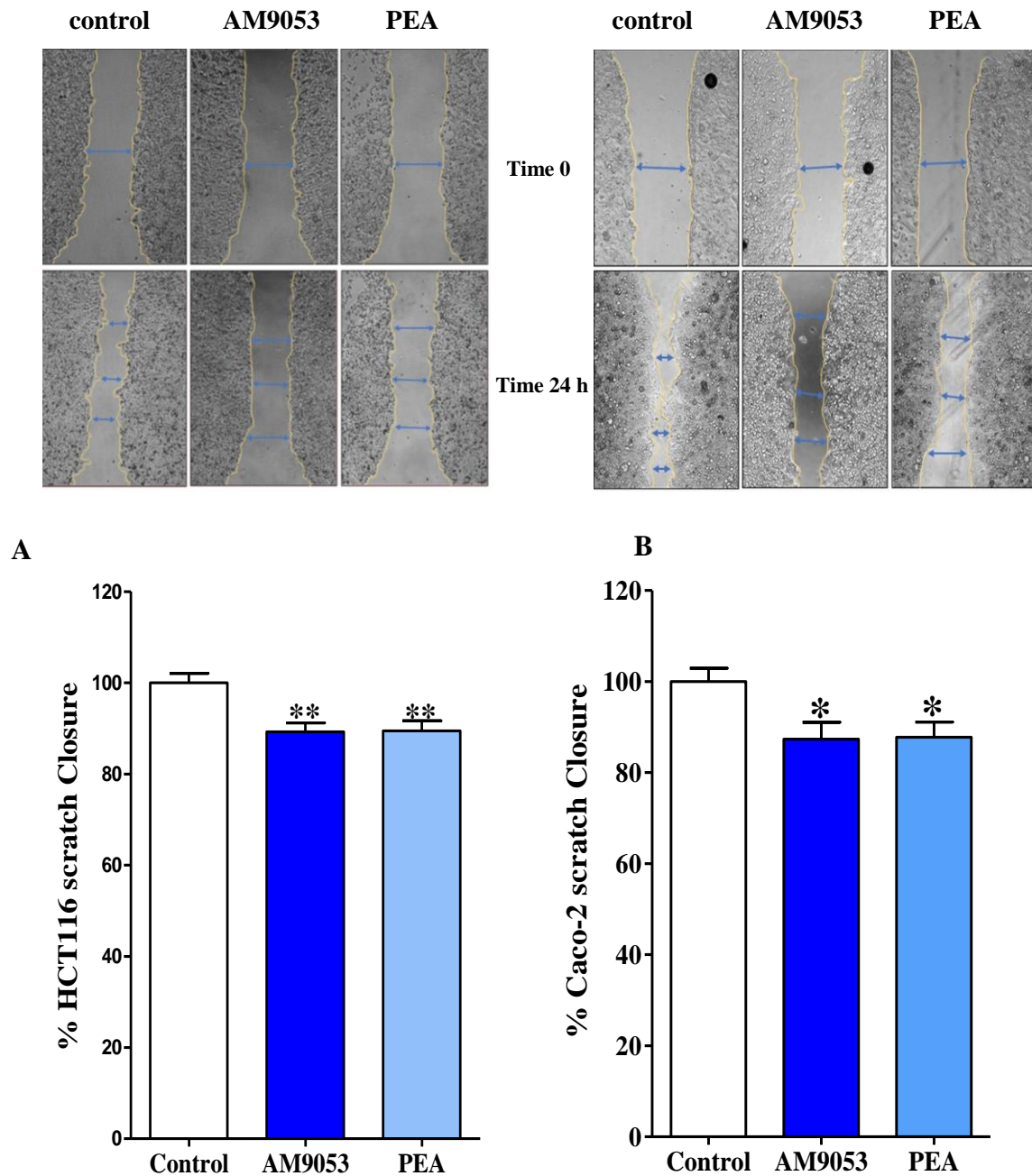


Figure 29. Effect of AM9053 (a NAAA inhibitor) and PEA on colorectal cancer cell migration
 Bottom: Effect of AM9053 (3 μ M) and PEA (30 μ M) in HCT116 (A) and in Caco-2 (B) monolayers after 24h treatment. The ordinates show the percentage of closure of the wound area. Each bar represents the mean \pm SEM of three independent experiments. * $p < 0.05$ and ** $P < 0.01$ vs control (vehicle-treated cells).
 Top: Representative pictures of CRC cells.

Chapter III. GPR35 promotes glycolysis, proliferation and colon tumorigenesis

1.1 *Gpr35*^{-/-} BMDM have reduced glucose uptake

GPR35 is abundantly expressed in macrophages and in colonic epithelial cells (Wang et al., 2006). Macrophages exhibit different functional states, which can be appraised *in vitro* by differentiation under MΦ (baseline), M1 (‘inflammatory’, IFNγ+LPS) and M2 (‘regenerative’, IL-4) conditions (Murray et al., 2014). We have found that bone marrow derived macrophages (BMDM) from *Gpr35*^{-/-} mice took up significant lower amounts of glucose compared to *Gpr35*^{+/+} macrophages (Figures 30A-C). These results were found in all phenotypes (MΦ, M1 and M2) of macrophages and were expressed as fmol of 2DG6P detected per cell after 10-60 min of 2DG incubation.

The reduced glucose uptake was not correlated with any difference in the expression of glucose transporters (i.e. GLUT1, SGLT1 and SGLT2) in MΦ, M1 and M2 macrophages between different genotypes (*Gpr35*^{+/+} vs *Gpr35*^{-/-}) (Figure 31). As expected, we found a 4-fold increase in GLUT1 expression induced by LPS and IFNγ polarization in both wild type and *Gpr35*^{-/-} M1 phenotype (Figure 31), confirming the importance of glucose as carbon source for pro-inflammatory macrophages. These data show that *Gpr35*^{-/-} macrophages may need a lower amount of glycolysis substrate, suggesting the involvement of GPR35 in the cellular metabolism.

1.2 The lack of GPR35 impairs the metabolic profile of macrophages

To investigate whether reduced glucose uptake influenced glycolytic metabolism, we measured the extracellular acidification rate (ECAR), an indicator of glycolysis, in wild-type and knockdown M1 macrophages using the Seahorse. Remarkably, metabolic study revealed that ECAR in *Gpr35*^{-/-} M1 was significantly lower compared to wild type cells (Figure 31A). In fact, as shown in the Figure 31A, the knockdown cells had both reduced glycolysis and glycolytic capacity. Moreover, we proved that the lactate accumulation, a hallmark of increased glycolysis, is significantly reduced in *Gpr35*^{-/-} M1 macrophages (Figure 31B).

Also, we assessed the metabolic profile of MΦ and M2 macrophages. Although inflammatory M1 macrophages support their energetic needs preferentially via aerobic glycolysis (Warburg effect), MΦ and M2 macrophages rely mostly on oxidative phosphorylation (OXPHOS) (Kelly and O'Neill, 2015). The oxygen consumption rate (OCR) was reduced in *Gpr35*^{-/-} MΦ and *Gpr35*^{-/-} M2 compared to wild-type cells which means that the lack of GPR35 impairs also the mitochondrial respiration in macrophages (Figures 31C-D). These data demonstrate that *Gpr35*^{-/-} macrophages have a reduction in glycolysis and OXPHOS compared with wild type cells, suggesting that the receptor may play a pivotal role in energy production and cellular energetic demand.

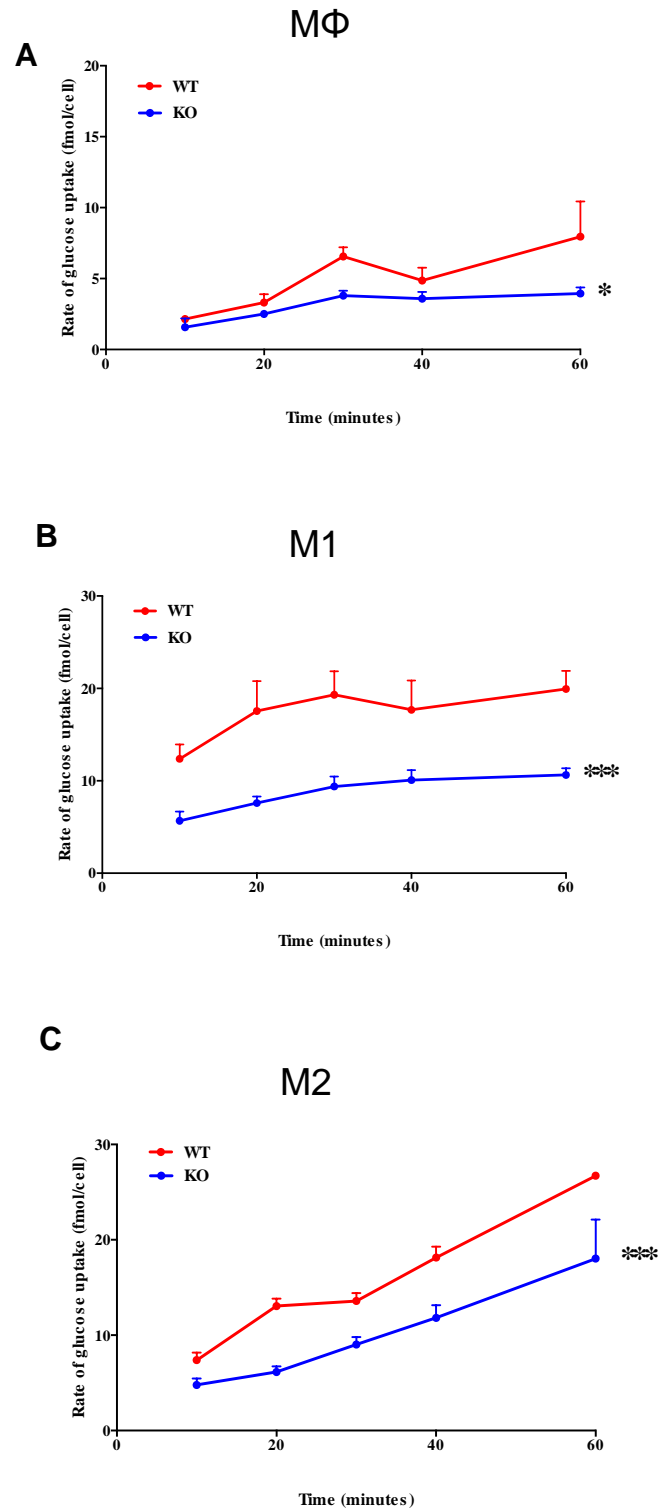


Figure 30. Glucose uptake in $Gpr35^{+/+}$ and $Gpr35^{-/-}$ bone marrow-derived macrophages (BMDM).

Rate of glucose uptake was measured in $Gpr35^{+/+}$ (red) and $Gpr35^{-/-}$ (blue) MΦ (A), M1 (B) and M2 (C) BMDM and was expressed as intracellular 2-deoxy-D-glucose-6-phosphate (2DG6P) concentration detected per cell after incubation of 2DG. * $P < 0.05$ and *** $P < 0.001$ vs wild-type cells.

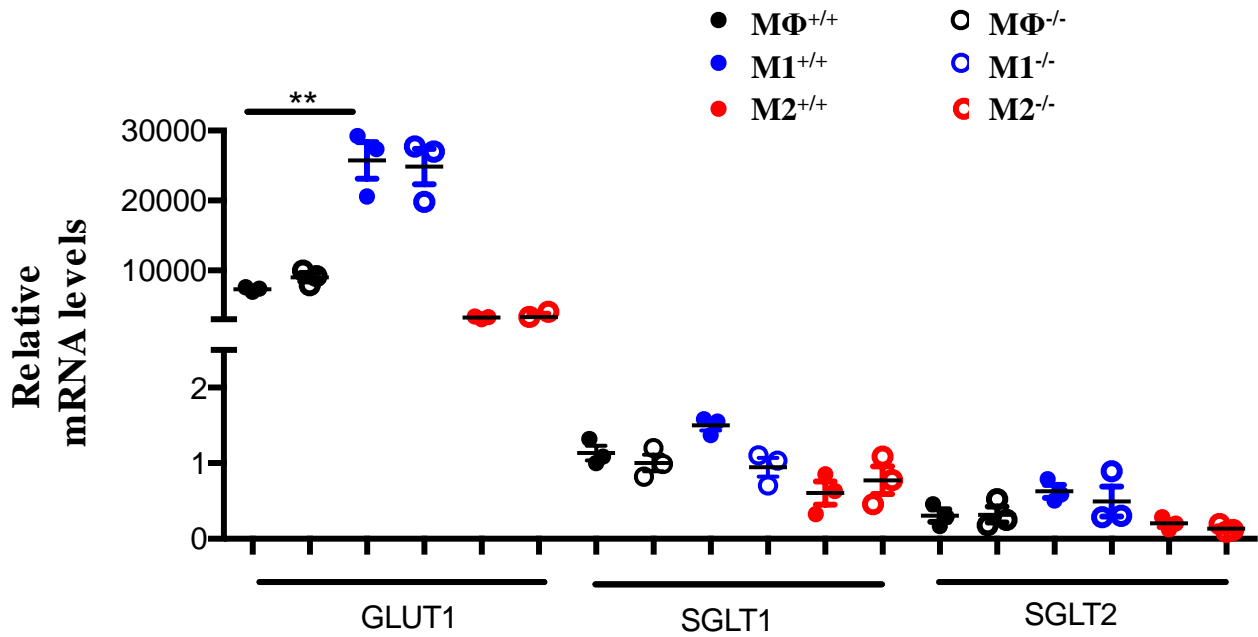


Figure 31. Expression of glucose transporters in *Gpr35*^{+/+} and *Gpr35*^{-/-} bone marrow-derived macrophages (BMDM).

Expression of GLUT1, SGLT1 and SGLT2 was evaluated in *Gpr35*^{+/+} (filled dots) and *Gpr35*^{-/-} (empty dots) MΦ (black), M1 (blue) and M2 (red) BMDM. Murine mRNA was evaluated by quantitative (real-time) RT-PCR analysis (mean ± SEM of 3 mice). **P < 0.01 vs MΦ BMDM.

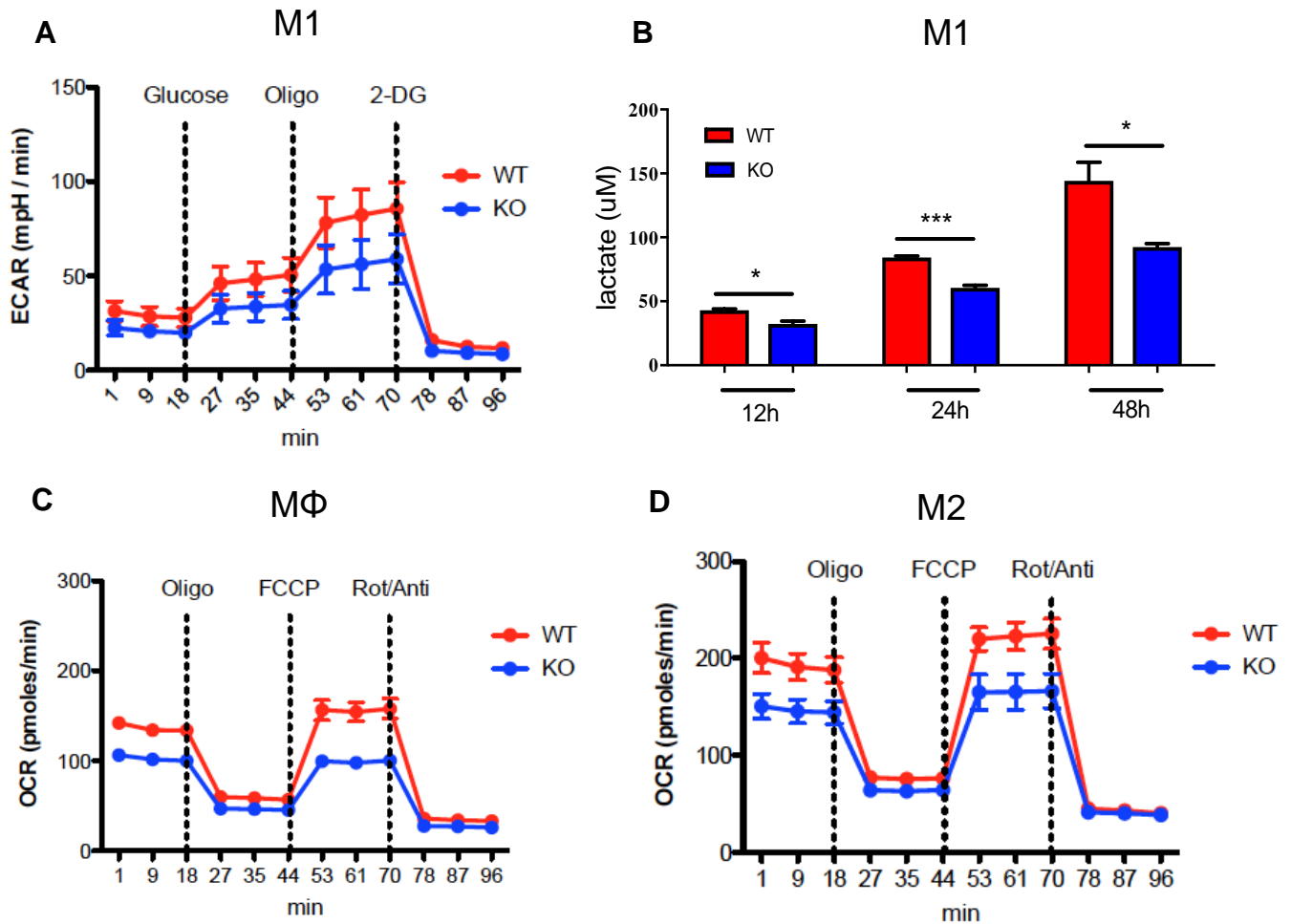


Figure 32. Effect of GPR35 deletion on metabolic profile of macrophages.

(A) Extracellular acidification rate (ECAR) and (B) lactate production were measured in *Gpr35*^{+/+}(red) and *Gpr35*^{-/-} (blue) M1 macrophages. ECAR was measured during sequential injection of Glucose, Oligomycin and 2-deoxyglucose (2-DG). **P* < 0.05 and ****P* < 0.001 vs wild-type BMDM (unpaired, Student's *t*-test).

The oxidative phosphorylation (OXPHOS) was measured in *Gpr35*^{+/+}(red) and *Gpr35*^{-/-}(blue) MΦ macrophages (C) and M2 macrophages (D), during sequential treatment with Oligomycin, FCCP and Rotenone/Antimycin. Data are from one experiment with three mice representative of three independent experiments. All data represented as mean ± SEM.

1.3 GPR35 influences angiogenesis via macrophages

Further, we explored the possible GPR35 function in the angiogenic process. CXCL1/GRO alpha, also known as KC in mouse, is a member of the CXC family of chemokines which promotes angiogenesis in colorectal cancer (Ohlsson et al., 2016). We measured the KC levels in supernatants of *Gpr35*^{+/+} and *Gpr35*^{-/-} MΦ, M1 and M2 macrophages. M2-phenotype macrophages are mostly involved in promoting angiogenesis and contributing to tissue remodeling and tumour progression (Dong et al., 2017). As expected, we found a higher levels of KC in the supernatant of M2 compared with MΦ and M1 macrophages (Figure 33A). Interestingly, *Gpr35*^{-/-} M2 macrophages produced a less amount of KC compared with wild type cells.

To investigate if macrophages may influence the formation of microvessel-like structures we assessed a co-culture system consisting of murine endothelial cell line (SVEC4-10) and M2-macrophages. SVEC cells were cultured for 6h at 37°C in presence of conditioned medium of wild type and knock-down M2 macrophages. *Gpr35*^{-/-} M2- stimulated SVEC4-10 showed a trend towards reduction in all angiogenetic parameters (nodes, junctions, segments) compared to wild-type M2 macrophages cultured endothelial cells (Figure 33B for the representative images and for the quantification of tube network).

Finally, we studied the mechanism of angiogenesis in the aortic ring model. This model is based on the capacity of mouse aortic explants to form new vessels (Aplin et al. 2008). The system is regulated by macrophages, pericytes and fibroblast through a complex molecular cascade (Nicosia, 2009). Interestingly, when assessing sprout numbers, we observed a 65% reduction of ‘neo-vessels’ in aortas from mice lacking GPR35 (Figure 34). GPR35 was identified as a potential receptor for CXCL17, a mucosal chemokine that promotes the tumour growth and angiogenesis (Maravillas-Montero et al. 2017, Weinstein et al. 2006). We took advantage of pro-angiogenic effect of CXCL17 in the aortic ring model, treating both *Gpr35*^{+/+} and *Gpr35*^{-/-} aortas. CXCL17 caused an increase (about 32%) of neo-vessels formation in *Gpr35*^{+/+} aortic rings, but not in KO aortas (Figure 34). These data confirm that the effect in aortic sprouts was mediated by GPR35.

All together these results show that the lack of GPR35 inhibits the formation of neovessels *in vitro* and *ex vivo* and interestingly the effect seems to be mediated by M2-macrophages.

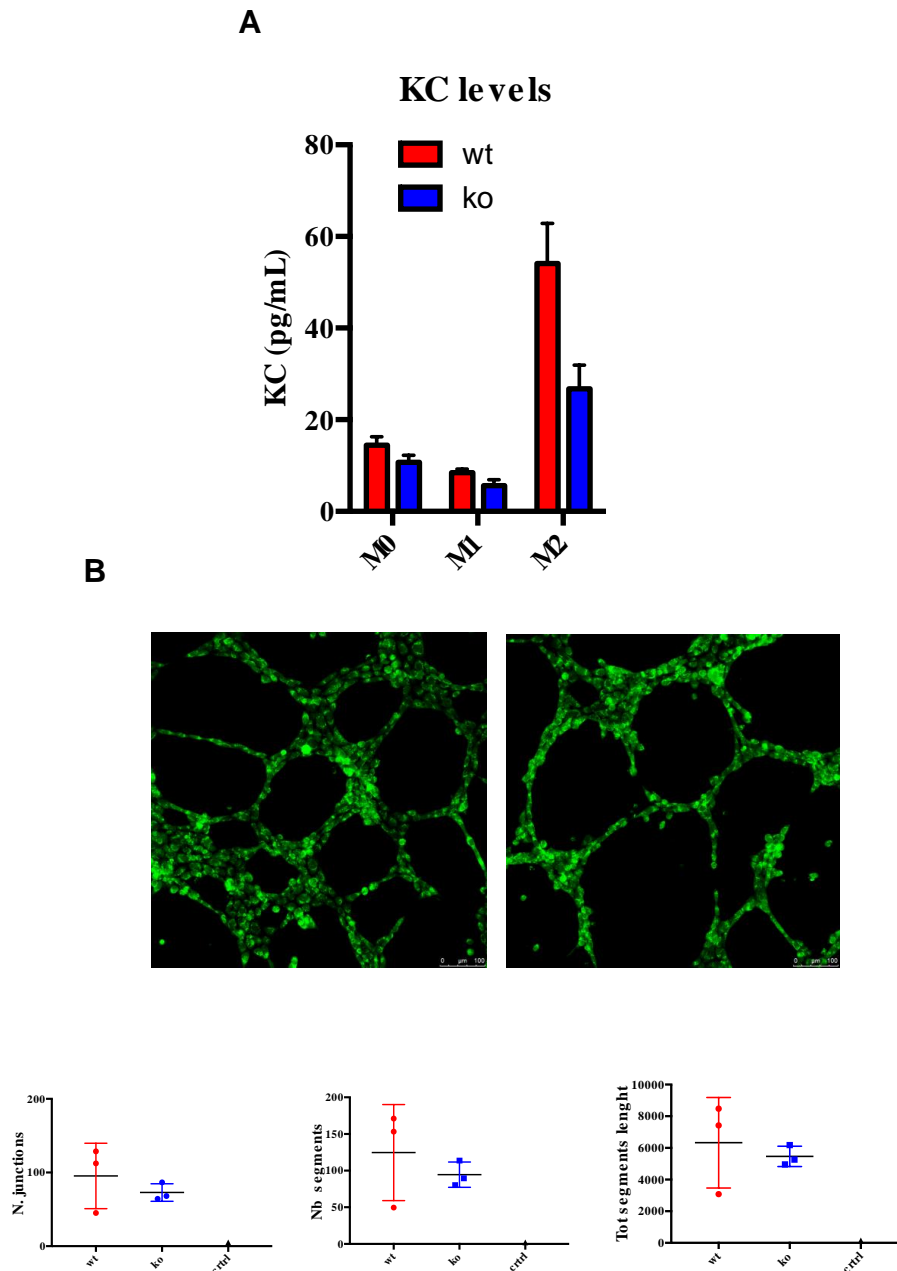


Figure 33. Effect of GPR35 deletion on angiogenesis via macrophages.

(A) CXCL1/GRO alpha, also known as KC in mouse is a member of the CXC family of chemokines. KC was detected in macrophages (MΦ, M1 and M2) supernatants.

(B) Representative images of SVEC cells incubated for 6h with conditioned media from *Gpr35*^{+/+} (M2 macrophages (left) and *Gpr35*^{-/-} M2 macrophages (right).

(C) Quantification of tube network (i.e. number of junctions, number of segments and length of segments) was assessed using Image J with the Angiogenesis Analyzer in SVEC cells incubated for 6h with conditioned media from *Gpr35*^{+/+} M2 macrophages (red) and *Gpr35*^{-/-} M2 macrophages (blue) or with RPMI (control, black). Data are from one experiment with three mice. All data represented as mean ± SEM.

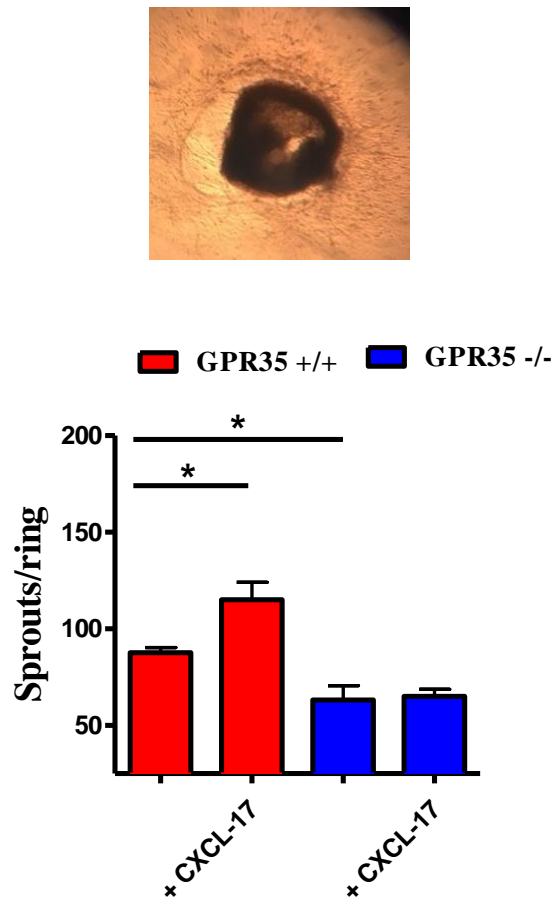


Figure 34. The effect of lack of GPR35 in aortic ring model.

(bottom) Quantification of aortic sprouts from *Gpr35*^{+/+} (red) and *Gpr35*^{-/-} (blue) mice (left), treated or not with CXCL17 (0.2 mg/ml), was counted by using the microscope. Results represent the mean \pm SEM of 5 mice * p <0.05.

(top) Representative image of aortic ring from wild-type mouse.

1.4 GPR35 is involved in experimental colitis-associated cancer and sporadic colon cancer

GPR35 is abundantly expressed in colonic epithelium; moreover, most cancer cells show conspicuous alterations in glucose metabolism. For this reason, we then evaluated whether GPR35 was involved in intestinal tumour progression using different models of intestinal tumour development.

In the CAC model, the number of colonic tumours significantly decreased in *Gpr35*^{-/-} mice treated with AOM and DSS compared with wild type mice (Figure 35A), suggesting that the absence of GPR35 reduced the intestinal tumour growth driven by colitis. Also, the lack of GPR35 partially protected the mice from AOM/DSS-induced weight loss, compared with wild-type mice (Figure 35B).

Moreover, we also observed a significant decrease in number of intestinal tumours of 15-week-old *Gpr35*^{-/-};*Apc*^{min} compared with *Gpr35*^{+/+};*Apc*^{min} and *Gpr35*^{+/-};*Apc*^{min} mice (Figure 35C). Therefore, the deletion of GPR35 protects mice from colitis-induced intestinal cancer and *Apc*^{Min}-dependent intestinal tumorigenesis.

As this result was observed in global GPR35 knock-out mice we also have generated a conditional mouse lacking GPR35 in the intestinal epithelium (*Gpr35*^{AIEC}). As shown in the Figure 35D *Gpr35*^{AIEC};*Apc*^{min} mice had a significant lower amount of tumours compared with non-transgenic *Apc*^{min} mice for GPR35 (*Gpr35*^{WT};*Apc*^{min}), suggesting that the effect in tumour progression could be selectively mediated by GPR35 in the intestinal epithelial cells.

1.5 GPR35 affects intestinal epithelial cell turn-over under homeostatic conditions

Then, we investigated the role of GPR35 in the baseline turn-over of intestinal epithelial cells (IECs). As depicted in Figure 36, the number of IECs that had migrated along the crypt-villous axis after a 24h pulse of BrdU was reduced by more than 50% in *Gpr35*^{-/-} compared to wild-type mice.

We subsequently investigated if GPR35 may act by directly promoting proliferation of the epithelial cells using colonic organoid cultures. This method allows long-term culture of isolated intestinal crypts or intestinal stem cells (Sato et al., 2009). The Figure 37 shows a representative image of colonic organoids from wild-type and GPR35-ko mice. Organoids from GPR35-ko mice had a significant lower number of Edu-positive cells compared with non-transgenic mice (Figure 37). This means that the lack of GPR35 reduced the cell proliferation as indicated by Edu-incorporation in intestinal stem cells, located at crypt bottom of colonic organoids (Figure 37). These data support the finding that GPR35 promotes intestinal tumorigenesis through an increase of proliferation.

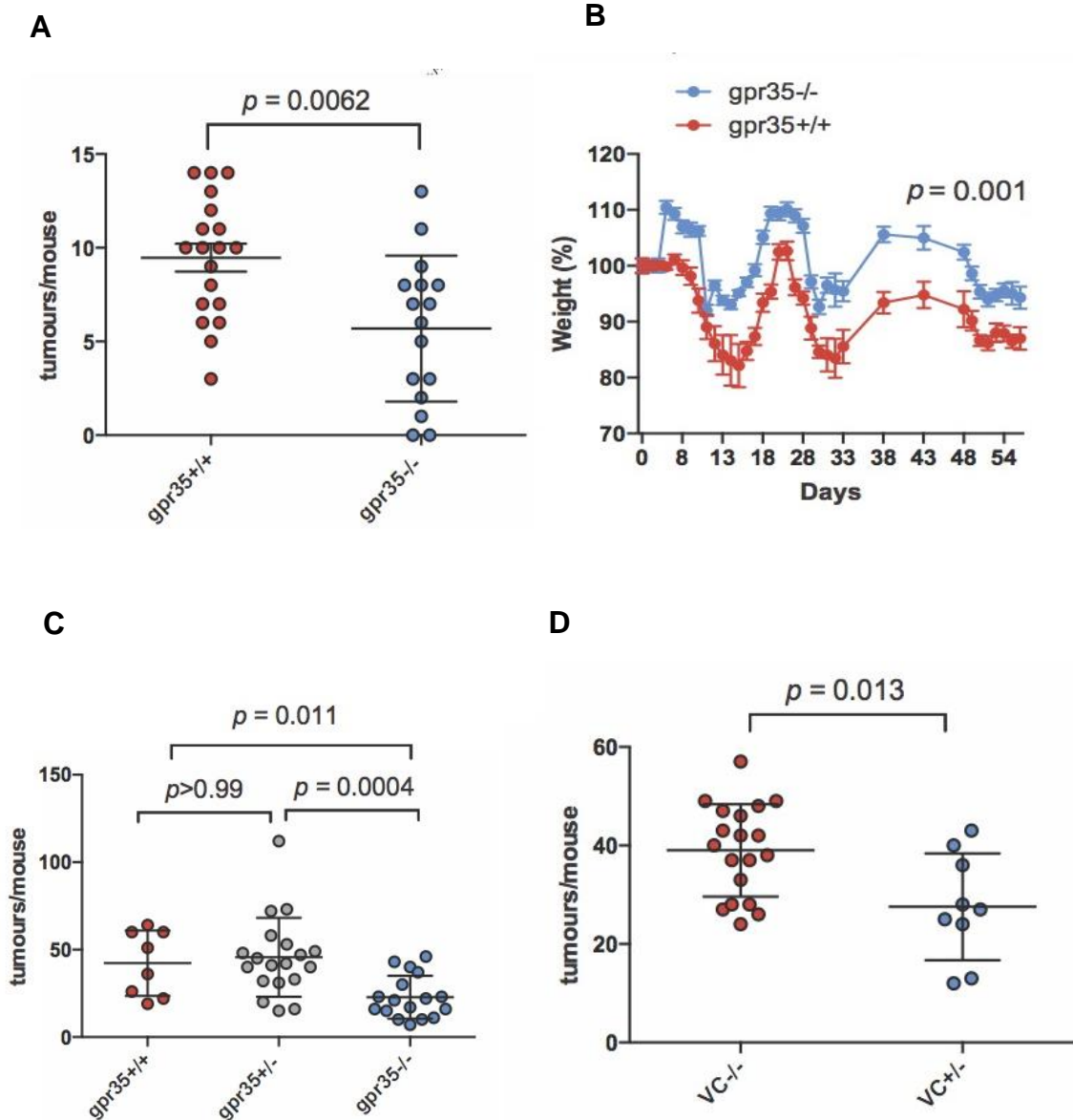


Figure 35. Role of GPR35 is involved in colitis-associated cancer and sporadic colon cancer.

(A) Number of tumours in the large intestine of 6-8 week-old *Gpr35*^{+/+} (red) and *Gpr35*^{-/-} (blue) mice in the AOM-DSS model.

(B) Body weight comparison between 6-8 week-old *Gpr35*^{+/+} (red, n=19) and *Gpr35*^{-/-} (blue, n=16) mice in the AOM-DSS model, normalized to day 0 within each cohort.

(C) Number of total tumours in the small and large intestine of 15-week-old *Gpr35*^{+/+}; *Apc*^{min}, *Gpr35*^{+/-}; *Apc*^{min} (grey) and *Gpr35*^{-/-}; *Apc*^{min} (blue) littermates.

(D) Number of total tumours in the small and large intestine of 15-week-old *Gpr35*^{WT}; *Apc*^{min} (red, VC^{-/-}) and *Gpr35*^{AIEC}; *Apc*^{min} (blue, VC^{+/-}) littermates.

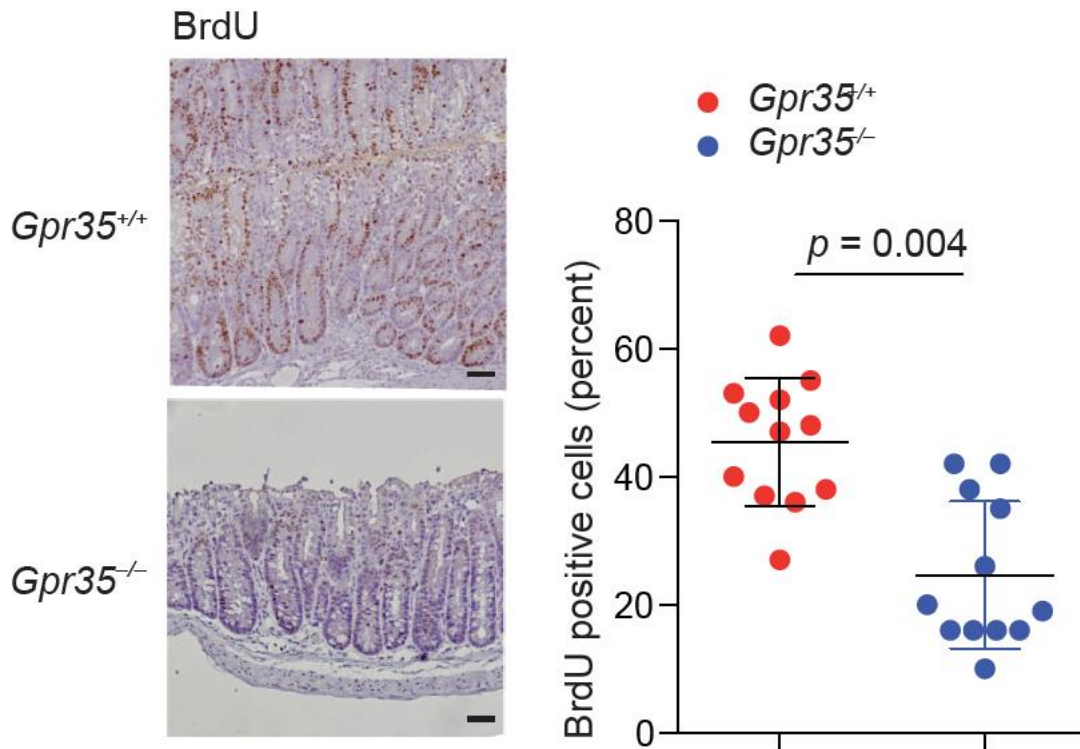
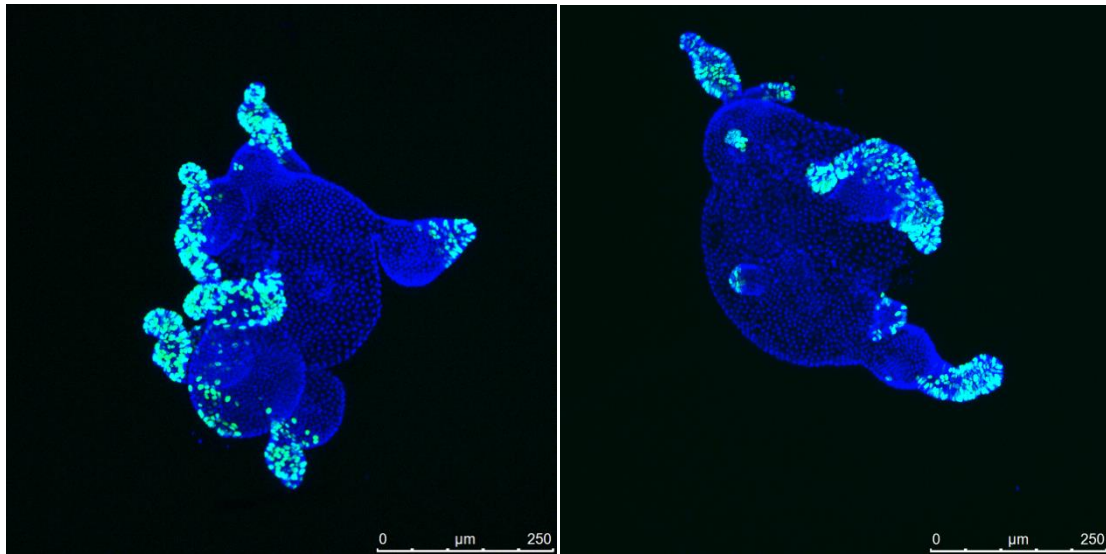


Figure 36. Role of GPR35 in the intestinal epithelial cell turnover under homeostatic conditions.

Immunohistochemistry of BrdU incorporation after a 24 hours pulse in intestinal sections from *Gpr35^{+/+}* (red) and *Gpr35^{-/-}* (blue) mice. Representative images (left panel). Quantification of cells staining positive for BrdU (right panel). Each data point represents one crypt villus axis from 3 individual mice per group.

A EdU/DAPI



B

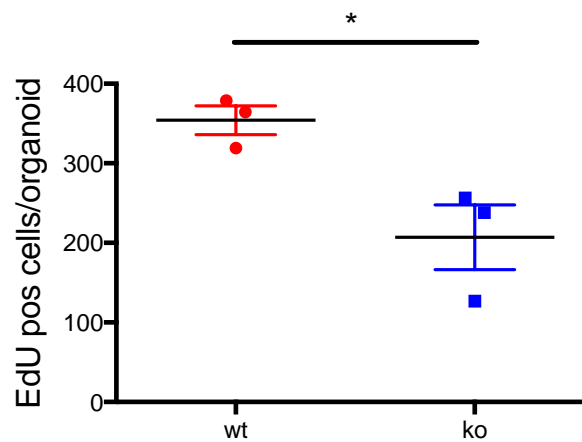


Figure 37. Role of GPR35 in the epithelial cell proliferation using colonic organoid cultures.

(A) Representative images of colonic organoids grown out of colonic crypts collected from *Gpr35*^{+/+} (left) and *Gpr35*^{-/-} (right) mice. Immunofluorescent staining of organoids was performed, and the cell proliferation was marked by incorporation of 5-ethynyl-2'-deoxyuridine (EdU, a thymidine analogue) into DNA.

(B) Quantification of number of EdU positive cells/organoid using Image J. All data represented as mean ± SEM. **P* < 0.05 vs positive cells/organoid in wild-type mice.

DISCUSSION

Part I. Pharmacological inhibition of MAGL reduces experimental colon tumorigenesis

MAGL is a serine hydrolase that plays a major role in the degradation of the endocannabinoid 2-AG. MAGL and 2-AG have been involved in a number of tumour types (Nomura et al. 2010; Melck et al. 2000; Orellana-Serradell et al., 2015; Ligresti et al., 2003; Nithipatikom et al., 2011; Nomura et al., 2011). However, the role of MAGL in colorectal cancer physiopathology is both under-researched and controversial (Sun et al., 2013; Ye et al., 2011), with no study attempting to relate MAGL and its main substrate 2-AG to angiogenesis. Here, we have shown that MAGL and 2-AG are present in tumour tissues and that pharmacological inhibition of MAGL results in chemopreventive (AOM model) and curative (xenograft model) effects in colon carcinogenesis.

1.1 Presence of MAGL and 2-AG in the xenograft tumour tissue

Monoacylglycerols such as the endocannabinoid 2-AG, are metabolized to free fatty acids and glycerol by MAGL. MAGL has been shown to be up-regulated in aggressive compared to non-aggressive tumour cell lines as well as in primary tumours (Mulvihill and Nomura, 2013; Van Dross et al., 2013). Here, we have shown that tumour tissues generated by injection of human colorectal cancer (HCT116) cells in nude mice express both mRNA MAGL and its related protein. Due to the use of specific human antibodies, it is very likely that the detected MAGL mRNA in the tumour xenograft derives from human epithelial cells, possibly underwent to phenotypic changes during tumour implantation and growth. Others have shown that MAGL was up-regulated in colorectal cancer patient tissues (Ye et al., 2011).

Because MAGL is the main enzyme responsible for 2-AG degradation, we measured its levels in the tumour mass. 2-AG, which is known to exert antiproliferative effects in colorectal cancer cells (Ligresti et al., 2003) was shown to be elevated in the mouse colon with aberrant crypt foci induced by AOM (Izzo et al., 2008) as well as in colorectal polyps and tumours of CRC patients (Ligresti et al., 2003). In our study we have revealed, in tumour tissues, amounts (300 pmol/mg of lipid extract) of 2-AG that were about four-fold higher than those detected in HCT116 cells and healthy tissues derived from the contralateral flank of xenografted mice (i.e. the flank not injected with xenografted cells).

1.2 Effect of URB602 on 2-AG levels, tumour progression and angiogenesis

In order to evaluate tumour progression, angiogenesis and 2-AG levels associated to MAGL inhibition, we selected the MAGL inhibitor URB602, i.e. the first compound reported with selectivity for MAGL over fatty acid amide hydrolase (FAAH) (Fowler, 2012). Although the *in vitro* selectivity of high concentrations of this compound (2-AG vs anandamide hydrolysis) has been questioned (Vandevoorde et al., 2007), its functional selectivity has been demonstrated by the

ability to elevate 2-AG levels in hippocampal slice cultures without affecting levels of other endocannabinoid-related molecules (Hohmann, et al., 2005; King et al., 2007). In contrast to directly-activating CB1 receptor agonists, URB602, given i.p. at doses less than 10 mg/kg, did not induce catalepsy and hypothermia (Comelli et al., 2007).

i) Effect of URB602 on 2-AG levels in xenograft tumour tissues.

We have found that URB602, at the daily dose of 5 mg/kg, which is significantly lower than that found to be active at, *e.g.*, reducing upper intestinal transit (Duncan et al., 2008), showed only a non-significant trend toward an increase in 2-AG levels in the xenograft tumour tissue. The failure of URB602 to significantly increase 2-AG levels could be due to the high levels of the endocannabinoid already present in the tumour tissue (see above). In fact, under the same experimental conditions, URB602 increased 2-AG levels in healthy tissues, where the basal levels of 2-AG are not so high like in tumour mass. Importantly, in this set of experiments, we found that URB602 significantly and selectively increased (by approximately four-fold) 2-AG levels, without significantly affecting the levels of anandamide (non-significant two-fold increase) and the related acylethanolamides (*i.e.* PEA and OEA).

ii) Effect of URB602 on xenograft tumour progression

Previous studies have shown that 2-AG as well as inhibitors of 2-AG hydrolysis exerted anti-tumorigenic (antiproliferative, inhibition of invasion and cell migration) effects in a number of cancer cell lines, including prostate, ovarian, breast and melanoma cells (Mulvihill and Nomura, 2013; Van Dross et al., 2013). However, the role of MAGL in colorectal cancer cells is controversial. Ye and colleagues found that colorectal cancer cell growth and invasion were inhibited by pharmacological and siRNA mediated MAGL knock-down (Ye et al., 2011). By contrast, a more recent paper highlighted the potential tumour suppressive role of MAGL in colorectal cancer cell lines, based on the findings that over-expression of MAGL suppressed colony formation in cell lines and knockdown of MAGL resulted in increased Akt phosphorylation (Sun et al., 2013). In the present study we have shown that URB602, at the daily dose of 5 mg/kg, reduced the growth of tumours generated by xenograft injection of colorectal cancer cells in athymic mice. It is important to further emphasize that URB602 reduced tumour growth at a dose devoid of central side effects (Comelli et al., 2007) and which selectively inhibits the metabolism of 2-AG without affecting the hydrolysis of anandamide and related acylethanolamide (present results, see above). Consistent with our data, Ye and colleagues showed that JZL184, a potent and selective MAGL inhibitor, reduced tumour formation generated by xenograft injection of colorectal cancer (Caco-2) cells in nude mice (Ye et al., 2011).

iii) Effect of URB602 on angiogenesis and proliferation in xenograft tumour tissues

A fundamental feature of tumour progression is the accomplishment of abundant vascular development to sustain the growing tumour mass (Hanahan and Folkman, 1996). Therefore, we evaluated the impact of URB602 on a number of angiogenesis markers in tumour-bearing mice. Although no specific study on 2-AG or MAGL on angiogenesis exists, cannabinoids, in addition to their cancer cell death promoting effects, have been also shown to normalize tumour vasculature (Blázquez et al., 2003; Pisanti et al., 2011; Pisanti et al., 2013; Velasco et al., 2015). In cancer cells, cannabinoids inhibit the activation of the vascular endothelial growth factor (VEGF) cascade, which is considered the most important and well-characterized pathway contributing to angiogenesis (Ferrara, 2004; Shibuya, 2011), and a number of elements of this cascade are down-regulated by cannabinoids, for example, in skin carcinomas, gliomas and thyroid carcinomas [see Velasco et al., 2016, for review].

Here, we have provided a number of evidences suggesting that URB602 acts via inhibition of angiogenesis. Indeed: URB602 i) reduced the expression of VEGF, which is considered the most important and the well-characterized contributor to angiogenesis (Ferrara, 2004; Shibuya, 2011); ii) reduced density, structure and composition of tumour vessels. Furthermore, using HUVEC we were able to recapitulate *in vitro* the anti-angiogenic effect of URB602. To the best of our knowledge, this represents the first demonstration about the involvement of MAGL and of its main substrate 2-AG in angiogenesis.

Lastly, our results show that the beneficial effect of URB602 was associated to down-regulation of cyclin D1, a specific cyclin required for tumour progression. Down-regulation of cyclin D1 is known to restrict the cell cycle progression to the G0/G1 phase. Conversely, cyclin D1 over-expression has been observed in 68.3% of human colorectal cancer, suggesting a role in human colorectal tumorigenesis (Bahnassy et al., 2004). Others have shown that the putative endocannabinoid noladin ether down-regulated cyclin D1 expression in prostate cancer cells and that Met-F-anandamide (a synthetic analogue of anandamide) in combination with the FAAH inhibitor URB597, induces G0/G1 cell cycle arrest by down-regulating cyclin D1 (Ravi et al., 2014). However, in the present study no significant effect of URB602 on the cycle-negative regulator p27KIP was observed.

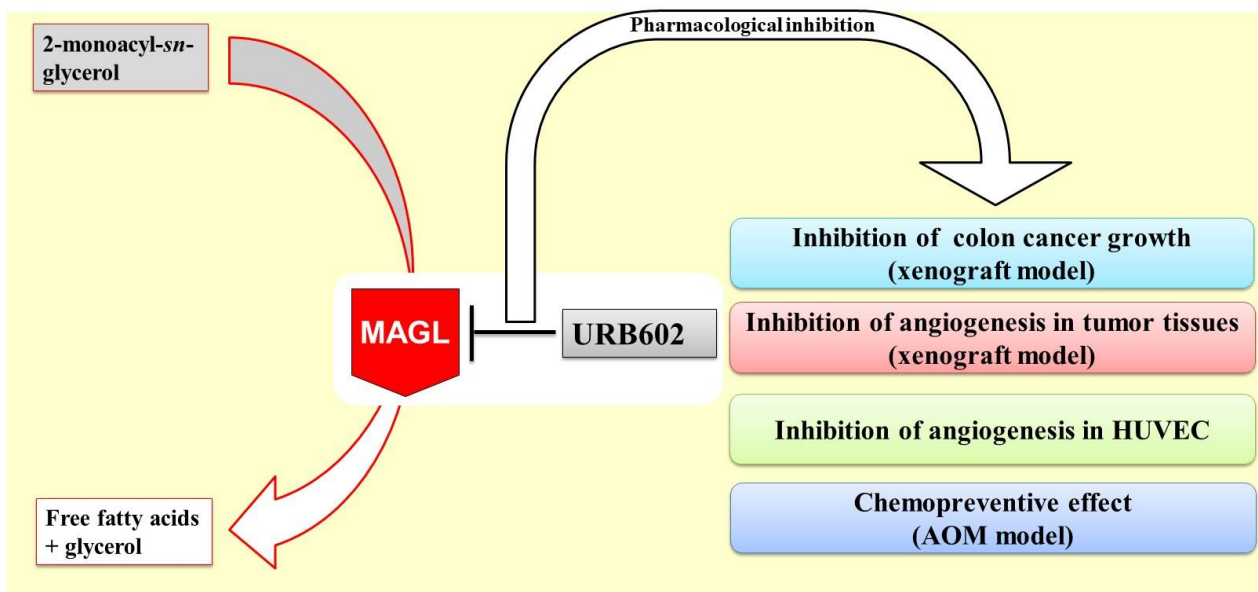
1.3 Effect of URB602 in the azoxymethane (AOM) model of colon carcinogenesis

In a different set of experiments, we evaluated the chemopreventive effect of URB602 in a model of colon carcinogenesis induced by AOM. Because the development of colon cancer spans about 10–15 years, chemoprevention is a great opportunity to counteract this fatal disease. The AOM model can experimentally induce carcinogenesis similar to the pathogenesis of human sporadic colon

cancer. In support to this assertion, there is the observation that sporadic CRC and the AOM model share several pathways and mechanisms, including K-ras, β -catenin and TGF β mutations. (Chen and Huang, 2009). Repetitive intra-peritoneal treatment of mice with AOM causes the formation of preneoplastic lesions (ACF), polyps and tumours in the distal colon. We have previously shown that the pharmacological enhancement of endocannabinoid levels (through inhibition of anandamide hydrolysis by the FAAH inhibitor N-arachidonoylserotonin) as well as the cannabinoid receptor agonist HU-210 attenuated the development of ACF in the mouse colon (Izzo et al., 2008). Here, we have shown that MAGL is over-expressed in the colon of AOM-treated mice and, more importantly, that URB602 reduced, approximately by one half, the number of ACF, polyps and tumours. Importantly, the effect of URB602 was absent in MAGL-deficient mice, thus suggesting that the drug is acting selectively via inhibition of MAGL and not through other potential unspecific mechanisms.

1.4 Concluding remarks

In summary, we have shown that MAGL and its main substrate 2-AG are abundantly present in the colorectal cancer tissues and that a pharmacological inhibition of the enzyme by URB602, which selectively increases 2-AG *in vivo*, resulted in chemopreventive and curative effects in experimental models of colon carcinogenesis. Importantly, the chemopreventive effect of URB602 was abrogated in *Mgll*-null mice. The antitumour effect of URB602 *in vivo* was associated to inhibition of angiogenic process and reduction of cyclin D1, a marker of cell proliferation. Furthermore, studies on human endothelial cells have shown that the URB602 exerted a direct antiangiogenic effect.



Part II. NAAA is crucially involved in proliferation, migration and *in vivo* colon tumorigenesis

NAAA is a lysosomal enzyme which hydrolyses a number of N-acyl ethanolamines at acidic pH. The preferred NAAA substrate is PEA, a lipid mediator chemically-related to the endocannabinoid anandamide.

Although NAAA role has been investigated in bladder and prostate cancer (Wang et al., 2008; Liu et al., 2014; Du et al., 2016; Vago et al., 2017), no information has been published to date about its possible physiopathological role in CRC. Here, we have shown that i) NAAA is down-regulated in human colorectal cancer biopsies and ii) pharmacological inhibition of NAAA – as well as PEA administration - reduces experimental colon carcinogenesis *in vivo* and decreases the proliferation and migration of human colorectal cancer cell lines.

1.1 NAAA and PPAR- α expression in human CRC

NAAA expression has been shown to be higher in non-aggressive prostate cancer (PC) - compared with aggressive PC - (Liu et al., 2014) and to be up-regulated in aggressive mouse ovarian cancer (Du et al., 2016). We observed a significant reduction in NAAA expression in CRC tissues compared to that detected in adjacent non-tumours tissues. Because NAAA is the main enzyme responsible of PEA degradation (Alhouayek et al., 2015), we next focused on the expression of the key targets of PEA in different TNM stages of CRC patients. PEA is a bioactive lipid that strongly alleviates pain and inflammation in animal models and in humans. Several studies demonstrated that PEA can act via direct activation of the PPAR- α (Lo Verme et al., 2005) and many of its pharmacological properties are generally mediated by PPAR- α (Alhouayek and Muccioli, 2014; Gugliandolo et al., 2018; Esposito and Cuzzocrea, 2013; Skaper et al., 2015; Iannotti et al., 2016). Here, we have found that PPAR- α was down-regulated in tumours of patients with stage pT3 and pT4 compared to normal tissues. PPAR- α function in cancer is still uncertain and currently under investigation, and it may be differently related to cancer/cell type of the tumour (Gou et al., 2017). Both PPAR- α agonists and antagonists have been shown to exert antiproliferative effects in cancer cells and to attenuate carcinogenesis *in vivo*. For example, PPAR- α activation increases proliferation in breast and renal cancer cell lines (Suchanek et al., 2002; Abu Aboud et al., 2013) and causes liver cancer in rodents, with PPAR- α null-mice to be resistant to hepatocarcinogenic effects of PPAR- α agonists (Peters et al., 1997; Zak et al., 2010; Li et al., 2014; Hann et al., 2013). On the other hand, the PPAR- α antagonists MK886 and NXT629 also inhibit chronic lymphocytic leukemia (CLL) cell proliferation (Spaner et al., 2013; Messmer et al., 2015).

1.2 Effect of AM9053 on experimental carcinogenesis

In order to assess the role of NAAA on experimental tumour progression, we took advantage of AM9053, a potent and selective NAAA inhibitor. Although its electrophilic isothiocyanate moiety,

AM9053 reversibly interacts with the enzyme (West et al., 2012; Malamas et al., 2015). AM9053 is the first NAAA inhibitor active following systemic administration *in vivo* (Alhouayek et al., 2015) and its selectivity has been demonstrated by the ability to increase PEA, but not AEA, levels in experimental colitis (Alhouayek et al., 2015).

i) Effect of AM9053 on xenograft tumour growth.

In the present study, we have demonstrated that AM9053, at dose of 20 mg/kg, reduced the xenograft tumour growth generated by injection of colorectal cancer cells (HCT116) in athymic mice. In line with our results, Alhouayek and colleagues showed that AM9053, at same dose, reduced colonic inflammation, an effect associated with a selective increase of endogenous PEA levels (Alhouayek et al., 2015). This observation is relevant in the well-established relationship existing between intestinal inflammation and CRC genesis and development (Terzic et al., 2010). Others have been shown that NAAA inhibitors are effective in experimental models of inflammation and pain (Bonezzi et al., 2016; Petrosino et al., 2015; Sasso et al., 2018; Alhouayek et al., 2015).

To further explore AM9053 mode of action, we considered the possible involvement of receptors (i.e. CB receptors, TRPV1, GPR55 and PPAR- α), which have been shown, based on pharmacodynamic studies, to be targeted by PEA (Petrosino and Di Marzo, 2017). Among PEA targets, we have found a reduction of PPAR- α expression only, following AM9053 treatment, suggesting a possible involvement of such target in the antitumoural effect of AM9053.

ii) Effect of AM9053 and exogenous PEA on tumours induced by azoxymethane (AOM)

We provided further evidence to support the role of NAAA in the experimental colon carcinogenesis by using the AOM model of colon cancer (Neufert et al., 2007). AOM is a potent carcinogen that cause a high number of tumours in the distal colon. This model is extensively used to study the mechanisms underlying human sporadic colon cancer as well as to evaluate drug potential chemopreventive effects (Neufert et al., 2007).

Previous studies have shown that pharmacological inhibition of FAAH and MAGL, by increasing the levels of AEA and 2-AG, respectively, reduced the development of tumours in the AOM model (Izzo et al., 2008, Pagano et al., 2017 see Chapter I). Here, we have shown that AM9053 reduced, approximately by 40%, the number of AOM-induced tumours. Similar to NAAA inhibition, exogenous administration of PEA produced a significant reduction in the tumours number caused by the injection of AOM.

1.3 Effect of AM9053 and exogenous PEA on proliferation and migration of colorectal cancer cells

We have here reported, for the first time, that NAAA mRNA is expressed in two different colorectal cancer cell lines, i.e. Caco-2 and HCT116. More importantly, we have found a down-regulation of NAAA in Caco-2 and HCT116 cells incubated with secretome derived from xenograft tumours. In recent years, the innovative proteomic technologies have greatly accelerated studies on the cancer secretome (Xue et al., 2008; Hsiao et al., 2017). Tumoural and stromal cells secrete a number of proteins, including growth factors, proteinase, immunoregulatory cytokines, cell motility factors or other bioactive molecules able to crucially regulate the tumour microenvironment (Hsiao et al., 2017; Cordani et al., 2016). Indeed, these cancer secreted proteins are essential in the processes of differentiation, invasion, metastasis and angiogenesis by regulating cell-to-cell and cell-to-extracellular matrix interaction (Xue et al., 2008; Cordani et al., 2016). The effect of cancer secretome (from xenograft model) on NAAA expression in Caco-2 cells adds further support to the observation that NAAA is dysregulated in colon cancer patients and that the tumoural microenvironment may be responsible of such change in gene expression.

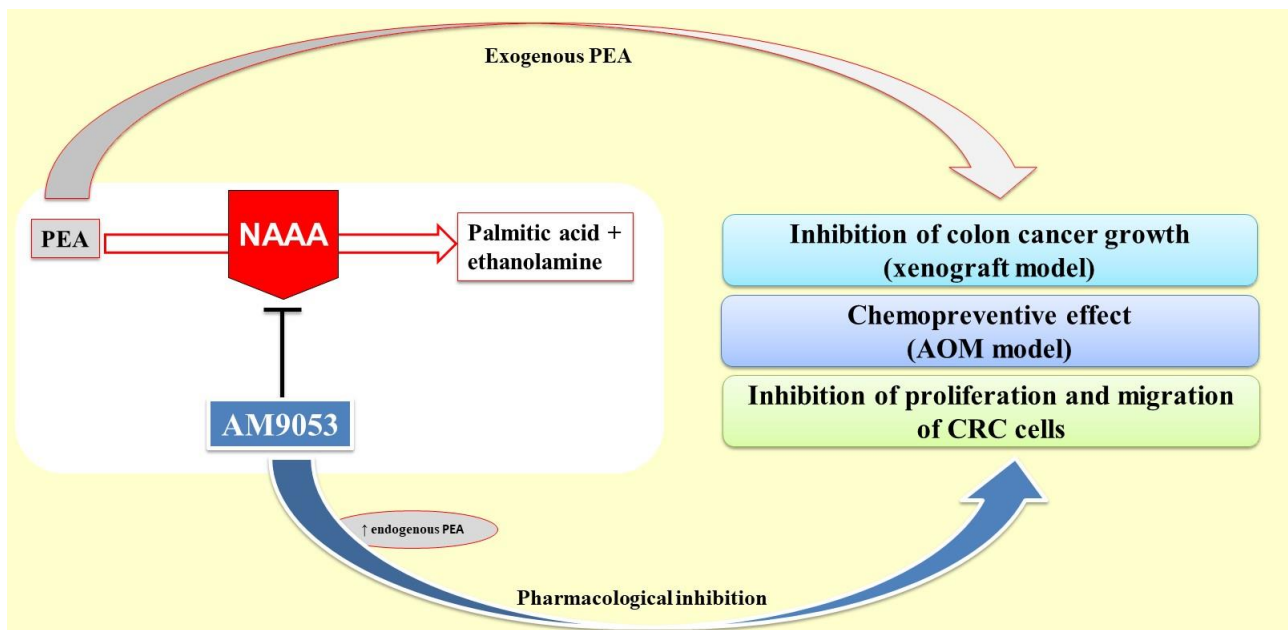
The antitumoral effects of the NAAA inhibitor AM9053 and of exogenous PEA were also depicted by the decreased proliferation and migration of CRC cells. Indeed, we have shown that, in a concentration- dependent manner, AM9053 and PEA reduced proliferation in two colorectal carcinoma cell lines, i.e. Caco-2 and HCT 116 cells. It is noteworthy that the antiproliferative effect of AM9053 was observed at concentrations which were able to inhibit NAAA, but not FAAH, in enzyme assays (Malamas et al., 2015).

Importantly from a translational viewpoint, the effect of both AM9053 and PEA was specific for colorectal carcinoma cells, showing no antiproliferative effects in healthy colonic epithelial cells. Others have shown that PEA caused a reduction in proliferation and VEGF signalling in Caco-2 cells through a selective PPAR- α - dependent inhibition of Akt/mTOR pathway (Sarnelli et al., 2016).

It is well established that tumour metastasis, i.e. the movement of tumour cells from a primary site, is the major responsible for the deaths of cancer patients and that cell migration is the first step in the metastatic process (Wirtz et al., 2011; Steeg, 2016). Therefore, we evaluated the impact of AM9053 and PEA on the capability of CRC cells to migrate. By using the scratch assay, a method that measures cell migration *in vitro*, we have here demonstrated that pharmacological inhibition of NAAA, which is expected to increase PEA levels, or exogenous administration of PEA reduced the migration of CRC cells.

1.4 Concluding remarks

In summary, we put forth the role of NAAA in colorectal cancer and propose NAAA inhibitors as a potential therapeutic strategy in CRC. Specifically, we have shown that NAAA inhibition results in antitumoural actions in two experimental models of colon cancer, i.e. the xenograft model and the model of chemoprevention induced by the carcinogenic agent AOM. Furthermore, studies on cells have shown that the NAAA inhibitor AM9053 reduced cell migration and exerted antiproliferative effects in tumoural – but not healthy – cells. Further studies using the genetic silencing of the enzyme will help us to confirm the role of NAAA in colon cancer development.



Part III. GPR35 promotes glycolysis, proliferation and colon tumorigenesis

GPR35, an orphan G protein coupled receptor, is mainly expressed in the colon and immune system (Wang et al., 2006). A GWAS identified the *GPR35*^{T108M} polymorphism as novel risk locus for UC and PSC, that are diseases with a high-risk developing cancer (Ellinghaus et al. 2013). GPR35 seems to be upregulated in breast, gastric and non-small-cell lung cancer tissues, although its role and the signalling pathways are unknown (Guo et al., 2017; Okumura et al., 2004). Here, we have shown that GPR35 deletion in mice results in a decrease of i) glucose metabolism in macrophages, ii) colonic epithelium turnover and iii) number of tumours in experimental models of colon cancer.

1.1 GPR35 controls macrophages metabolism

Macrophages display a spectrum of functional activation phenotypes depending on the composition of microenvironment [*e.g.* variations in concentrations of metabolites (O'Neill, 2011; Tannahill et al., 2013; Rodriguez-Prados et al., 2010), lipids (El Kasmi et al., 2013), oxygen tension (Kelly and O'Neill, 2015), and cytokines (Hashimoto-Kataoka et al., 2015; Idzko et al., 2014)] (El Kasmi and Stenmark, 2015). Despite this huge range of *stimuli*, two distinct macrophage activation states (also called 'canonical activation') have been recognized, namely the M1 (or classically activated) macrophages and the M2 (or alternative activated) macrophages (Biswas and Mantovani, 2010). Polarized macrophages show also a distinct regulation of glucose metabolism, thus M1 phenotype displays a metabolic shift toward the anaerobic glycolytic pathway (Kelly and O'Neill, 2015).

In order to explore the GPR35 role in cell metabolism, we used the canonical activation of macrophages towards M1 and M2. We found that glucose uptake was deeply reduced in *Gpr35*^{-/-} BMDM, irrespective of polarizing conditions. Importantly, the reduced glucose uptake was not due to a different expression of glucose transporters, although a predominant role of GLUT1 was revealed functionally. GLUT1 mediates the constitutive glucose uptake, which occurs by facilitated diffusion in most cells and tissues (Lee et al., 2015) This suggests that the amount of consumed glucose drives the uptake. Therefore, *Gpr35*^{-/-} macrophages may need a lower amount of glycolysis substrate, suggesting an involvement of GPR35 in the cell energetic demand.

Thereafter, we assessed the metabolic profile of MΦ, M1 and M2 BMDM. The increased glycolysis in M1-polarized macrophages is permissive to quickly trigger microbicidal activity and cope with a hypoxic tissue microenvironment (Biswas and Mantovani, 2013). Interestingly, we proved that the lack of GPR35 resulted in a reduction in glycolysis and glycolytic capacity (as showed by extracellular acidification rate) in M1 BMDM compared to *Gpr35*^{+/+} BMDM, with a consequent decrease in lactic acid, the final product of aerobic glycolysis.

Although inflammatory M1 macrophages support their energetic needs preferentially via aerobic glycolysis (Warburg effect), MΦ and M2 macrophages rely mostly on oxidative phosphorylation

(OXPHOS) (Kelly and O'Neill, 2015). Additionally, here we have shown that oxygen consumption rate (OCR), a measure of OXPHOS was also reduced in *Gpr35*^{-/-} MΦ and M2 BMDM compared to wild-type cells, thus confirming that GPR35 is a key actor in cell energetic demand and production.

1.2 GPR35 affects angiogenesis

M2-polarized macrophages are known to contribute to tissue remodeling, repair, and wound healing under pathophysiological conditions (Biswas and Mantovani, 2010). Also, M2 macrophages may influence angiogenesis via both direct and indirect mechanisms, including elevated production of key angiogenic factors and secretion of matrix metalloproteinases, thus facilitating endothelial cell migration and tube formation (Zajac et al., 2013).

To verify if GPR35 interferes in the pro-angiogenic role of M2-macrophages, we used a co-culture system consisting of murine endothelial cells and M2-macrophages. Endothelial cells showed a reduction in the formation of microvessel-like structures when incubated with conditioned medium of *Gpr35*^{-/-} M2 BMDM. Furthermore, we have showed that *Gpr35*^{-/-} M2 BMDM produced lower amounts CXCL1 compared to wild type cells, which could explain the effect of conditioned medium on endothelial cells first mentioned. CXCL1 is the most significant cytokines derived from tumour-associated macrophages for inducing breast cancer metastasis (Wang et al., 2018). Also, CXCL1 high levels promote tumorigenicity and serve as a poor prognostic biomarker in metastatic CRC patients (le Rolle et al., 2015).

Finally, we observed that the capacity of the aortic endothelium to form neo-vessels was reduced (about 65%) in *Gpr35*^{-/-} mice. The aortic ring model is one of the most widely used methods to study angiogenesis and its mechanism, including the regulation of angiogenesis by macrophages, pericytes and fibroblasts (Aplin et al., 2008). It is worthy to note that CXCL17, i.e. a supposed GPR35 ligand, increased the neo-vessels formation only in the aortic cultures of wild type mice, but not in *Gpr35*^{-/-} aortic endothelium.

In conclusion, we provided evidence that the lack of GPR35 reduced neo-vessels formation, with M2 macrophages playing a crucial role.

1.3 GPR35 has a role in colonic proliferation and tumorigenesis

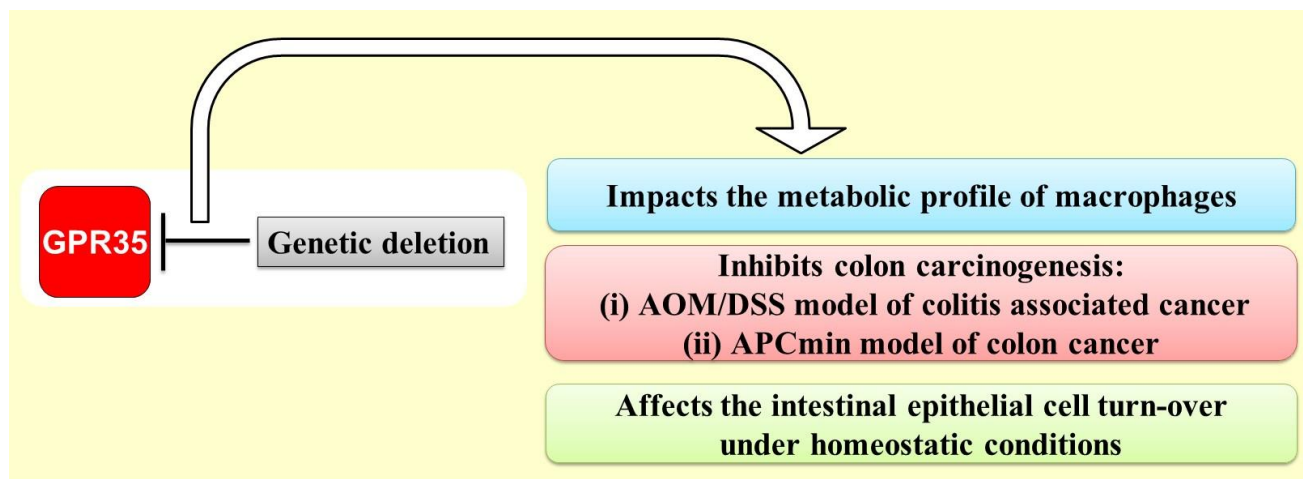
Because GPR35 is highly expressed in the intestine, we investigated the possible role of GPR35 in the intestinal epithelial cells (IECs). The number of IECs that migrated along the crypt-villous axis after a 24h treatment of BrdU was reduced by more than 50% in *Gpr35*^{-/-} compared to wild-type mice. Similarly, colonic organoids derived from *Gpr35*^{-/-} mice exhibited decreased proliferation as determined by fewer cells incorporating EdU compared to cultures derived from wild-type mice. These data demonstrated a ~40% reduction in the turn-over of the intestinal epithelium in the

absence of GPR35. The 3D organoid model is the most useful and innovative long-term culture of primary murine colonic epithelial cells mimicking intestinal epithelial function (Sato et al. 2009). Finally, we observed a protective effect of *GPR35* deletion, resulting in a reduction of tumours, in the *Apc^{min}* model of CRC sporadic and in the AOM/DSS model of CAC. Additionally, in the *Apc^{min}* model we have demonstrated that the protective effect was selectively mediated by GPR35. Indeed, *Gpr35^{ΔIEC}* (conditional mice lacking GPR35 in the intestinal epithelium); *Apc^{min}* mice had a significant lower number of tumours compared to non-transgenic *Apc^{min}* mice for GPR35 (*Gpr35^{WT}*; *Apc^{min}*).

1.4 Concluding remarks

We have shown that GPR35 plays a key role in cell energetic demand, as revealed in metabolic studies on macrophages. Moreover, the deletion of GPR35 in M2-macrophages resulted in a reduced ability to produce pro-angiogenic factors. Finally, GPR35 regulated the formation of neo-vessels in the aortic epithelium.

In vivo, the deletion of GPR35 reduced the turnover of intestinal epithelial cells in physiological conditions and protected mice from tumours formation in two different models of colon cancer. The effect on colon tumorigenesis could be due to GPR35 impact on cell metabolic profile, since it has been demonstrated that cancer cells rewire their metabolism to promote growth, survival, proliferation, and long-term maintenance.



GENERAL CONCLUSIONS

Colorectal cancer (CRC) is the most common gastrointestinal malignancy. Despite the continuous progresses in CRC diagnostic and therapeutic systems, which have reduced recurrence rates and are prolonging survival, steps forward can be achieved only by pointing to a better understanding of its pathogenesis.

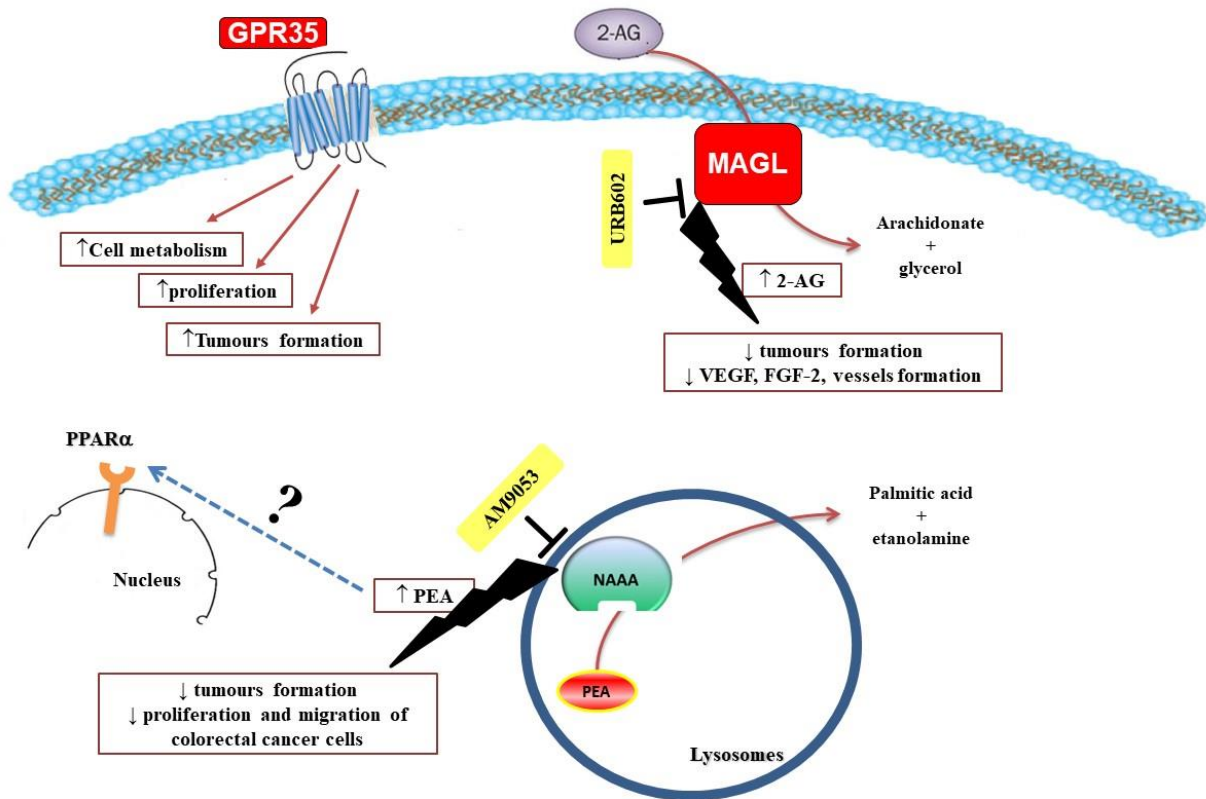
The experiments depicted in this PhD thesis highlight three potential targets, i.e. MAGL, NAAA and GPR35, implicated in colon carcinogenesis (see graphical conclusion).

Briefly, we have shown that:

- MAGL inhibition with URB602 was effective at increasing the endogenous levels of the endocannabinoid 2-AG and resulted in antitumour effects *in vivo*. The pharmacological inhibition of URB602 was selective for MAGL as demonstrated in *Mgll*-null mice. More in depth studies have demonstrated that tumour growth reduction may due to both proliferation and angiogenesis inhibition.
- NAAA was down-regulated in human and mouse colon cancer tissues. Both NAAA inhibition, by AM9053, and exogenous administration of PEA (i.e. the NAAA main physiological substrate) caused a reduction of colon cancer growth *in vivo*. AM9053 and PEA were effective antiproliferative agents, showing a selectivity toward CRC vs healthy colonic cells. It is worthy to emphasise that PEA is safe in humans and it is commercially available – as foods for special medical purposes – to alleviate inflammatory and painful conditions.
- GPR35 deletion impaired cell energetic demand in macrophages and reduced their ability to stimulate neo-vessels formation in the endothelium. Also, GPR35 physiologically regulated the turnover of intestinal epithelial cells in both *in vivo* and *ex vivo* models. Finally, GPR35 deletion protected mice from tumours formation in two different models of colon carcinogenesis. Notably, inactivation of conditional GPR35 by villin-cre, which results in a selective GPR35 deletion in the intestine, caused less tumours development in *APC^{min}* mice.

In conclusion, this PhD thesis contributes to elucidate the physiopathological role of MAGL, NAAA and GPR35 in colon carcinogenesis and thus may offer novel future pharmacological opportunities for colon cancer prevention and cure.

Graphical conclusion



REFERENCES

- Abu Aboud O, Wettersten HI, Weiss RH. Inhibition of PPAR α induces cell cycle arrest and apoptosis, and synergizes with glycolysis inhibition in kidney cancer cells. *PLoS One*. 2013;8(8):e71115.
- Ahmed D, Eide PW, Eilertsen IA, Danielsen SA, Eknæs M, Hektoen M, Lind GE, Lothe RA. Epigenetic and genetic features of 24 colon cancer cell lines. *Oncogenesis*. 2013;2:e71.
- Ahn JY, Lee JS, Min HY, Lee HY. Acquired resistance to 5-fluorouracil via HSP90/Src-mediated increase in thymidylate synthase expression in colon cancer. *Oncotarget*. 2015;6(32):32622-33.
- Ahn K, McKinney MK, Cravatt BF. Enzymatic pathways that regulate endocannabinoid signaling in the nervous system. *Chem Rev*. 2008;108(5):1687-707. Review.
- Alexander SP, Fabbro D, Kelly E, Marrion N, Peters JA, Benson HE, Faccenda E, Pawson AJ, Sharman JL, Southan C, Davies JA; CGTP Collaborators. The Concise Guide to PHARMACOLOGY 2015/16: Enzymes. *Br J Pharmacol*. 2015;172(24):6024-109.
- Alhouayek M, Bottemanne P, Subramanian KV, Lambert DM, Makriyannis A, Cani PD, Muccioli GG. N-Acylethanolamine-hydrolyzing acid amidase inhibition increases colon N-palmitoylethanolamine levels and counteracts murine colitis. *FASEB J*. 2015;29(2):650-61.
- Alhouayek M, Muccioli GG. Harnessing the anti-inflammatory potential of palmitoylethanolamide. *Drug Discov Today*. 2014;19(10):1632-9. Review.
- Ambrosino P, Soldovieri MV, De Maria M, Russo C, Tagliatela M. Functional and biochemical interaction between PPAR α receptors and TRPV1 channels: Potential role in PPAR α agonists-mediated analgesia. *Pharmacol Res*. 2014;87:113-22.
- Ambrosino P, Soldovieri MV, Russo C, Tagliatela M. Activation and desensitization of TRPV1 channels in sensory neurons by the PPAR α agonist palmitoylethanolamide. *Br J Pharmacol*. 2013;168(6):1430-44.
- Aplin AC, Fogel E, Zorzi P, Nicosia RF. The aortic ring model of angiogenesis. *Methods Enzymol*. 2008;443:119-36.
- Baba Y, Funakoshi T, Mori M, Emoto K, Masugi Y, Ekmekcioglu S, Amagai M, Tanese K. Expression of monoacylglycerol lipase as a marker of tumour invasion and progression in malignant melanoma. *J Eur Acad Dermatol Venereol*. 2017;31(12):2038-2045.
- Baggelaar MP, Maccarrone M, van der Stelt M. 2-Arachidonoylglycerol: A signaling lipid with manifold actions in the brain. *Prog Lipid Res*. 2018;71:1-17. Review.

Bahnassy AA, Zekri AR, El-Houssini S, El-Shehaby AM, Mahmoud MR, Abdallah S, El-Serafi M. Cyclin A and cyclin D1 as significant prognostic markers in colorectal cancer patients. *BMC Gastroenterol.* 2004;4:22.

Baker M, Robinson SD, Lechertier T, Barber PR, Tavora B, D'Amico G, Jones DT, Vojnovic B, Hodivala-Dilke K. Use of the mouse aortic ring assay to study angiogenesis. *Nat Protoc.* 2011;7(1):89-104.

Bandiera T, Ponzano S, Piomelli D. Advances in the discovery of N-acylethanolamine acid amidase inhibitors. *Pharmacol Res.* 2014;86:11-7. Review.

Ben-Shabat S, Fride E, Sheskin T, Tamiri T, Rhee MH, Vogel Z, Bisogno T, De Petrocellis L, Di Marzo V, Mechoulam R. An entourage effect: inactive endogenous fatty acid glycerol esters enhance 2-arachidonoyl-glycerol cannabinoid activity. *Eur J Pharmacol.* 1998;353(1):23-31.

Bergers G, Benjamin LE. Tumorigenesis and the angiogenic switch. *Nat Rev Cancer.* 2003;3(6):401-10. Review.

Bernstein CN, Blanchard JF, Kliewer E, Wajda A. Cancer risk in patients with inflammatory bowel disease: a population-based study. *Cancer.* 2001;91(4):854-62.

Biswas SK, Mantovani A. Macrophage plasticity and interaction with lymphocyte subsets: cancer as a paradigm. *Nat Immunol.* 2010;11(10):889-96.

Biswas SK, Allavena P, Mantovani A. Tumor-associated macrophages: functional diversity, clinical significance, and open questions. *Semin Immunopathol.* 2013;35(5):585-600.

Blankman JL, Simon GM, Cravatt BF. A comprehensive profile of brain enzymes that hydrolyze the endocannabinoid 2-arachidonoylglycerol. *Chem Biol.* 2007;14(12):1347-56.

Blázquez C, Casanova ML, Planas A, Gómez Del Pulgar T, Villanueva C, Fernández-Aceñero MJ, Aragonés J, Huffman JW, Jorcano JL, Guzmán M. Inhibition of tumor angiogenesis by cannabinoids. *FASEB J.* 2003;17(3):529-31.

Bluff JE, Menakuru SR, Cross SS, Higham SE, Balasubramanian SP, Brown NJ, Reed MW, Staton CA. Angiogenesis is associated with the onset of hyperplasia in human ductal breast disease. *Br J Cancer.* 2009;101(4):666-72.

Bonezzi FT, Sasso O, Pontis S, Realini N, Romeo E, Ponzano S, Nuzzi A, Fiasella A, Bertozzi F, Piomelli D. An Important Role for N-Acylethanolamine Acid Amidase in the Complete Freund's Adjuvant Rat Model of Arthritis. *J Pharmacol Exp Ther.* 2016;356(3):656-63.

Borrelli F, Pagano E, Romano B, Panzera S, Maiello F, Coppola D, De Petrocellis L, Buono L, Orlando P, Izzo AA. Colon carcinogenesis is inhibited by the TRPM8 antagonist cannabigerol, a Cannabis-derived non-psychotropic cannabinoid. *Carcinogenesis*. 2014;35(12):2787-97.

Borrelli F, Romano B, Petrosino S, Pagano E, Capasso R, Coppola D, Battista G, Orlando P, Di Marzo V, Izzo AA. Palmitoylethanolamide, a naturally occurring lipid, is an orally effective intestinal anti-inflammatory agent. *Br J Pharmacol*. 2015;172(1):142-58.

Bossi P, Viale G, Lee AK, Alfano R, Coggi G, Bosari S. Angiogenesis in colorectal tumors: microvessel quantitation in adenomas and carcinomas with clinicopathological correlations. *Cancer Res*. 1995;55(21):5049-53.

Bottemanne P, Muccioli GG, Alhouayek M. N-acylethanolamine hydrolyzing acid amidase inhibition: tools and potential therapeutic opportunities. *Drug Discov Today*. 2018;23(8):1520-1529. Review.

Bouaboula M, Hilairat S, Marchand J, Fajas L, Le Fur G, Casellas P. Anandamide induced PPARgamma transcriptional activation and 3T3-L1 preadipocyte differentiation. *Eur J Pharmacol*. 2005;517(3):174-81.

Calvert PM, Frucht H. The genetics of colorectal cancer. *Ann Intern Med*. 2002;137(7):603-12. Review.

Campbell AP, Smrcka AV. Targeting G protein-coupled receptor signalling by blocking G proteins. *Nat Rev Drug Discov*. 2018. Review.

Carmeliet P. VEGF as a key mediator of angiogenesis in cancer. *Oncology*. 2005;69 Suppl 3:4-10. Review.

Chanda PK, Gao Y, Mark L, Btesh J, Strassle BW, Lu P, Piesla MJ, Zhang MY, Bingham B, Uveges A, Kowal D, Garbe D, Kouranova EV, Ring RH, Bates B, Pangalos MN, Kennedy JD, Whiteside GT, Samad TA. Monoacylglycerol lipase activity is a critical modulator of the tone and integrity of the endocannabinoid system. *Mol Pharmacol*. 2010;78(6):996-1003.

Chen J, Huang XF. The signal pathways in azoxymethane-induced colon cancer and preventive implications. *Cancer Biol Ther*. 2009;8(14):1313-7.

Coburn AF, Graham CE, Haninger J. The effect of egg yolk in diets on anaphylactic arthritis (passive Arthus phenomenon) in the guinea pig. *J Exp Med*. 1954;100(5):425-35.

Comelli F, Giagnoni G, Bettoni I, Colleoni M, Costa B. The inhibition of monoacylglycerol lipase by URB602 showed an anti-inflammatory and anti-nociceptive effect in a murine model of acute inflammation. *Br J Pharmacol*. 2007;152(5):787-94.

Cordani M, Pacchiana R, Butera G, D'Orazi G, Scarpa A, Donadelli M. Mutant p53 proteins alter cancer cell secretome and tumour microenvironment: Involvement in cancer invasion and metastasis. *Cancer Lett.* 2016;376(2):303-9.

Costa MA, Fonseca BM, Keating E, Teixeira NA, Correia-da-Silva G. 2-arachidonoylglycerol effects in cytotrophoblasts: metabolic enzymes expression and apoptosis in BeWo cells. *Reproduction.* 2014;147(3):301-11.

Curtis MJ, Bond RA, Spina D, Ahluwalia A, Alexander SP, Giembycz MA, Gilchrist A, Hoyer D, Insel PA, Izzo AA, Lawrence AJ, MacEwan DJ, Moon LD, Wonnacott S, Weston AH, McGrath JC. Experimental design and analysis and their reporting: new guidance for publication in *BJP*. *Br J Pharmacol.* 2015;172(14):3461-71.

De Palma M, Biziato D, Petrova TV. Microenvironmental regulation of tumour angiogenesis. *Nat Rev Cancer.* 2017;17(8):457-474. Review.

De Petrocellis L, Bisogno T, Ligresti A, Bifulco M, Melck D, Di Marzo V. Effect on cancer cell proliferation of palmitoylethanolamide, a fatty acid amide interacting with both the cannabinoid and vanilloid signalling systems. *Fundam Clin Pharmacol.* 2002;16(4):297-302.

De Petrocellis L, Davis JB, Di Marzo V. Palmitoylethanolamide enhances anandamide stimulation of human vanilloid R1 receptors. *FEBS Lett.* 2001;506(3):253-6.

Dejea CM, Fathi P, Craig JM, Boleij A, Taddese R, Geis AL, Wu X, DeStefano Shields CE, Hechenbleikner EM, Huso DL, Anders RA, Giardiello FM, Wick EC, Wang H, Wu S, Pardoll DM, Housseau F, Sears CL. Patients with familial adenomatous polyposis harbor colonic biofilms containing tumorigenic bacteria. *Science.* 2018;359(6375):592-597.

Des Guetz G, Uzzan B, Nicolas P, Cucherat M, Morere JF, Benamouzig R, Breau JL, Perret GY. Microvessel density and VEGF expression are prognostic factors in colorectal cancer. Meta-analysis of the literature. *Br J Cancer.* 2006;94(12):1823-32.

Di Marzo V, Melck D, Orlando P, Bisogno T, Zagoory O, Bifulco M, Vogel Z, De Petrocellis L. Palmitoylethanolamide inhibits the expression of fatty acid amide hydrolase and enhances the anti-proliferative effect of anandamide in human breast cancer cells. *Biochem J.* 2001;358(Pt 1):249-55.

Di Marzo V, Capasso R, Matias I, Aviello G, Petrosino S, Borrelli F, Romano B, Orlando P, Capasso F, Izzo AA. The role of endocannabinoids in the regulation of gastric emptying: alterations in mice fed a high-fat diet. *Br J Pharmacol.* 2008;153(6):1272-80.

Dinh TP, Freund TF, Piomelli D. A role for monoglyceride lipase in 2-arachidonoylglycerol inactivation. *Chem Phys Lipids.* 2002;121(1-2):149-58. Review.

Dinh TP, Kathuria S, Piomelli D. RNA interference suggests a primary role for monoacylglycerol lipase in the degradation of the endocannabinoid 2-arachidonoylglycerol. *Mol Pharmacol*. 2004;66(5):1260-4.

Divorcy N, Mackenzie AE, Nicklin SA, Milligan G. G protein-coupled receptor 35: an emerging target in inflammatory and cardiovascular disease. *Front Pharmacol*. 2015;6:41. Review.

Dong R, Gong Y, Meng W, Yuan M, Zhu H, Ying M, He Q, Cao J, Yang B. The involvement of M2 macrophage polarization inhibition in fenretinide-mediated chemopreventive effects on colon cancer. *Cancer Lett*. 2017;388:43-53.

Donnini S, Solito R, Giachetti A, Granger HJ, Ziche M, Morbidelli L. Fibroblast growth factor-2 mediates Angiotensin-converting enzyme inhibitor-induced angiogenesis in coronary endothelium. *J Pharmacol Exp Ther*. 2006;319(2):515-22.

Du F, Li Y, Zhang W, Kale SP, McFerrin H, Davenport I, Wang G, Skripnikova E, Li XL, Bowen NJ, McDaniels LB, Meng YX, Polk P, Liu YY, Zhang QJ. Highly and moderately aggressive mouse ovarian cancer cell lines exhibit differential gene expression. *Tumour Biol*. 2016;37(8):11147-11162.

Duncan M, Thomas AD, Cluny NL, Patel A, Patel KD, Lutz B, Piomelli D, Alexander SP, Sharkey KA. Distribution and function of monoacylglycerol lipase in the gastrointestinal tract. *Am J Physiol Gastrointest Liver Physiol*. 2008;295(6):G1255-65.

Duranti A, Tontini A, Antonietti F, Vacondio F, Fioni A, Silva C, Lodola A, Rivara S, Solorzano C, Piomelli D, Tarzia G, Mor M. N-(2-oxo-3-oxetanyl)carbamic acid esters as N-acylethanolamine acid amidase inhibitors: synthesis and structure-activity and structure-property relationships. *J Med Chem*. 2012;55(10):4824-36.

El Kasmi KC, Anderson AL, Devereaux MW, Vue PM, Zhang W, Setchell KD, Karpen SJ, Sokol RJ. Phytosterols promote liver injury and Kupffer cell activation in parenteral nutrition-associated liver disease. *Sci Transl Med*. 2013;5(206):206ra137.

El Kasmi KC, Stenmark KR. Contribution of metabolic reprogramming to macrophage plasticity and function. *Semin Immunol*. 2015;27(4):267-75.

Ellinghaus D, Folseraas T, Holm K, Ellinghaus E, Melum E, Balschun T, Laerdahl JK, Shiryayev A, Gotthardt DN, Weismüller TJ, Schramm C, Wittig M, Bergquist A, Björnsson E, Marschall HU, Vatn M, Teufel A, Rust C, Gieger C, Wichmann HE, Runz H, Sterneck M, Rupp C, Braun F, Weersma RK, Wijmenga C, Ponsioen CY, Mathew CG, Rutgeerts P, Vermeire S, Schrupf E, Hov JR, Manns MP, Boberg KM, Schreiber S, Franke A, Karlsen TH. Genome-wide association analysis in primary sclerosing cholangitis and ulcerative colitis identifies risk loci at GPR35 and TCF4. *Hepatology*. 2013;58(3):1074-83.

Esposito E, Cuzzocrea S. Palmitoylethanolamide in homeostatic and traumatic central nervous system injuries. *CNS Neurol Disord Drug Targets*. 2013;12(1):55-61. Review.

Fang S, Salven P. Stem cells in tumor angiogenesis. *J Mol Cell Cardiol*. 2011;50(2):290-5. Review.

Fearon ER. Molecular genetics of colorectal cancer. *Annu Rev Pathol*. 2011;6:479-507. Review.

Ferrara N, Mass RD, Campa C, Kim R. Targeting VEGF-A to treat cancer and age-related macular degeneration. *Annu Rev Med*. 2007;58:491-504. Review.

Ferrara N. Vascular endothelial growth factor as a target for anticancer therapy. *Oncologist*. 2004;9 Suppl 1:2-10. Review.

Fidoamore A, Cristiano L, Antonosante A, d'Angelo M, Di Giacomo E, Astarita C, Giordano A, Ippoliti R, Benedetti E, Cimini A. Glioblastoma Stem Cells Microenvironment: The Paracrine Roles of the Niche in Drug and Radioresistance. *Stem Cells Int*. 2016;2016:6809105.

Finetti F, Terzuoli E, Bocci E, Coletta I, Polenzani L, Mangano G, Alisi MA, Cazzolla N, Giachetti A, Ziche M, Donnini S. Pharmacological inhibition of microsomal prostaglandin E synthase-1 suppresses epidermal growth factor receptor-mediated tumor growth and angiogenesis. *PLoS One*. 2012;7(7):e40576.

Fowler CJ. Monoacylglycerol lipase - a target for drug development? *Br J Pharmacol*. 2012;166(5):1568-85. Review.

Fukumura D, Yuan F, Monsky WL, Chen Y, Jain RK. Effect of host microenvironment on the microcirculation of human colon adenocarcinoma. *Am J Pathol*. 1997;151(3):679-88.

Ganley OH, Graessle OE, Robinson HJ. Anti-inflammatory activity on compounds obtained from egg yolk, peanut oil, and soybean lecithin. *J Lab Clin Med*. 1958;51(5):709-14.

Gao Y, Vasilyev DV, Goncalves MB, Howell FV, Hobbs C, Reisenberg M, Shen R, Zhang MY, Strassle BW, Lu P, Mark L, Piesla MJ, Deng K, Kouranova EV, Ring RH, Whiteside GT, Bates B, Walsh FS, Williams G, Pangalos MN, Samad TA, Doherty P. Loss of retrograde endocannabinoid signaling and reduced adult neurogenesis in diacylglycerol lipase knock-out mice. *J Neurosci*. 2010;30(6):2017-24.

Geeraerts X, Bolli E, Fendt SM, Van Ginderachter JA. Macrophage Metabolism As Therapeutic Target for Cancer, Atherosclerosis, and Obesity. *Front Immunol*. 2017 ;8:289. Review.

Gelmon K, Eisenhauer E, Bryce C, Tolcher A, Mayer L, Tomlinson E, Zee B, Blackstein M, Tomiak E, Yau J, Batist G, Fisher B, Iglesias J. Randomized phase II study of high-dose paclitaxel

with or without amifostine in patients with metastatic breast cancer. *J Clin Oncol.* 1999;17(10):3038-47.

Goetz MP, Erlichman C, Windebank AJ, Reid JM, Sloan JA, Atherton P, Adjei AA, Rubin J, Pitot H, Galanis E, Ames MM, Goldberg RM. Phase I and pharmacokinetic study of two different schedules of oxaliplatin, irinotecan, Fluorouracil, and leucovorin in patients with solid tumors. *J Clin Oncol.* 2003;21(20):3761-9.

Goparaju SK, Ueda N, Yamaguchi H, Yamamoto S. Anandamide amidohydrolase reacting with 2-arachidonoylglycerol, another cannabinoid receptor ligand. *FEBS Lett.* 1998;422(1):69-73.

Gou Q, Gong X, Jin J, Shi J, Hou Y. Peroxisome proliferator-activated receptors (PPARs) are potential drug targets for cancer therapy. *Oncotarget.* 2017;8(36):60704-60709. Review.

Gouveia-Figueira S, Nording ML. Development and validation of a sensitive UPLC-ESI-MS/MS method for the simultaneous quantification of 15 endocannabinoids and related compounds in milk and other biofluids. *Anal Chem.* 2014;86(2):1186-95.

Greten FR, Eckmann L, Greten TF, Park JM, Li ZW, Egan LJ, Kagnoff MF, Karin M. IKKbeta links inflammation and tumorigenesis in a mouse model of colitis-associated cancer. *Cell.* 2004;118(3):285-96.

Gugliandolo E, D'amico R, Cordaro M, Fusco R, Siracusa R, Crupi R, Impellizzeri D, Cuzzocrea S, Di Paola R. Effect of PEA-OXA on neuropathic pain and functional recovery after sciatic nerve crush. *J Neuroinflammation.* 2018;15(1):264.

Guo YJ, Zhou YJ, Yang XL, Shao ZM, Ou ZL. The role and clinical significance of the CXCL17-CXCR8 (GPR35) axis in breast cancer. *Biochem Biophys Res Commun.* 2017;493(3):1159-1167.

Gupta RB, Harpaz N, Itzkowitz S, Hossain S, Matula S, Kornbluth A, Bodian C, Ullman T. Histologic inflammation is a risk factor for progression to colorectal neoplasia in ulcerative colitis: a cohort study. *Gastroenterology.* 2007;133(4):1099-105.

Gustavsson B, Carlsson G, Machover D, Petrelli N, Roth A, Schmoll HJ, Tveit KM, Gibson F. A review of the evolution of systemic chemotherapy in the management of colorectal cancer. *Clin Colorectal Cancer.* 2015;14(1):1-10. Review.

Hamtaux L, Masquelier J, Muccioli GG, Bouzin C, Feron O, Gallez B, Lambert DM. The association of N-palmitoylethanolamine with the FAAH inhibitor URB597 impairs melanoma growth through a supra-additive action. *MC Cancer.* 2012;12:92.

Hanahan D, Folkman J. Patterns and emerging mechanisms of the angiogenic switch during tumorigenesis. *Cell.* 1996;86(3):353-64. Review.

Hann SS, Zheng F, Zhao S. Targeting 3-phosphoinositide-dependent protein kinase 1 by N-acetylcysteine through activation of peroxisome proliferators activated receptor alpha in human lung cancer cells, the role of p53 and p65. *J Exp Clin Cancer Res.* 2013;32:43.

Hashimoto-Kataoka T, Hosen N, Sonobe T, Arita Y, Yasui T, Masaki T, Minami M, Inagaki T, Miyagawa S, Sawa Y, Murakami M, Kumanogoh A, Yamauchi-Takahara K, Okumura M, Kishimoto T, Komuro I, Shirai M, Sakata Y, Nakaoka Y. Interleukin-6/interleukin-21 signaling axis is critical in the pathogenesis of pulmonary arterial hypertension. *Proc Natl Acad Sci U S A.* 2015;112(20):E2677-86.

Hawinkels LJ, Zuidwijk K, Verspaget HW, de Jonge-Muller ES, van Duijn W, Ferreira V, Fontijn RD, David G, Hommes DW, Lamers CB, Sier CF. VEGF release by MMP-9 mediated heparan sulphate cleavage induces colorectal cancer angiogenesis. *Eur J Cancer.* 2008;44(13):1904-13.

Ho WS, Barrett DA, Randall MD. 'Entourage' effects of N-palmitoylethanolamide and N-oleoylethanolamide on vasorelaxation to anandamide occur through TRPV1 receptors. *Br J Pharmacol.* 2008;155(6):837-46.

Hohmann AG, Suplita RL, Bolton NM, Neely MH, Fegley D, Mangieri R, Krey JF, Walker JM, Holmes PV, Crystal JD, Duranti A, Tontini A, Mor M, Tarzia G, Piomelli D. An endocannabinoid mechanism for stress-induced analgesia. *Nature.* 2005;435(7045):1108-12.

Hsiao YC, Chu LJ, Chen JT, Yeh TS, Yu JS. Proteomic profiling of the cancer cell secretome: informing clinical research. *Expert Rev Proteomics.* 2017;14(9):737-756.

Iannotti FA, Panza E, Barrese V, Viggiano D, Soldovieri MV, Taglialatela M. Expression, localization, and pharmacological role of Kv7 potassium channels in skeletal muscle proliferation, differentiation, and survival after myotoxic insults. *J Pharmacol Exp Ther.* 2010;332(3):811-20.

Iannotti FA, Di Marzo V, Petrosino S. Endocannabinoids and endocannabinoid-related mediators: Targets, metabolism and role in neurological disorders. *Prog Lipid Res.* 2016;62:107-28. Review.

Iannotti and Piscitelli. Endocannabinoidome. In: eLS. John Wiley & Sons, Ltd: Chichester. November 2018. In press

Idzko M, Ferrari D, Eltzschig HK. Nucleotide signalling during inflammation. *Nature.* 2014 May 15;509(7500):310-7. Review.

Insel PA, Tang CM, Hahntow I, Michel MC. Impact of GPCRs in clinical medicine: monogenic diseases, genetic variants and drug targets. *Biochim Biophys Acta.* 2007;1768(4):994-1005. Review.

Itzkowitz SH, Harpaz N. Diagnosis and management of dysplasia in patients with inflammatory bowel diseases. *Gastroenterology*. 2004;126(6):1634-48. Review.

Iwasaki Y, Saito O, Tanabe M, Inayoshi K, Kobata K, Uno S, Morita A, Watanabe T. Monoacylglycerols activate capsaicin receptor, TRPV1. *Lipids*. 2008;43(6):471-83.

Izzo AA, Aviello G, Petrosino S, Orlando P, Marsicano G, Lutz B, Borrelli F, Capasso R, Nigam S, Capasso F, Di Marzo V; Endocannabinoid Research Group. Increased endocannabinoid levels reduce the development of precancerous lesions in the mouse colon. *J Mol Med (Berl)*. 2008;86(1):89-98.

Izzo AA, Camilleri M. Cannabinoids in intestinal inflammation and cancer. *Pharmacol Res*. 2009;60(2):117-25. Review.

Izzo AA, Muccioli GG, Ruggieri MR, Schicho R. Endocannabinoids and the Digestive Tract and Bladder in Health and Disease. *Handb Exp Pharmacol*. 2015;231:423-47. Review.

Jenkins L, Alvarez-Curto E, Campbell K, de Munnik S, Canals M, Schlyer S, Milligan G. Agonist activation of the G protein-coupled receptor GPR35 involves transmembrane domain III and is transduced via $G\alpha_{13}$ and β -arrestin-2. *Br J Pharmacol*. 2011;162(3):733-48.

Jenkins L, Brea J, Smith NJ, Hudson BD, Reilly G, Bryant NJ, Castro M, Loza MI, Milligan G. Identification of novel species-selective agonists of the G-protein-coupled receptor GPR35 that promote recruitment of β -arrestin-2 and activate $G\alpha_{13}$. *Biochem J*. 2010;432(3):451-9.

Jenkins L, Harries N, Lappin JE, MacKenzie AE, Neetoo-Isseljee Z, Southern C, McIver EG, Nicklin SA, Taylor DL, Milligan G. Antagonists of GPR35 display high species ortholog selectivity and varying modes of action. *J Pharmacol Exp Ther*. 2012;343(3):683-95.

Jubb AM, Cesario A, Ferguson M, Congedo MT, Gatter KC, Lococo F, Mulè A, Pezzella F. Vascular phenotypes in primary non-small cell lung carcinomas and matched brain metastases. *Br J Cancer*. 2011;104(12):1877-81.

Karlsen TH, Folseraas T, Thorburn D, Vesterhus M. Primary sclerosing cholangitis - a comprehensive review. *J Hepatol*. 2017;67(6):1298-1323. Review.

Karlsson M, Reue K, Xia YR, Lusi AJ, Langin D, Tornqvist H, Holm C. Exon-intron organization and chromosomal localization of the mouse monoglyceride lipase gene. *Gene*. 2001;272(1-2):11-8.

Kelly B, O'Neill LA. Metabolic reprogramming in macrophages and dendritic cells in innate immunity. *Cell Res*. 2015 Jul;25(7):771-84. Review.

Kenakin T. New concepts in drug discovery: collateral efficacy and permissive antagonism. *Nat Rev Drug Discov.* 2005 Nov;4(11):919-27. Review.

Kilaru A, Blancaflor EB, Venables BJ, Tripathy S, Mysore KS, Chapman KD. The N-acylethanolamine-mediated regulatory pathway in plants. *Chem Biodivers.* 2007;4(8):1933-55. Review.

King AR, Duranti A, Tontini A, Rivara S, Rosengarth A, Clapper JR, Astarita G, Geaga JA, Luecke H, Mor M, Tarzia G, Piomelli D. URB602 inhibits monoacylglycerol lipase and selectively blocks 2-arachidonoylglycerol degradation in intact brain slices. *Chem Biol.* 2007;14(12):1357-65.

Kozak KR, Gupta RA, Moody JS, Ji C, Boeglin WE, DuBois RN, Brash AR, Marnett LJ. 15-Lipoxygenase metabolism of 2-arachidonoylglycerol. Generation of a peroxisome proliferator-activated receptor alpha agonist. *J Biol Chem.* 2002;277(26):23278-86.

Krawczyk CM, Holowka T, Sun J, Blagih J, Amiel E, DeBerardinis RJ, Cross JR, Jung E, Thompson CB, Jones RG, Pearce EJ. Toll-like receptor-induced changes in glycolytic metabolism regulate dendritic cell activation. *Blood.* 2010;115(23):4742-9.

Krugliak Cleveland N, Rubin DT, Hart J, Weber CR, Meckel K, Tran AL, Aelvoet AS, Pan I, Gonsalves A, Gaetano JN, Williams KM, Wroblewski K, Jabri B, Pekow J. Patients With Ulcerative Colitis and Primary Sclerosing Cholangitis Frequently Have Subclinical Inflammation in the Proximal Colon. *Clin Gastroenterol Hepatol.* 2018;16(1):68-74.

Lagerström MC, Schiöth HB. Structural diversity of G protein-coupled receptors and significance for drug discovery. *Nat Rev Drug Discov.* 2008;7(4):339-57. Review. Erratum in: *Nat Rev Drug Discov.* 2008;7(6):542.

Lahmar Q, Keirsse J, Laoui D, Movahedi K, Van Overmeire E, Van Ginderachter JA. Tissue-resident versus monocyte-derived macrophages in the tumor microenvironment. *Biochim Biophys Acta.* 2016;1865(1):23-34. Review.

Lane JR, Beukers MW, Mulder-Krieger T, Ijzerman AP. The endocannabinoid 2-arachidonoylglycerol is a negative allosteric modulator of the human A3 adenosine receptor. *Biochem Pharmacol.* 2010;79(1):48-56.

Lankman JL, Simon GM, Cravatt BF. A comprehensive profile of brain enzymes that hydrolyze the endocannabinoid 2-arachidonoylglycerol. *Chem Biol.* 2007;14(12):1347-56.

Lao VV, Grady WM. Epigenetics and colorectal cancer. *Nat Rev Gastroenterol Hepatol.* 2011;8(12):686-700. Review.

Lee EE, Ma J, Sacharidou A, Mi W, Salato VK, Nguyen N, Jiang Y, Pascual JM, North PE, Shaul PW, Mettlen M, Wang RC. A Protein Kinase C Phosphorylation Motif in GLUT1 Affects Glucose Transport and is Mutated in GLUT1 Deficiency Syndrome. *Mol Cell*. 2015;58(5):845-53.

le Rolle AF, Chiu TK, Fara M, Shia J, Zeng Z, Weiser MR, Paty PB, Chiu VK. The prognostic significance of CXCL1 hypersecretion by human colorectal cancer epithelia and myofibroblasts. *J Transl Med*. 2015;13:199.

Levoye A, Dam J, Ayoub MA, Guillaume JL, Jockers R. Do orphan G-protein-coupled receptors have ligand-independent functions? New insights from receptor heterodimers. *EMBO Rep*. 2006;7(11):1094-8. Review.

Li T, Zhang Q, Zhang J, Yang G, Shao Z, Luo J, Fan M, Ni C, Wu Z, Hu X. Fenofibrate induces apoptosis of triple-negative breast cancer cells via activation of NF- κ B pathway. *BMC Cancer*. 2014;14:96.

Liang CC, Park AY, Guan JL. In vitro scratch assay: a convenient and inexpensive method for analysis of cell migration in vitro. *Nat Protoc*. 2007;2(2):329-33.

Ligresti A, Bisogno T, Matias I, De Petrocellis L, Cascio MG, Cosenza V, D'argenio G, Scaglione G, Bifulco M, Sorrentini I, Di Marzo V. Possible endocannabinoid control of colorectal cancer growth. *Gastroenterology*. 2003;125(3):677-87.

Liu Y, Chen J, Sethi A, Li QK, Chen L, Collins B, Gillet LC, Wollscheid B, Zhang H, Aebersold R. Glycoproteomic analysis of prostate cancer tissues by SWATH mass spectrometry discovers N-acylethanolamine acid amidase and protein tyrosine kinase 7 as signatures for tumor aggressiveness. *Mol Cell Proteomics*. 2014;13(7):1753-68.

Lo Verme J, Fu J, Astarita G, La Rana G, Russo R, Calignano A, Piomelli D. The nuclear receptor peroxisome proliferator-activated receptor- α mediates the anti-inflammatory actions of palmitoylethanolamide. *Mol Pharmacol*. 2005;67(1):15-9.

Long JZ, Nomura DK, Cravatt BF. Characterization of monoacylglycerol lipase inhibition reveals differences in central and peripheral endocannabinoid metabolism. *Chem Biol*. 2009a;16(7):744-53.

Long JZ, Li W, Booker L, Burston JJ, Kinsey SG, Schlosburg JE, Pavón FJ, Serrano AM, Selley DE, Parsons LH, Lichtman AH, Cravatt BF. Selective blockade of 2-arachidonoylglycerol hydrolysis produces cannabinoid behavioral effects. *Nat Chem Biol*. 2009b;5(1):37-44.

Lynch HT, de la Chapelle A. Hereditary colorectal cancer. *N Engl J Med*. 2003;348(10):919-32. Review.

Maccarrone M, Attinà M, Cartoni A, Bari M, Finazzi-Agrò A. Gas chromatography-mass spectrometry analysis of endogenous cannabinoids in healthy and tumoral human brain and human cells in culture. *J Neurochem.* 2001;76(2):594-601.

MacKenzie AE, Caltabiano G, Kent TC, Jenkins L, McCallum JE, Hudson BD, Nicklin SA, Fawcett L, Markwick R, Charlton SJ, Milligan G. The antiallergic mast cell stabilizers Iodoxamide and bufrolin as the first high and equipotent agonists of human and rat GPR35. *Mol Pharmacol.* 2014;85(1):91-104.

Malamas, M. Makriyannis A., et al. Preparation of isothiocyanatoalkylbenzene derivatives and analogs for use as N-acylethanolamine hydrolyzing acid amidase inhibitors. 2015 Patent: WO2015179190A1.

Malvezzi M, Carioli G, Bertuccio P, Boffetta P, Levi F, La Vecchia C, Negri E. European cancer mortality predictions for the year 2017, with focus on lung cancer. *Ann Oncol.* 2017;28(5):1117-1123.

Maravillas-Montero JL, Burkhardt AM, Hevezi PA, Carnevale CD, Smit MJ, Zlotnik A. Cutting edge: GPR35/CXCR8 is the receptor of the mucosal chemokine CXCL17. *J Immunol.* 2015;194(1):29-33.

Markowitz SD, Bertagnolli MM. Molecular origins of cancer: Molecular basis of colorectal cancer. *N Engl J Med.* 2009;361(25):2449-60. Review.

Marley AR, Nan H. Epidemiology of colorectal cancer. *Int J Mol Epidemiol Genet.* 2016;7(3):105-114. Review.

Marrs WR, Blankman JL, Horne EA, Thomazeau A, Lin YH, Coy J, Bodor AL, Muccioli GG, Hu SS, Woodruff G, Fung S, Lafourcade M, Alexander JP, Long JZ, Li W, Xu C, Möller T, Mackie K, Manzoni OJ, Cravatt BF, Stella N. The serine hydrolase ABHD6 controls the accumulation and efficacy of 2-AG at cannabinoid receptors. *Nat Neurosci.* 2010;13(8):951-7.

Melck D, De Petrocellis L, Orlando P, Bisogno T, Laezza C, Bifulco M, Di Marzo V. Suppression of nerve growth factor Trk receptors and prolactin receptors by endocannabinoids leads to inhibition of human breast and prostate cancer cell proliferation. *Endocrinology.* 2000;141(1):118-26.

Messmer D, Lorrain K, Stebbins K, Bravo Y, Stock N, Cabrera G, Correa L, Chen A, Jacintho J, Chiorazzi N, Yan XJ, Spaner D, Prasit P, Lorrain D. A Selective Novel Peroxisome Proliferator-Activated Receptor (PPAR)- α Antagonist Induces Apoptosis and Inhibits Proliferation of CLL Cells In Vitro and In Vivo. *Mol Med.* 2015;21:410-9.

Milligan G. Orthologue selectivity and ligand bias: translating the pharmacology of GPR35. *Trends Pharmacol Sci.* 2011 May;32(5):317-25. Review.

Monti M, Donnini S, Giachetti A, Mochly-Rosen D, Ziche M. deltaPKC inhibition or varepsilonPKC activation repairs endothelial vascular dysfunction by regulating eNOS post-translational modification. *J Mol Cell Cardiol.* 2010;48(4):746-56.

Morikawa S, Baluk P, Kaidoh T, Haskell A, Jain RK, McDonald DM. Abnormalities in pericytes on blood vessels and endothelial sprouts in tumors. *Am J Pathol.* 2002;160(3):985-1000.

Morrissey C, True LD, Roudier MP, Coleman IM, Hawley S, Nelson PS, Coleman R, Wang YC, Corey E, Lange PH, Higano CS, Vessella RL. Differential expression of angiogenesis associated genes in prostate cancer bone, liver and lymph node metastases. *Clin Exp Metastasis.* 2008;25(4):377-88.

Motokura T, Arnold A. Cyclins and oncogenesis. *Biochim Biophys Acta.* 1993;1155(1):63-78. Review.

Mulvihill MM, Nomura DK. Therapeutic potential of monoacylglycerol lipase inhibitors. *Life Sci.* 2013;92(8-9):492-7. Review.

Murataeva N, Straiker A, Mackie K. Parsing the players: 2-arachidonoylglycerol synthesis and degradation in the CNS. *Br J Pharmacol.* 2014;171(6):1379-91. Review.

Murray PJ, Allen JE, Biswas SK, Fisher EA, Gilroy DW, Goerdt S, Gordon S, Hamilton JA, Ivashkiv LB, Lawrence T, Locati M, Mantovani A, Martinez FO, Mege JL, Mosser DM, Natoli G, Saeij JP, Schultze JL, Shirey KA, Sica A, Suttles J, Udalova I, van Ginderachter JA, Vogel SN, Wynn TA. Macrophage activation and polarization: nomenclature and experimental guidelines. *Immunity.* 2014;41(1):14-20.

Neufert C, Becker C, Neurath MF. An inducible mouse model of colon carcinogenesis for the analysis of sporadic and inflammation-driven tumor progression. *Nat Protoc.* 2007;2(8):1998-2004.

Nicosia RF. The aortic ring model of angiogenesis: a quarter century of search and discovery. *J Cell Mol Med.* 2009;13(10):4113-36.

Nithipatikom K, Isbell MA, Endsley MP, Woodliff JE, Campbell WB. Anti-proliferative effect of a putative endocannabinoid, 2-arachidonoylglycerol in prostate carcinoma cells. *Prostaglandins Other Lipid Mediat.* 2011;94(1-2):34-43.

Nomura DK, Long JZ, Niessen S, Hoover HS, Ng SW, Cravatt BF. Monoacylglycerol lipase regulates a fatty acid network that promotes cancer pathogenesis. *Cell.* 2010;140(1):49-61.

Nomura DK, Morrison BE, Blankman JL, Long JZ, Kinsey SG, Marcondes MC, Ward AM, Hahn YK, Lichtman AH, Conti B, Cravatt BF. Endocannabinoid hydrolysis generates brain prostaglandins that promote neuroinflammation. *Science*. 2011a;334(6057):809-13.

Nomura DK, Lombardi DP, Chang JW, Niessen S, Ward AM, Long JZ, Hoover HH, Cravatt BF. Monoacylglycerol lipase exerts dual control over endocannabinoid and fatty acid pathways to support prostate cancer. *Chem Biol*. 2011b;18(7):846-56.

Nuzzi A, Fiasella A, Ortega JA, Pagliuca C, Ponzano S, Pizzirani D, Bertozzi SM, Ottonello G, Tarozzo G, Reggiani A, Bandiera T, Bertozzi F, Piomelli D. Potent α -amino- β -lactam carbamic acid ester as NAAA inhibitors. Synthesis and structure-activity relationship (SAR) studies. *Eur J Med Chem*. 2016;111:138-59.

O'Dowd BF, Nguyen T, Marchese A, Cheng R, Lynch KR, Heng HH, Kolakowski LF Jr, George SR. Discovery of three novel G-protein-coupled receptor genes. *Genomics*. 1998;47(2):310-3.

Ohlsson L, Hammarström ML, Lindmark G, Hammarström S, Sitohy B. Ectopic expression of the chemokine CXCL17 in colon cancer cells. *Br J Cancer*. 2016;114(6):697-703.

Ohshiro H, Tonai-Kachi H, Ichikawa K. GPR35 is a functional receptor in rat dorsal root ganglion neurons. *Biochem Biophys Res Commun*. 2008;365(2):344-8.

Oka S, Ota R, Shima M, Yamashita A, Sugiura T. GPR35 is a novel lysophosphatidic acid receptor. *Biochem Biophys Res Commun*. 2010;395(2):232-7.

Okumura S, Baba H, Kumada T, Nanmoku K, Nakajima H, Nakane Y, Hioki K, Ikenaka K. Cloning of a G-protein-coupled receptor that shows an activity to transform NIH3T3 cells and is expressed in gastric cancer cells. *Cancer Sci*. 2004;95(2):131-5.

O'Neill LA. A critical role for citrate metabolism in LPS signalling. *Biochem J*. 2011;438(3):e5-6.

Orellana-Serradell O, Poblete CE, Sanchez C, Castellón EA, Gallegos I, Huidobro C, Llanos MN, Contreras HR. Proapoptotic effect of endocannabinoids in prostate cancer cells. *Oncol Rep*. 2015;33(4):1599-608.

Pantel A, Teixeira A, Haddad E, Wood EG, Steinman RM, Longhi MP. Direct type I IFN but not MDA5/TLR3 activation of dendritic cells is required for maturation and metabolic shift to glycolysis after poly IC stimulation. *PLoS Biol*. 2014;12(1):e1001759.

Pagano E, Borrelli F, Orlando P, Romano B, Monti M, Morbidelli L, Aviello G, Imperatore R, Capasso R, Piscitelli F, Buono L, Di Marzo V, Izzo AA. Pharmacological inhibition of MAGL attenuates experimental colon carcinogenesis. *Pharmacol Res*. 2017;119:227-236.

Pancione M, Remo A, Colantuoni V. Genetic and epigenetic events generate multiple pathways in colorectal cancer progression. *Patholog Res Int.* 2012;2012:509348.

Park SJ, Lee SJ, Nam SY, Im DS. GPR35 mediates Iodoxamide-induced migration inhibitory response but not CXCL17-induced migration stimulatory response in THP-1 cells; is GPR35 a receptor for CXCL17? *Br J Pharmacol.* 2018;175(1):154-161.

Pavlopoulos S, Pelekoudas DN, Benchama O, Rawlins CM, Agar JN, West JM, Malamas M, Zvonok N, Makriyannis A. Secretion, isotopic labeling and deglycosylation of N-acylethanolamine acid amidase for biophysical studies. *Protein Expr Purif.* 2018;145:108-117.

Persano L, Rampazzo E, Della Puppa A, Pistollato F, Basso G. The three-layer concentric model of glioblastoma: cancer stem cells, microenvironmental regulation, and therapeutic implications. *ScientificWorldJournal.* 2011;11:1829-41. Review.

Pertwee RG. GPR55: a new member of the cannabinoid receptor clan? *Br J Pharmacol.* 2007;152(7):984-6. Review.

Peters JM, Cattley RC, Gonzalez FJ. Role of PPAR alpha in the mechanism of action of the nongenotoxic carcinogen and peroxisome proliferator Wy-14,643. *Carcinogenesis.* 1997;18(11):2029-33.

Petrosino S, Ahmad A, Marcolongo G, Esposito E, Allarà M, Verde R, Cuzzocrea S, Di Marzo V. Diacerein is a potent and selective inhibitor of palmitoylethanolamide inactivation with analgesic activity in a rat model of acute inflammatory pain. *Pharmacol Res.* 2015;91:9-14.

Petrosino S, Schiano Moriello A, Cerrato S, Fusco M, Puigdemont A, De Petrocellis L, Di Marzo V. The anti-inflammatory mediator palmitoylethanolamide enhances the levels of 2-arachidonoyl-glycerol and potentiates its actions at TRPV1 cation channels. *Br J Pharmacol.* 2016;173(7):1154-62.

Petrosino S, Di Marzo V. The pharmacology of palmitoylethanolamide and first data on the therapeutic efficacy of some of its new formulations. *Br J Pharmacol.* 2017 Jun;174(11):1349-1365. Review.

Pisanti S, Picardi P, D'Alessandro A, Laezza C, Bifulco M. The endocannabinoid signaling system in cancer. *Trends Pharmacol Sci.* 2013;34(5):273-82. Review.

Pisanti S, Picardi P, Prota L, Proto MC, Laezza C, McGuire PG, Morbidelli L, Gazzero P, Ziche M, Das A, Bifulco M. Genetic and pharmacologic inactivation of cannabinoid CB1 receptor inhibits angiogenesis. *Blood.* 2011;117(20):5541-50.

Ponzano S, Bertozzi F, Mengatto L, Dionisi M, Armirotti A, Romeo E, Berteotti A, Fiorelli C, Tarozzo G, Reggiani A, Duranti A, Tarzia G, Mor M, Cavalli A, Piomelli D, Bandiera T. Synthesis and structure-activity relationship (SAR) of 2-methyl-4-oxo-3-oxetanylcarbamic acid esters, a class of potent N-acylethanolamine acid amidase (NAAA) inhibitors. *J Med Chem.* 2013;56(17):6917-34.

Potente M, Gerhardt H, Carmeliet P. Basic and therapeutic aspects of angiogenesis. *Cell.* 2011;146(6):873-87. Review.

Qian BZ, Pollard JW. Macrophage diversity enhances tumor progression and metastasis. *Cell.* 2010;141(1):39-51. Review.

Qin H, Ruan ZH. The role of monoacylglycerol lipase (MAGL) in the cancer progress. *Cell Biochem Biophys.* 2014;70(1):33-6. Review.

Ravi J, Sneh A, Shilo K, Nasser MW, Ganju RK. FAAH inhibition enhances anandamide mediated anti-tumorigenic effects in non-small cell lung cancer by downregulating the EGF/EGFR pathway. *Oncotarget.* 2014;5(9):2475-86.

Ribeiro A, Pontis S, Mengatto L, Armirotti A, Chiurchiù V, Capurro V, Fiasella A, Nuzzi A, Romeo E, Moreno-Sanz G, Maccarrone M, Reggiani A, Tarzia G, Mor M, Bertozzi F, Bandiera T, Piomelli D. A Potent Systemically Active N-Acylethanolamine Acid Amidase Inhibitor that Suppresses Inflammation and Human Macrophage Activation. *ACS Chem Biol.* 2015;10(8):1838-46.

Richard ML, Liguori G, Lamas B, Brandi G, da Costa G, Hoffmann TW, Pierluigi Di Simone M, Calabrese C, Poggioli G, Langella P, Campieri M, Sokol H. Mucosa-associated microbiota dysbiosis in colitis associated cancer. *Gut Microbes.* 2018;9(2):131-142.

Risau W. Mechanisms of angiogenesis. *Nature.* 1997;386(6626):671-4. Review.

Rodríguez-Prados JC, Través PG, Cuenca J, Rico D, Aragonés J, Martín-Sanz P, Cascante M, Boscá L. Substrate fate in activated macrophages: a comparison between innate, classic, and alternative activation. *J Immunol.* 2010;185(1):605-14.

Rustgi AK. The genetics of hereditary colon cancer. *Genes Dev.* 2007;21(20):2525-38. Review.

Ryberg E, Larsson N, Sjögren S, Hjorth S, Hermansson NO, Leonova J, Elebring T, Nilsson K, Drmota T, Greasley PJ. The orphan receptor GPR55 is a novel cannabinoid receptor. *Br J Pharmacol.* 2007;152(7):1092-101.

Sakura Y, Tsuboi K, Uyama T, Zhang X, Taoka R, Sugimoto M, Kakehi Y, Ueda N. A quantitative study on splice variants of N-acylethanolamine acid amidase in human prostate cancer cells and other cells. *Biochim Biophys Acta*. 2016;1861(12 Pt A):1951-1958.

Santos R, Ursu O, Gaulton A, Bento AP, Donadi RS, Bologa CG, Karlsson A, Al-Lazikani B, Hersey A, Oprea TI, Overington JP. A comprehensive map of molecular drug targets. *Nat Rev Drug Discov*. 2017;16(1):19-34. Review.

Sarnelli G, Gigli S, Capoccia E, Iuvone T, Cirillo C, Seguella L, Nobile N, D'Alessandro A, Pesce M, Steardo L, Cuomo R, Esposito G. Palmitoylethanolamide Exerts Antiproliferative Effect and Downregulates VEGF Signaling in Caco-2 Human Colon Carcinoma Cell Line Through a Selective PPAR- α -Dependent Inhibition of Akt/mTOR Pathway. *Phytother Res*. 2016;30(6):963-70.

Sasso O, Moreno-Sanz G, Martucci C, Realini N, Dionisi M, Mengatto L, Duranti A, Tarozzo G, Tarzia G, Mor M, Bertorelli R, Reggiani A, Piomelli D. Antinociceptive effects of the N-acylethanolamine acid amidase inhibitor ARN077 in rodent pain models. *Pain*. 2013;154(3):350-60.

Sato T, Vries RG, Snippert HJ, van de Wetering M, Barker N, Stange DE, van Es JH, Abo A, Kujala P, Peters PJ, Clevers H. Single Lgr5 stem cells build crypt-villus structures in vitro without a mesenchymal niche. *Nature*. 2009;459(7244):262-5.

Schicho R, Storr M. Alternative targets within the endocannabinoid system for future treatment of gastrointestinal diseases. *Can J Gastroenterol*. 2011;25(7):377-83. Review.

Schlosburg JE, Blankman JL, Long JZ, Nomura DK, Pan B, Kinsey SG, Nguyen PT, Ramesh D, Booker L, Burston JJ, Thomas EA, Selley DE, Sim-Selley LJ, Liu QS, Lichtman AH, Cravatt BF. Chronic monoacylglycerol lipase blockade causes functional antagonism of the endocannabinoid system. *Nat Neurosci*. 2010;13(9):1113-9.

Shibuya M. Vascular Endothelial Growth Factor (VEGF) and Its Receptor (VEGFR) Signaling in Angiogenesis: A Crucial Target for Anti- and Pro-Angiogenic Therapies. *Genes Cancer*. 2011;2(12):1097-105.

Siegel RL, Miller KD, Jemal A. Cancer statistics, 2018. *CA Cancer J Clin*. 2018;68(1):7-30.

Sigel E, Baur R, Rácz I, Marazzi J, Smart TG, Zimmer A, Gertsch J. The major central endocannabinoid directly acts at GABA(A) receptors. *Proc Natl Acad Sci U S A*. 2011;108(44):18150-5.

Simpson CM, Itabe H, Reynolds CN, King WC, Glomset JA. Swiss 3T3 cells preferentially incorporate sn-2-arachidonoyl monoacylglycerol into sn-1-stearoyl-2-arachidonoyl phosphatidylinositol. *J Biol Chem*. 1991;266(24):15902-9. Erratum in: *J Biol Chem* 1991;266(29):19865.

Skaper SD, Facci L, Barbierato M, Zusso M, Bruschetta G, Impellizzeri D, Cuzzocrea S, Giusti P. N-Palmitoylethanolamine and Neuroinflammation: a Novel Therapeutic Strategy of Resolution. *Mol Neurobiol.* 2015;52(2):1034-42. Review.

Solorzano C, Zhu C, Battista N, Astarita G, Lodola A, Rivara S, Mor M, Russo R, Maccarrone M, Antonietti F, Duranti A, Tontini A, Cuzzocrea S, Tarzia G, Piomelli D. Selective N-acylethanolamine-hydrolyzing acid amidase inhibition reveals a key role for endogenous palmitoylethanolamide in inflammation. *Proc Natl Acad Sci U S A.* 2009;106(49):20966-71.

Spaner DE, Lee E, Shi Y, Wen F, Li Y, Tung S, McCaw L, Wong K, Gary-Gouy H, Dalloul A, Ceddia R, Gorzycynski R. PPAR-alpha is a therapeutic target for chronic lymphocytic leukemia. *Leukemia.* 2013;27(5):1090-9.

Steeg PS. Targeting metastasis. *Nat Rev Cancer.* 2016;16(4):201-18.

Stock K, Kumar J, Synowitz M, Petrosino S, Imperatore R, Smith ES, Wend P, Purfürst B, Nuber UA, Gurok U, Matyash V, Wälzlein JH, Chirasani SR, Dittmar G, Cravatt BF, Momma S, Lewin GR, Ligresti A, De Petrocellis L, Cristino L, Di Marzo V, Kettenmann H, Glass R. Neural precursor cells induce cell death of high-grade astrocytomas through stimulation of TRPV1. *Nat Med.* 2012;18(8):1232-8.

Suchanek KM, May FJ, Robinson JA, Lee WJ, Holman NA, Monteith GR, Roberts-Thomson SJ. Peroxisome proliferator-activated receptor alpha in the human breast cancer cell lines MCF-7 and MDA-MB-231. *Mol Carcinog.* 2002;34(4):165-71.

Sugiura T, Kodaka T, Nakane S, Miyashita T, Kondo S, Suhara Y, Takayama H, Waku K, Seki C, Baba N, Ishima Y. Evidence that the cannabinoid CB1 receptor is a 2-arachidonoylglycerol receptor. Structure-activity relationship of 2-arachidonoylglycerol, ether-linked analogues, and related compounds. *J Biol Chem.* 1999;274(5):2794-801.

Sugiura T, Kondo S, Kishimoto S, Miyashita T, Nakane S, Kodaka T, Suhara Y, Takayama H, Waku K. Evidence that 2-arachidonoylglycerol but not N-palmitoylethanolamine or anandamide is the physiological ligand for the cannabinoid CB2 receptor. Comparison of the agonistic activities of various cannabinoid receptor ligands in HL-60 cells. *J Biol Chem.* 2000;275(1):605-12.

Sun H, Jiang L, Luo X, Jin W, He Q, An J, Lui K, Shi J, Rong R, Su W, Lucchesi C, Liu Y, Sheikh MS, Huang Y. Potential tumor-suppressive role of monoglyceride lipase in human colorectal cancer. *Oncogene.* 2013;32(2):234-41.

Sun YV, Bielak LF, Peyser PA, Turner ST, Sheedy PF 2nd, Boerwinkle E, Kardia SL. Application of machine learning algorithms to predict coronary artery calcification with a sibship-based design. *Genet Epidemiol.* 2008;32(4):350-60.

Tai T, Tsuboi K, Uyama T, Masuda K, Cravatt BF, Houchi H, Ueda N. Endogenous molecules stimulating N-acylethanolamine-hydrolyzing acid amidase (NAAA). *ACS Chem Neurosci*. 2012;3(5):379-85.

Taniguchi Y, Tonai-Kachi H, Shinjo K. Zaprinas, a well-known cyclic guanosine monophosphate-specific phosphodiesterase inhibitor, is an agonist for GPR35. *FEBS Lett*. 2006;580(21):5003-8.

Tanimura A, Yamazaki M, Hashimoto Y, Uchigashima M, Kawata S, Abe M, Kita Y, Hashimoto K, Shimizu T, Watanabe M, Sakimura K, Kano M. The endocannabinoid 2-arachidonoylglycerol produced by diacylglycerol lipase α mediates retrograde suppression of synaptic transmission. *Neuron*. 2010;65(3):320-7.

Tannahill GM, Curtis AM, Adamik J, Palsson-McDermott EM, McGettrick AF, Goel G, Frezza C, Bernard NJ, Kelly B, Foley NH, Zheng L, Gardet A, Tong Z, Jany SS, Corr SC, Haneklaus M, Caffrey BE, Pierce K, Walmsley S, Beasley FC, Cummins E, Nizet V, Whyte M, Taylor CT, Lin H, Masters SL, Gottlieb E, Kelly VP, Clish C, Auron PE, Xavier RJ, O'Neill LA. Succinate is an inflammatory signal that induces IL-1 β through HIF-1 α . *Nature*. 2013;496(7444):238-42.

Terzić J, Grivennikov S, Karin E, Karin M. Inflammation and colon cancer. *Gastroenterology*. 2010;138(6):2101-2114.e5. Review.

Trédan O, Galmarini CM, Patel K, Tannock IF. Drug resistance and the solid tumor microenvironment. *J Natl Cancer Inst*. 2007;99(19):1441-54. Review.

Tsuboi K, Sun YX, Okamoto Y, Araki N, Tonai T, Ueda N. Molecular characterization of N-acylethanolamine-hydrolyzing acid amidase, a novel member of the cholesterylglycine hydrolase family with structural and functional similarity to acid ceramidase. *J Biol Chem*. 2005;280(12):11082-92.

Ueda N, Tsuboi K, Uyama T. Metabolism of endocannabinoids and related N-acylethanolamines: canonical and alternative pathways. *FEBS J*. 2013;280(9):1874-94. Review.

Ullman T. Histologic inflammation is a risk factor for progression to colorectal neoplasia in ulcerative colitis: a cohort study. *Gastroenterology*. 2007;133(4):1099-105.

Ullman TA, Itzkowitz SH. Intestinal inflammation and cancer. *Gastroenterology*. 2011;140(6):1807-16. Review.

Vago R, Bettiga A, Salonia A, Ciuffreda P, Ottria R. Development of new inhibitors for N-acylethanolamine-hydrolyzing acid amidase as promising tool against bladder cancer. *Bioorg Med Chem*. 2017;25(3):1242-1249.

- Van Dross R, Soliman E, Jha S, Johnson T, Mukhopadhyay S. Receptor-dependent and receptor-independent endocannabinoid signaling: a therapeutic target for regulation of cancer growth. *Life Sci.* 2013;92(8-9):463-6. Review.
- Vandevoorde S, Jonsson KO, Labar G, Persson E, Lambert DM, Fowler CJ. Lack of selectivity of URB602 for 2-oleoylglycerol compared to anandamide hydrolysis in vitro. *Br J Pharmacol.* 2007;150(2):186-91.
- Velasco G, Hernández-Tiedra S, Dávila D, Lorente M. The use of cannabinoids as anticancer agents. *Prog Neuropsychopharmacol Biol Psychiatry.* 2016;64:259-66. Review.
- Velasco G, Sánchez C, Guzmán M. Anticancer mechanisms of cannabinoids. *Curr Oncol.* 2016;23(2):S23-32. Review.
- Venables BJ, Waggoner CA, Chapman KD. N-acylethanolamines in seeds of selected legumes. *Phytochemistry.* 2005;66(16):1913-8.
- Wang CI, Lewis RJ. Emerging opportunities for allosteric modulation of G-protein coupled receptors. *Biochem Pharmacol.* 2013;85(2):153-62. Review.
- Wang J, Simonavicius N, Wu X, Swaminath G, Reagan J, Tian H, Ling L. Kynurenic acid as a ligand for orphan G protein-coupled receptor GPR35. *J Biol Chem.* 2006;281(31):22021-8.
- Wang J, Zhao LY, Uyama T, Tsuboi K, Wu XX, Kakehi Y, Ueda N. Expression and secretion of N-acylethanolamine-hydrolysing acid amidase in human prostate cancer cells. *J Biochem.* 2008;144(5):685-90.
- Wang W, Han T, Tong W, Zhao J, Qiu X. Overexpression of GPR35 confers drug resistance in NSCLC cells by β -arrestin/Akt signaling. *Onco Targets Ther.* 2018;11:6249-6257.
- Warburg O. On the origin of cancer cells. *Science.* 1956;123(3191):309-14.
- Weinstein EJ, Head R, Griggs DW, Sun D, Evans RJ, Swearingen ML, Westlin MM, Mazzarella R. VCC-1, a novel chemokine, promotes tumor growth. *Biochem Biophys Res Commun.* 2006;350(1):74-81.
- West JM, Zvonok N, Whitten KM, Vadivel SK, Bowman AL, Makriyannis A. Biochemical and mass spectrometric characterization of human N-acylethanolamine-hydrolyzing acid amidase inhibition. *PLoS One.* 2012;7(8):e43877.
- West NR, McCuaig S, Franchini F, Powrie F. Emerging cytokine networks in colorectal cancer. *Nat Rev Immunol.* 2015;15(10):615-29. Review.

Wirtz D, Konstantopoulos K, Searson PC. The physics of cancer: the role of physical interactions and mechanical forces in metastasis. *Nat Rev Cancer*. 2011;11(7):512-22.

Wynder EL, Kajitani T, Ishikawa S, Dodo H, Takano A. Environmental factors of cancer of the colon and rectum. II. Japanese epidemiological data. *Cancer*. 1969;23(5):1210-20.

Xue H, Lu B, Lai M. The cancer secretome: a reservoir of biomarkers. *J Transl Med*. 2008;6:52.

Yang L, Li L, Chen L, Li Y, Chen H, Li Y, Ji G, Lin D, Liu Z, Qiu Y. Potential analgesic effects of a novel N-acylethanolamine acid amidase inhibitor F96 through PPAR- α . *Sci Rep*. 2015;5:13565.

Ye L, Zhang B, Seviour EG, Tao KX, Liu XH, Ling Y, Chen JY, Wang GB. Monoacylglycerol lipase (MAGL) knockdown inhibits tumor cells growth in colorectal cancer. *Cancer Lett*. 2011;307(1):6-17.

Zajac E, Schweighofer B, Kupriyanova TA, Juncker-Jensen A, Minder P, Quigley JP, Deryugina EI. Angiogenic capacity of M1- and M2-polarized macrophages is determined by the levels of TIMP-1 complexed with their secreted proMMP-9. *Blood*. 2013;122(25):4054-67.

Zak Z, Gelebart P, Lai R. Fenofibrate induces effective apoptosis in mantle cell lymphoma by inhibiting the TNF α /NF-kappaB signaling axis. *Leukemia*. 2010;24(8):1476-86.